공학박사 학위 논문

로봇 매니퓰레이터를 위한 관찰자 기반 제어 설계 기술

OBSERVER-BASED CONTROL DESIGN TECHNIQUES FOR ROBOT MANIPULATORS

울산대학교 대학원

기계자동차 공학과

DAO HOANG VU

OBSERVER-BASED CONTROL DESIGN TECHNIQUES FOR ROBOT MANIPULATORS

A thesis submitted in partial fulfillment of the requirement for the Degree of

Doctor of Philosophy to the School of Mechanical and Automotive

Engineering, University of Ulsan, Korea

By

DAO HOANG VU

June 2023

로봇 매니퓰레이터를 위한 관찰자 기반 제어 설계 기술

OBSERVER-BASED CONTROL DESIGN TECHNIQUES FOR ROBOT MANIPULATORS

지도교수 **안경관**

이논문을 공학박사 학위 논문으로 제출함

2023 년 06 월

울산대학교 대학원

기계자동차공학과

OBSERVER-BASED CONTROL DESIGN TECHNIQUES FOR ROBOT MANIPULATORS

This certifies that the dissertation of

DAO HOANG VU is approved by

Committee Chairman: **Prof. BYUNG RYONG LEE**

Committee Member: **Prof. KYOUNG KWAN AHN**

Committee Member: **Prof. CHEOLKEUN HA**

Committee Member: **Prof. GI-SEO PARK**

Committee Member: **Prof. JI-SUNG JANG**

School of Mechanical and Automotive Engineering

University of Ulsan, Korea

June 2023

Acknowledgment

Five years of Ph.D. study brought me a lot of experiences and knowledge, which truly changed the way I think and look at many aspects of my life and career. Therefore, I would like to express my gratitude to the people who helped and encouraged me a lot during my time in Ulsan.

Firstly, I would like to thank my advisor, Prof. Ahn Kyoung Kwan, who led me from the very beginning of my research path, gave me a lot of valuable experience in research, contributed greatly to my scientific achievements, and opened a new horizon for my future career. I will never forget his presence in my life.

Secondly, I would like to thank the graduate thesis defense committee members, Prof. Lee Byung Ryong, Prof. Ha Cheolkeun, Prof. Park Gi-Seo, and Prof. Jang Ji-Sung for their insightful comments, fair assessment, and suggestions to improve the quality of my dissertation in many aspects. At the same time, I highly appreciate Ulsan University as well as the Korean government for their financial support in my research, which helped me realize my dream of studying abroad.

Next, I would like to thank my brothers at FPMI Lab who have helped me a lot in both academic and daily life. We have shared both the joys and sorrows of life, overcoming many difficulties and challenges to achieve what we are now. Thank you, my big brother, Dr. Ho Cong Minh who has accompanied me, from the first day to the last day he was here, he is a shining example of the will, energy, and unpretentiousness to overcome adversity and optimism into a bright future. Thank you, my big brother, Mr. Nguyen Manh Hung who always takes a lot of time to listen to my stories and share with me his experiences and views on life.

Finally, I would like to express my deep gratitude to my family for their silent sacrifices. For me, my family is the greatest motivation and spiritual support for me to be strong enough to overcome all challenges and difficulties.

Ulsan, Korea, June 2023

Dao Hoang Vu

Contents

List of Figures

List of Tables

Abbreviations

DUEA   Disturbances and uncertainties estimation and attenuation

DOB   Disturbance observer

ESO   Extended state observer

ESMO   Extended sliding mode observer

SMO   Sliding mode observer

FTC   Fault-tolerant control

TCF   Task coordinate frame

CCC   Cross-coupled control

BLF   Barrier Lyapunov function

NN   Neural network

ABSTRACT

Due to the capability of performing repetitive tasks with high speeds and accuracies, robot manipulators have been developed and used in many fields such as industrial automation, robotic surgery, and in-space missions. Besides the development of hardware components such as mechanical and electric subsystems, control design plays an important role to ensure that the robot manipulators operate precisely and achieve the desired performance. Recently, advanced control techniques have been proposed to deal with practical problems such as model uncertainties and external disturbances, output and state constraints, control input saturation, convergence time, and their combinations. Among them, uncertainty and disturbance attenuation are essential to guarantee nominal control performance before considering any further problems. This thesis proposes advanced control techniques for robot manipulators suffering from nonlinear dynamics, model uncertainties, external disturbances, and unmeasurable joint velocities. Firstly, the kinematics and dynamics of a general n-degree-of-freedom (n-DOF) series manipulator are established by the Lagrangian method. Based on that, several observers such as sliding mode observer (SMO), and extended sliding mode observer (ESMO) are firstly designed to simultaneously estimate both lumped uncertainties/disturbances and unknown joint velocities. Then, the estimated values are feedback to the main controller which is constructed by the backstepping framework to guarantee the robustness of the control system with those difficulties. In addition, to further improve the position tracking control accuracy, the barrier Lyapunov function (BLF) is adopted to guarantee prescribed position tracking performance. For some specific applications while the contouring performance is primary compared to the general tracking performance, the task coordinate frame (TCF), which transforms the tracking error into the contouring error and other error components, is integrated into the original backstepping framework together with advanced observers to achieve high accuracy contouring performance. Finally, the proposed observer techniques are utilized in not only position control tasks but also force control tasks, i.e., admittance control architecture which regulates the relationship between the end-effector position and interaction forces with the environment.

Chapter 1
INTRODUCTION

1.1. Overview

In recent decades, robot manipulators play an important role in the development of human society, from traditional applications such as material handling [1], assembly [2], and machining tasks [3] in general industry to recent trends such as surgery assistants [4], robot teachers [5], robot maids [6], etc. due to the characteristics of high accuracy and flexibility. Overall, a typical robot manipulator is constructed with many components such as mechanical, electric, electronic, and control subsystems in a sophisticated way. Among them, the control algorithm is primary to guarantee the tasks are properly conducted during robot operation. However, the control design for robot manipulators is difficult and has received much attention from both academics and the industry.

The overall control performance can be classified into nominal control performance and uncertainties/disturbances attenuation. In terms of the nominal control performance, the controller is designed based on the nominal robot model to guarantee that the desired criterions such as position tracking accuracy, force tracking accuracy, or the force/position relationship, i.e., impedance behavior, can be achieved. Depending on the availability of the system information, control approaches can be listed as proportional-integral-derivative control [7], computed torque control [8], adaptive control [9], backstepping control [10], sliding mode control [11], etc. Besides guaranteeing nominal control performance, these control algorithms still have the robustness to uncertainties/disturbances if high control gains are selected. For example, the sliding mode control approaches not even attenuate to matched uncertainties/disturbances due to the adoption of the signum function, but also provide finite-time convergence. However, for robotic systems with large uncertainties/disturbances, the high control gain approach can cause instabilities in the robotic systems. Therefore, the uncertainties/disturbance attenuation is necessary to release the burden to the main controller, and also decouple the nominal control performance from the disturbance rejection and uncertainty suppression.

For a long time, disturbance/uncertainty estimation and attenuation (DUEA) have been investigated for robot manipulator applications [12]. Overall, the DUEA approaches can be classified into adaptive methods and disturbance observer methods. Originally, adaptive methods [13, 14] have been proposed to deal with structured uncertainties with known dynamic

functions and unknown model parameters. Adaptive laws are designed to estimate the unknown model parameters with the assumption that these parameters are constant or slow-varying. However, these laws are directly coupled with the tracking control errors and the parameter estimation accuracy is not guaranteed. Recently, the applications of the adaptive methods are broadened into unstructured uncertainties by assuming that they can be ideally approximated by neural networks (NNs) with bounded approximation errors [15, 16]. Then, adaptive laws are designed to estimate the weighting factors of the NNs. However, the problems of assuming constant weighting factors and their convergences still exist. Furthermore, these methods are only effective for model uncertainties, i.e., state-dependent terms, not for external disturbances. The remaining approach is the disturbance observer approach, which handles both the external disturbances and model uncertainties. For example, time delay estimation (TDE) has been applied to estimate the lumped uncertainties/disturbances in the position tracking control of the robotics system based on the time delay estimation mechanism [17, 18]. However, joint velocities and accelerations are needed which requires other state observers or sensors in the robotic system. Similarly, the nonlinear disturbance observer (NDOB) was also proposed to utilize the nonlinear dynamics of the robot manipulators in its design to successfully estimate the lumped uncertainties/disturbances [19]. Asymptotically estimation can be achieved in case of slow-varying or constant disturbances. Furthermore, acceleration information is omitted here, but the velocity information is still required to construct the observer. Another DUEA approach called "generalized momentum observer" (GMO) has been proposed to deal with the contact force estimation when the robot manipulator end-effector interacts with the environment [20]. Nevertheless, the problem of velocity estimation still occurs. To overcome these issues, the extended-state observer (ESO) was designed to simultaneously estimate both joint velocities and lumped disturbances/uncertainties [21]. Compared to the above-mentioned DUEAs, no further state observers are needed. Furthermore, after the estimation, both kinds of information are fed back into the main controller, which completes the design of the general control approach. From the author's point of view, until now, the problem of active disturbance rejection control design for robot manipulators with different applications is still open and needs more investigation.

1.2. Research objectives

This thesis investigates and presents observer-based control techniques for different applications of robot manipulators suffering from nonlinear dynamics, external disturbances, model uncertainties, unknown joint velocities, and actuator faults. The main controllers are

designed following the backstepping approach, which is effective to deal with the nonlinear dynamics of robot manipulators and allows easy implementation of the various kinds of state and disturbance observers. The Lyapunov theory is utilized to analyze the stability of the control systems. Simulation results verify the effectiveness of the proposed control algorithm compared to previous studies.

In detail, the objectives of the thesis are mentioned as follows:

- To introduce some advanced state and disturbance observers for robot manipulator control purposes. The extended sliding mode observer (ESMO) and the sliding mode observer (SMO) are presented which improve both the transient response and the steadstate estimation performance of both velocities and lumped disturbances. The Lyapunov analysis is utilized to validate the effectiveness of the proposed observers compared to the well-known ESO.
- To investigate the applications of observer-based control approach for hydraulic robot manipulators in terms of position tracking with fault diagnosis and fault tolerant control problem. The internal leakage in the hydraulic actuators is considered the main problem here together with other difficulties. The ESOs play an important role in both estimating the matched and mismatched disturbances and detecting the internal leakage fault. Then, the fault is identified based on an adaptive identification algorithm.
- To investigate the applications of the observer-based control approach for hydraulic robot manipulators in terms of interaction control with the environment. An extended sliding observer (ESMO) is designed to estimate the contact force and contribute to the cascade control framework.
- To investigate the applications of the observer-based control approach for semi-autonomous robotic excavators in terms of contouring accuracy. The task coordinate approach is adopted to separate the original tracking errors into contouring errors and the other error components. An ESO is designed to estimate joint velocities and disturbances. Based on that, the main control is designed following the backstepping framework with further improvement by considering the output constraint problem with help of the barrier Lyapunov function.

1.3. Limitations

In this work, advanced observer-based control techniques have been conducted to improve the control performance of robot manipulators in different applications. However, some limitations remain as follows:

- The derivatives of the lumped uncertainties/disturbances are assumed to be bounded.
- The nominal models of the robot manipulators are available.
- Only simulation results are presented to validate the proposed control algorithm. Experiment results are not available due to some obstacles during the building of the test benches.

1.4. Thesis outline

The dissertation outlines are presented as follows:

- Chapter 1 present the research motivations, objectives, limitation, and the outlines of the thesis.
- Chapter 2 introduces some state and disturbance observers for robot manipulator control applications.
- Chapter 3 derives an active fault-tolerant control for hydraulic manipulators based on ESOs and adaptive fault identification algorithm.
- Chapter 4 describes a force-sensorless admittance control design for hydraulic manipulators with ESMO which estimates the unknown contact force at the end-effector.
- Chapter 5 provides a high-accuracy contouring control algorithm for robotic excavators to complete the surface-flattening tasks based on the task-coordinate frame approach and ESO.
- Chapter 6 concludes the thesis and gives a discussion about future works.

Chapter 2

OBSERVER DESIGN TECHNIQUES FOR ROBOT MANIPULATORS

2.1. Introduction

Before investigating the applications of the observer-based control techniques in the next chapters, in this chapter, the robot manipulator dynamics is presented with some assumptions to realize the design of the state and disturbance observers. Based on that, the design of ESO, ESMO, and SMO are presented, and observer stabilities are analyzed by the Lyapunov theorem. Finally, some discussions about the performance of observers are given.

2.2. Robot manipulator dynamics

The manipulator dynamics are given as follows:

$$M(q)\ddot{q} + C(q,\dot{q})\dot{q} + G(q) = u + \tau_d \tag{2.1}$$

where $q \in R^n, M(q), C(q,\dot{q})$, and $G(q)$ are the vector of joint angles, inertia matrix, Coriolis and centrifugal matrix, and gravity matrix, respectively. u is the control force/torque and τ_d is the vector of lumped disturbances and uncertainties existing in the system.

To design the proposed observer more conveniently, the manipulator dynamics is rewritten in the following form:

$$\begin{aligned}\dot{x}_1 &= x_2 \\ \dot{x}_2 &= f_1(x_1)u + f_2(x_1, x_2) + d\end{aligned} \tag{2.2}$$

where $x_1 = q, x_2 = \dot{q}, d = M(x_1)^{-1}\tau_d, f_1 = M(x_1)^{-1}$, and $f_2 = -M(x_1)^{-1}(C(x_1, x_2)x_2 + G(x_1))$.

Assumption 1: There exists a constant $\alpha > 0$ so that the following Lipchitz condition holds:

$$\|f_2(x_1, x_2 + \Delta x_2) - f_2(x_1, x_2)\| \le \alpha \|\Delta x_2\| \tag{2.3}$$

Assumption 2: The derivative of the lumped disturbances and uncertainties is bounded, i.e., $\|\dot{d}\| \le \delta_h$ where $\delta_h > 0$.

Remark 1: The joint angles are measurable. The problem is how to estimate both joint velocities and lumped disturbances and uncertainties.

2.3. Extended state observer

The ESO is designed as follows [21]:

$$
\begin{aligned}
\dot{\hat{x}}_1 &= \hat{x}_2 + 3\omega(x_1 - \hat{x}_1) \\
\dot{\hat{x}}_2 &= f_1(x_1)u + f_2(x_1, \hat{x}_2) + \hat{x}_3 + 3\omega^2(x_1 - \hat{x}_1) \\
\dot{\hat{x}}_3 &= \omega^3(x_1 - \hat{x}_1)
\end{aligned}
\tag{2.4}
$$

where ω is the observer gain.

Theorem 1: The ESO can achieved globally uniformly ultimately bounded (GUUB) estimation performances of both unmeasurable joint velocities and lumped uncertainties/disturbances for the robot manipulator.

Proof: Set $\tilde{x} = x - \hat{x}$. The error dynamics become

$$
\begin{aligned}
\dot{\tilde{x}}_1 &= \tilde{x}_2 - 3\omega\tilde{x}_1 \\
\dot{\tilde{x}}_2 &= \tilde{f}_2 + \tilde{x}_3 - 3\omega^2\tilde{x}_1 \\
\dot{\tilde{x}}_3 &= h - \omega^3\tilde{x}_1
\end{aligned}
\tag{2.5}
$$

Set $\varepsilon = [\tilde{x}_1, \tilde{x}_2/\omega, \tilde{x}_3/\omega^2]^T$. The scaled estimation error dynamics are derived by

$$
\begin{aligned}
\dot{\varepsilon}_1 &= \omega\varepsilon_2 - 3\omega\varepsilon_1 \\
\dot{\varepsilon}_2 &= \omega\varepsilon_3 - 3\omega\varepsilon_1 + \frac{\tilde{f}_2}{\omega} \\
\dot{\varepsilon}_3 &= -\omega\varepsilon_1 + \frac{h}{\omega^2}
\end{aligned}
\tag{2.6}
$$

Transferring above equation into matrix form, one obtains:

$$
\dot{\varepsilon} = \omega A\varepsilon + D_1\frac{\tilde{f}_2}{\omega} + D_2\frac{h}{\omega^2}
\tag{2.7}
$$

where $A = \begin{bmatrix} -3I_n & I_n & 0_{n\times n} \\ -3I_n & 0_{n\times n} & I_n \\ -I_n & 0_{n\times n} & 0_{n\times n} \end{bmatrix}; D_1 = \begin{bmatrix} 0_{n\times n} \\ I_n \\ 0_{n\times n} \end{bmatrix}; D_2 = \begin{bmatrix} 0_{n\times n} \\ 0_{n\times n} \\ I_n \end{bmatrix}$.

Since the matrix A is Hurwitz, there exists a positive-definite matrix P satisfying the Lyapunov equation as follows:

$$
A^T P + PA = -2I_{3n}
\tag{2.8}
$$

Consider the following Lyapunov function

$$
V = \frac{1}{2}\varepsilon^T P\varepsilon
\tag{2.9}
$$

6

Taking the derivative of it, one obtains

$$\dot{V} = -\omega \boldsymbol{\varepsilon}^T \boldsymbol{\varepsilon} + \boldsymbol{\varepsilon}^T \boldsymbol{PD}_1 \frac{\tilde{\boldsymbol{f}}_2}{\omega} + \boldsymbol{\varepsilon}^T \boldsymbol{PD}_2 \frac{\boldsymbol{h}}{\omega^2}$$

$$\leq -\omega \boldsymbol{\varepsilon}^T \boldsymbol{\varepsilon} + \frac{1}{2} \boldsymbol{\varepsilon}^T \boldsymbol{\varepsilon} + \frac{1}{2\omega^2}{}^T \tilde{\boldsymbol{f}}_2{}^T \boldsymbol{Y}_1 \tilde{\boldsymbol{f}}_2$$

$$+ \frac{1}{2} \boldsymbol{\varepsilon}^T \boldsymbol{\varepsilon} + \frac{1}{2\omega^4} \boldsymbol{h}^T \boldsymbol{Y}_2 \boldsymbol{h} \tag{2.10}$$

$$\leq -\left(\omega - 1 - \frac{\lambda_{Y1}\alpha^2}{2\omega^2} \right) \frac{2}{\lambda_{P1}} V + \frac{1}{2\omega^4} \lambda_{Y2} \delta_h{}^2$$

$$= -aV + b$$

where $\lambda_{Y1} = \lambda_{\min}((\boldsymbol{PD}_1)^T \boldsymbol{PD}_1)$, $\lambda_{Y2} = \lambda_{\min}((\boldsymbol{PD}_2)^T \boldsymbol{PD}_2)$, and $\lambda_{P1} = \lambda_{\max}(\boldsymbol{P})$.

This completes the proof.

Based on that, one obtains:

$$\|\hat{\boldsymbol{x}}_2 - \boldsymbol{x}_2\| \leq \frac{\delta_h}{\omega^{3/2}} \sqrt{\frac{\lambda_{Y2}\lambda_{P1}}{2\lambda_{P2}\left(1 - \frac{1}{\omega} - \frac{\lambda_{Y1}\alpha^2}{2\omega}\right)}}$$

$$\|\hat{\boldsymbol{x}}_3 - \boldsymbol{x}_3\| \leq \frac{\delta_h}{\omega^{1/2}} \sqrt{\frac{\lambda_{Y2}\lambda_{P1}}{2\lambda_{P2}\left(1 - \frac{1}{\omega} - \frac{\lambda_{Y1}\alpha^2}{2\omega}\right)}} \tag{2.11}$$

where $\lambda_{P2} = \lambda_{\min}(\boldsymbol{P})$.

2.4. Extended sliding mode observer

The ESMO is designed as follows [22]:

$$\begin{cases} \dot{\hat{\boldsymbol{x}}}_1 = \hat{\boldsymbol{x}}_2 + \boldsymbol{v} \\ \dot{\hat{\boldsymbol{x}}}_2 = \boldsymbol{f}_1(\boldsymbol{x}_1)\boldsymbol{u} + \boldsymbol{f}_2(\boldsymbol{x}_1, \hat{\boldsymbol{x}}_2) + \hat{\boldsymbol{x}}_3 + 2\omega \boldsymbol{v} \\ \dot{\hat{\boldsymbol{x}}}_3 = \omega^2 \boldsymbol{v} \end{cases} \tag{2.12}$$

where the switching function is defined as

$$\boldsymbol{v} = \begin{cases} \eta \dfrac{\boldsymbol{x}_1 - \hat{\boldsymbol{x}}_1}{\|\boldsymbol{x}_1 - \hat{\boldsymbol{x}}_1\|} & \text{if } \|\boldsymbol{x}_1 - \hat{\boldsymbol{x}}_1\| \neq 0 \\ \boldsymbol{0}_{n \times 1} & \text{otherwise} \end{cases} \tag{2.13}$$

Theorem 2: The ESMO guarantees arbitrarily bounded velocity and disturbance estimation errors the bandwidth of the observer ω is chosen with a large enough value.

Proof: Define the estimation errors $\tilde{x}_i = x_i - \hat{x}_i$ $(i = 1, 2, 4)$ and $\tilde{f}_2 = f_2(x_1, x_2) - f_2(x_1, \hat{x}_2)$. One obtains:

$$
\begin{aligned}
\dot{\tilde{x}}_1 &= \tilde{x}_2 - v \\
\dot{\tilde{x}}_2 &= \tilde{f}_2 + \tilde{x}_3 - 2\omega v \\
\dot{\tilde{x}}_3 &= h - \omega^2 v
\end{aligned}
\tag{2.14}
$$

A Lyapunov function is defined as $V_1 = 0.5\tilde{x}_1^T \tilde{x}_1$. Taking the derivative of it, one obtains

$$
\dot{V}_1 = \tilde{x}_1^T(\tilde{x}_2 - v) \leq -\|\tilde{x}_1\|(\eta - \|\tilde{x}_2\|)
\tag{2.15}
$$

In the domain that $\|\tilde{x}_2\| \leq \eta - \eta_0$, $\eta_0 > 0$, the following condition holds:

$$
\dot{V}_1 \leq -\eta_0 \|\tilde{x}_1\| = -\eta_0 \sqrt{2V_1}
\tag{2.16}
$$

Hence, finite-time convergence is achieved. After that, one obtains the equivalent switching action $v_{eq} = \tilde{x}_2$. Hence, the remaining error dynamics become

$$
\begin{aligned}
\dot{\tilde{x}}_2 &= \tilde{f}_2 + \tilde{x}_3 - 2\omega\tilde{x}_2 \\
\dot{\tilde{x}}_3 &= h - \omega^2 \tilde{x}_2
\end{aligned}
\tag{2.17}
$$

Define a scaled estimation error $\varepsilon = [\tilde{x}_2^T, \tilde{x}_3^T / \omega]^T$. The error dynamics are rewritten as

$$
\dot{\varepsilon} = \omega A \varepsilon + D_1 \tilde{f}_2 + D_2 h / \omega
\tag{2.18}
$$

where $A = \begin{bmatrix} -2I_n & I_n \\ -I_n & 0_{n \times n} \end{bmatrix}$; $D_1 = \begin{bmatrix} I_n \\ 0_{n \times n} \end{bmatrix}$; $D_2 = \begin{bmatrix} 0_{n \times n} \\ I_n \end{bmatrix}$.

Because the matrix A is negative definite, there exists a solution P of the following Lyapunov equation:

$$
A^T P + PA = -2I_{2n}
\tag{2.19}
$$

A Lyapunov function is defined as $V = 0.5\varepsilon^T P \varepsilon$. Taking the derivative of it, one obtains

$$
\dot{V} = -\omega\varepsilon^T \varepsilon + \varepsilon^T P(D_1 \tilde{f}_2 + D_2 h / \omega)
\tag{2.20}
$$

Define $Y_1 = D_{\varepsilon 1}^T P_\varepsilon^T P_\varepsilon D_{\varepsilon 1}$ and $Y_2 = D_{\varepsilon 2}^T P_\varepsilon^T P_\varepsilon D_{\varepsilon 2}$. The following inequality holds:

$$
\dot{V} \leq -aV + b
\tag{2.21}
$$

where

8

$$a = \frac{2}{\lambda_{P1}}\left(\omega - \frac{1}{2}\alpha^2\lambda_{Y1} - 1\right), b = \frac{1}{2\omega^2}\lambda_{Y2}\delta_h^2,$$

$$\lambda_{Y1} = \lambda_{\max}(\boldsymbol{Y}_1), \lambda_{P1} = \lambda_{\max}(\boldsymbol{P}) \tag{2.22}$$

This completes the proof.

In the steady state, one obtains:

$$\|\hat{\boldsymbol{x}}_2 - \boldsymbol{x}_2\| \le \frac{\delta_h}{\omega^{3/2}}\sqrt{\frac{\lambda_{Y2}\lambda_{P1}}{2\lambda_{P2}\left(1 - \frac{1}{\omega} - \frac{\lambda_{Y1}\alpha^2}{2\omega}\right)}}$$

$$\|\hat{\boldsymbol{x}}_3 - \boldsymbol{x}_3\| \le \frac{\delta_h}{\omega^{1/2}}\sqrt{\frac{\lambda_{Y2}\lambda_{P1}}{2\lambda_{P2}\left(1 - \frac{1}{\omega} - \frac{\lambda_{Y1}\alpha^2}{2\omega}\right)}} \tag{2.23}$$

2.5. Sliding mode observer

The proposed SMO is expressed as follows [23]:

$$\begin{cases} \dot{\boldsymbol{s}}_1 = \boldsymbol{s}_2 + \boldsymbol{v} \\ \dot{\boldsymbol{s}}_2 = f(\boldsymbol{x}_1)\boldsymbol{u} + \boldsymbol{f}_2(\boldsymbol{x}_1, \boldsymbol{s}_2) + \omega\boldsymbol{v} \end{cases} \tag{2.24}$$

where $\boldsymbol{s}_1$ and $\boldsymbol{s}_2$ are the states of the observer, and ω is the observer gain. The symbol $\boldsymbol{v}$ denotes a switching function of the observation error, which is defined by

$$\boldsymbol{v} = \begin{cases} \dfrac{\eta(\boldsymbol{x}_1 - \boldsymbol{s}_1)}{\|\boldsymbol{x}_1 - \boldsymbol{s}_1\|} & \text{if } \|\boldsymbol{x}_1 - \boldsymbol{s}_1\| \ne 0 \\ 0 & \text{otherwise} \end{cases} \tag{2.25}$$

where η is a positive parameter.

Theorem 4: Based on Assumptions 1 and 2, the proposed SMO ensures arbitrarily bounded estimation performance for the system if the observer parameters are selected with large enough values.

Proof: Denote the error term $\tilde{\boldsymbol{s}} = \boldsymbol{x} - \boldsymbol{s}$. The error dynamics are expressed as follows:

$$\begin{aligned} \dot{\tilde{\boldsymbol{s}}}_1 &= \tilde{\boldsymbol{s}}_2 - \boldsymbol{v} \\ \dot{\tilde{\boldsymbol{s}}}_2 &= \tilde{\boldsymbol{f}} + \boldsymbol{d} - \omega\boldsymbol{v} \end{aligned} \tag{2.26}$$

Define a Lyapunov function $V_{s1} = 1/2\,\tilde{\boldsymbol{s}}_1^T\tilde{\boldsymbol{s}}_1$. Differentiating it and substituting into, it becomes

$$\dot{V}_{s1} = \tilde{\boldsymbol{s}}_1(\tilde{\boldsymbol{s}}_2 - \boldsymbol{v}) \le -\|\tilde{\boldsymbol{s}}_1\|(\eta - \|\tilde{\boldsymbol{s}}_2\|) \tag{2.27}$$

where the observer parameter η is selected with a large enough value so that there exists a positive constant η_0 satisfying $\|\tilde{s}_2\| \leq \eta - \eta_0$. Therefore, one obtains

$$\dot{V}_{s1} \leq -\sqrt{2}\eta_0\sqrt{V_{s1}} \tag{2.28}$$

Based on this, s_1 converges to zero in finite time. After that, from the first equation of, it is observed that the switching function v is equivalent to the error $\tilde{s}_2$. Substituting it into the second equation of, it becomes

$$\dot{\tilde{s}}_2 = \tilde{f} + d - \omega\tilde{s}_2 \tag{2.29}$$

Another Lyapunov function is designed as $V_{s2} = 1/2\,\tilde{s}_2^T\tilde{s}_2$. The derivative of it is derived as

$$\begin{aligned}
\dot{V}_{s2} &= \tilde{s}_2^T(\tilde{f} + d - \omega\tilde{s}_2) \\
&\leq -\omega\tilde{s}_2^T\tilde{s}_2 + \tilde{s}_2^T\tilde{s}_2 + \frac{1}{2}\tilde{f}^T\tilde{f} + \frac{1}{2}d^Td
\end{aligned} \tag{2.30}$$

Combining with Assumptions 1 and 2, it becomes

$$\begin{aligned}
\dot{V}_{s2} &\leq -\left(\omega - \frac{1}{2}\alpha_f^2 - 1\right)\tilde{s}_2^T\tilde{s}_2 + \frac{1}{2}\Delta_d^2 \\
&\leq -\lambda_{s2}V_{s2} + \Delta_{s2}
\end{aligned} \tag{2.31}$$

This completes the proof.

2.6. Discussion

This chapter provides a proof theory for some state and disturbance observers which will be utilized for different applications of robot manipulators. Comparison between observers is given as follows:

- The ESO covers the states and disturbance estimation in case disturbance is limited in change rate.
- The ESMO improves the state and disturbance estimation compared to the ESO. However, parameter selection for initial conditions needs to be careful.
- Different from the above observers, the SMO handles the states and disturbances while the disturbance is limited, not the change rate of it. However, the proof theory cannot be strictly maintained.

Chapter 3
APPLICATION TO FAULT-TOLERANT CONTROL PROBLEM OF HYDRAULIC MANIPULATORS

3.1. Introduction

Electrohydraulic servomechanism has a high-power-to-weight ratio and large force/torque output compared to servo systems driven by pneumatic or electrical actuators [24]. As a result, electrohydraulic systems have been widely applied in industrial automation applications and/or military applications including active suspensions [25], rolling mills [26], aircraft actuators [27], robot manipulators [14, 28-31], and construction machines [32]. However, the performance of the servo system driven by electrohydraulic actuators usually is strongly affected by high nonlinearities, modeling uncertainties (e.g., Bulk modulus, friction, and leakage), and external disturbance (e.g., load variations) [33, 34]. To deal with these problems, several approaches have been proposed. Assuming that exact model parameters are available, the highly nonlinear behavior of the hydraulic system is effectively treated by the feedback linearization control [35]. To deal with parametric uncertainties, the adaptive mechanism is integrated into the nonlinear control design which adapts the unknown parameters based on the projection mapping function [33, 36]. To increase the robustness of the adaptive control under unmodeled disturbance and uncertain model parameters, the adaptive robust control (ARC) is proposed for a single-rod hydraulic actuator which guarantees bounded tracking performance [37]. Furthermore, the applications of ARC are realized in current works relating to not only valve-controlled hydraulic systems, but also pump-controlled hydraulic systems [38], and pump and valves combined hydraulic systems [39]. However, under the assumption that the unmodeled disturbance and its derivative are bounded, asymptotic tracking performance can be achieved by integrating a novel robust integral of the sign of the error (RISE) feedback in the adaptive backstepping control design [40]. To cancel or attenuate the effect of external disturbance on the system performance, disturbance, the DOB is proposed to estimate it with the assumption that its derivative is bounded [34, 41-43]. Compared to the adaptive mechanism, the disturbance estimation performance is completely guaranteed and does not depend on the tracking performance. However, in the above-mentioned works, the problems are limited in healthy working conditions, not faulty conditions, which not only severely influents the high-accuracy tracking performance, but also poses a threat to the system safety [44-47].

In the electrohydraulic system, there are many types of faults as actuator faults including internal leakage, external leakage, drop in supply pressure, and sensor faults including pressure sensor faults and position sensor faults [48, 49]. Among them, internal leakage fault is the most popular problem which has been widely considered in previous studies. In [50], a robust leakage detection algorithm has been proposed for the electrohydraulic actuators disturbed by model uncertainty and external disturbance by using an adaptive nonlinear observer and a decision-making mechanism. However, in this work, only a single actuator fault is considered with the fault detection problem. In [48], taking the advantage of the nonlinear unknown input observer (NUIO), model-based fault detection and isolation (FDI) scheme is proposed for a rudder servo system. Many types of faults are presented in this work including actuator faults and sensor faults with simulation and experimental validation. However, the simultaneous faulty conditions have not been investigated and the fault identification and FTC were not involved. In [51], an FTC design is proposed to effectively control a redundant hydraulic actuation system with internal leakage fault and force synchronization problem. However, in these studies, the problem of internal leakage fault is only considered for one-DOF system, which does not suffer from the nonlinear dynamics as the n-DOF mechanical system and limits the application of the proposed algorithm. To the best of authors' knowledge, the problem of internal leakage faults in n-DOF electrohydraulic servosystem has not been studied in previous works.

In a certain aspect, faults can be considered as parametric uncertainty or external disturbance that exceeds an allowable threshold [45, 52]. As a result, the approaches mentioned above to deal with modeling uncertainty and external disturbance can be utilized in the design of FTC [53]. Taking the advantage of these approaches, in recent years, some efforts are trying to integrate the DOB and adaptive mechanism into the control design to simultaneously handle external disturbance and unknown model parameters in a more effective way. In [54], Yao. et. al. proposed a backstepping control scheme using a combination of an extended state observer (ESO) and a parameter adaption with projection mapping for a double-rod hydraulic servo system where the adapted parameters are utilized in the design of the ESO. However, the approach seems not practical because the disturbance estimation error, which is unknown, is used in the design of the adaptive function to adapt the unknown model parameters. In contrast, in [55], Wang. et. al. proposed a nonlinear adaptive control with a novel ESO for estimating both matched and mismatched lumped disturbances and uncertainties for a hydraulic valve-controlled single-rod actuator system. Different from [54], the design of the proposed ESO only utilizes the nominal model parameters and the parameter adaption is adopted to update "virtual" nominal model parameters, which gives more freedom in the control design. However, there is no proof theory

to guarantee the convergence of the adapted parameters to the physical ones. Overall, merging the DOB and parameter adaption law is still an open problem [35].

In this paper, the problem of internal leakage faults in an n-DOF electrohydraulic servo system is studied for the first time by a novel active fault-tolerant control design system. In the normal control mode, the internal leakage fault detection is achieved based on a decision-making mechanism that compared the estimated matched disturbance from the ESO to a preset value. After the fault is detected, the controller is reconfigured, i.e., the ESO which is utilized to estimate the matched disturbance is turned off, and the online identification algorithm based on adaptive law is turned on to effectively estimate the internal leakage fault coefficient which is the dominant component compared to the matched disturbance due to the severity of its effects on the system performance. Based on this approach, merging the DOB and adaptive mechanism is achieved in this work to effectively take advantage of both techniques. Moreover, the proposed control scheme can handle not only single-fault conditions but also simultaneous-fault conditions and entirely decouple the faulty effect from a faulty actuator to the remaining actuators. To attenuate the effect of mismatched disturbances/uncertainties on the control system, another ESO is designed and integrated with the above-mentioned techniques in the backstepping framework. Based on the Lyapunov stability analysis, bounded tracking performance is guaranteed. To verify the effectiveness of the proposed FTC, numerical simulations are conducted using a 2-DOF hydraulic manipulator model. The simulation results show that the proposed approach achieves acceptable tracking performance under a bunch of faulty conditions and difficulties.

This paper is organized as follows. In Section II, a general mathematical model of the n-DOF hydraulic system is presented. The fault detection and FTC design are developed in Section III. Stability analysis is conducted in Section IV and numerical simulation is presented in Section V. Finally, section VI concludes this paper.
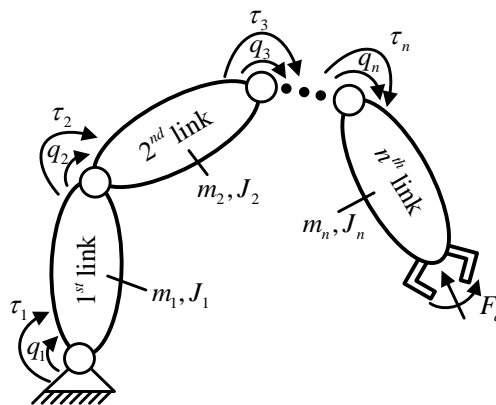
Fig. 3-1: Schematic diagram of an n-DOF manipulator

3.2. System dynamics
3.2.1.Mechanical system

The general structure of an n-DOF series-type manipulator is described in **Fig. 3-1**. The dynamics of the n-DOF manipulator is given by [56, 57]

$$M(q)\ddot{q} + C(q,\dot{q})\dot{q} + G(q) + \tau_d = \tau \tag{3.1}$$

where q is the joint displacement vector, $M(q) \in R^{n \times n}$ is the nominal inertia matrix which is symmetric positive-define, $C(q,\dot{q})\dot{q} \in R^n$ represents the nominal vector of centrifugal and Coriolis moments, $G(q) \in R^n$ is the nominal vector of gravity, $\tau_d \in R^n$ denotes the lumped disturbance and uncertainty in the mechanical system, and $\tau \in R^n$ is the actuator force/torque vector.

Assumption 1: The Coulomb friction is assumed to be differentiable, which is proportional to the function $\tanh(\bullet)$, instead of the signum function $\text{sgn}(\bullet)$, where $(\bullet)$ is the investigated velocity [57, 58].

Based on Assumption 1, the vector τ_d including parametric uncertainty, viscous friction, Coulomb friction, and external disturbance F_d is expressed as below

$$\begin{aligned} \tau_d &= \Delta M(q)\ddot{q} + \Delta C(q,\dot{q})\dot{q} + \Delta G(q) \\ &+ B_v \dot{q} + B_C \tanh(\dot{q}) - J^T F_d \end{aligned} \tag{3.2}$$

where ΔM, ΔC, and ΔG denotes uncertain matrices and vectors caused by model parameter uncertainties. B_v and B_C represent the unknown viscous and Coulomb friction matrices of the joints. The Jacobian matrix $J = \partial x_E / \partial q$ is defined based on the relation between end-effector position x_E and joint angles q.

The actuator force/torque τ is computed based on the force/torque generated by the hydraulic power as

$$\begin{aligned} \tau &= J_a^T(q)(F - F_a) \\ F_a &= D_v J_a(q)\dot{q} + D_C \tanh(J_a(q)\dot{q}) \end{aligned} \tag{3.3}$$

where D_v and D_C denote the viscous friction and Coulomb friction matrices of the actuator. The Jacobian matrix from manipulator space to actuator space $J_a = \partial c / \partial q$ is calculated based on the geometric relation between joint angles q and actuator displacements c.

From (3.1)-(3.3), the manipulator dynamics is re-written as

$$M(q)\ddot{q} + C(q,\dot{q})\dot{q} + G(q) + d = J_a^T(q)F \tag{3.4}$$

where $d = \tau_d + J_a^T(q)F_a$ represents lumped disturbance and uncertainty vector.
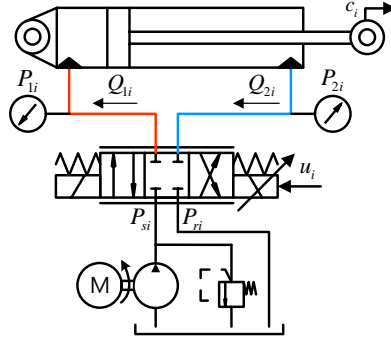
Fig. 3-2: A typical electrohydraulic actuation system

3.2.2. Hydraulic system

A typical electrohydraulic actuation system is described in Error! Reference source not found. i ncluding a 4-way-3-position servo valve and a hydraulic actuator which can be a cylinder or a rotary actuator. The force/torque generated by the ith hydraulic actuator as mentioned in (3.3) and (3.4) is computed by

$$F_i = A_{1i}P_{1i} - A_{2i}P_{2i} \tag{3.5}$$

where P_{1i} and P_{2i} are the pressures of both chambers. A_{1i} and A_{2i} denote the areas of both sides of the actuator.

The pressure dynamics of each actuator is given as [34]

$$\dot{P}_{1i} = \frac{\beta_e}{V_{1i}}\left(-A_{1i}J_{ai}\dot{q}_i - q_{Li} + Q_{1i}\right) + w_{1i}$$

$$\dot{P}_{2i} = \frac{\beta_e}{V_{2i}}\left(A_{2i}J_{ai}\dot{q}_i + q_{Li} - Q_{2i}\right) + w_{2i} \tag{3.6}$$

where $V_{1i} = V_{01i} + A_{1i}c_i, V_{2i} = V_{02i} - A_{2i}c_i$, are the volumes trapped in both chambers of the ith cylinder $(i = \overline{1,n})$ while V_{01i}, V_{02i} are the initial volumes. β_e denotes the nominal value of Bulk modulus. q_{Li}, Q_{1i}, Q_{2i}, and w_{1i}, w_{2i} denote the internal leakage flow rate, flow rates going to/from both chambers, and the modeling errors in the pressure dynamics of the ith actuator, respectively.

The internal leakage is modeled as follows:

$$q_{Li} = C_{0i}(P_{1i} - P_{2i}) + C_{ti}\sqrt{P_{1i} - P_{2i}}\,\text{sgn}(P_{1i} - P_{2i}) \qquad (3.7)$$

where C_{0i} is a known coefficient and C_{ti} is an unknown faulty coefficient. When C_{ti} is large enough, the internal leakage fault happens and seriously affects the system performance.

With the assumption that the spool dynamics is neglected, i.e., $x_{vi} = k_{ui}u_i$ where u_i is the control signal which is the voltage applied to the ith servo valve, the supplied flow rate to the 1st chamber and the return flow rate of the 2nd chamber are derived by

$$Q_{1i} = k_{qi}k_{ui}u_i[s^*(u_i)\sqrt{P_{si} - P_{1i}} + s^*(-u_i)\sqrt{P_{1i} - P_{ri}}]$$
$$Q_{2i} = k_{qi}k_{ui}u_i[s^*(u_i)\sqrt{P_{2i} - P_{ri}} + s^*(-u_i)\sqrt{P_{si} - P_{2i}}] \qquad (3.8)$$

where k_{qi} is the hydraulic coefficient depending on the discharge coefficient, spool valve area gradient, and the density of the oil. The function $s^*(x)$ is defined as

$$s^*(x) = \begin{cases} 1, & \text{if } x \geq 0 \\ 0, & \text{if } x < 0 \end{cases} \qquad (3.9)$$

3.2.3. Total system dynamics

To consider both the mechanical system and hydraulic system, a new state variable is defined as $x = [q^T, \dot{q}^T, (A_1 P_1 - A_2 P_2)^T]^T$. The total system model can be summarized as follows:

$$\begin{cases} \dot{x}_1 = x_2 \\ \dot{x}_2 = M(x_1)^{-1}(J_a(x_1)^T x_3 - C(x_1, x_2)x_2 - G(x_1) - d) \\ \dot{x}_3 = f_1(x_1)u - f_2(x_1, x_2) - f_3(x_1)C_t + f \end{cases} \qquad (3.10)$$

where $A_1 = \text{diag}(A_{11}, A_{12}, ... A_{1n})$, $A_2 = \text{diag}(A_{21}, A_{22}, ... A_{2n})$, $C_t = [C_{t1}, C_{t2}, ..., C_{tn}]^T$, $P_1 = [P_{11}, P_{12}, ..., P_{1n}]^T$, $P_2 = [P_{21}, P_{22}, ..., P_{2n}]^T$, $f_1 = \text{diag}(f_{11}, f_{12}, ..., f_{1n})$, $f_2 = [f_{21}, f_{22}, ..., f_{2n}]^T$, $f_3 = \text{diag}(f_{31}, f_{32}, ..., f_{3n})$, $f = \text{diag}(f_1, f_2, ..., f_n)$.

The detailed description of each element in the above matrices and vectors is given as

$$f_{1i} = \frac{A_{1i}\beta_e}{V_{1i}}k_{qi}k_{ui}R_{1i} + \frac{A_{2i}\beta_e}{V_{2i}}k_{qi}k_{ui}R_{2i}; f_{2i} = \frac{A_{1i}\beta_e}{V_{1i}}\left[A_{1i}J_{aii}x_{2i} + C_{0i}(P_{1i} - P_{2i})\right]$$

$$+ \frac{A_{2i}\beta_e}{V_{2i}}\left[A_{2i}J_{aii}x_{2i} + C_{0i}(P_{1i} - P_{2i})\right]$$

$$\qquad (3.11)$$

$$f_{3i} = \left(\frac{A_{1i}\beta_e}{V_{1i}} + \frac{A_{2i}\beta_e}{V_{2i}}\right)\sqrt{|P_{1i} - P_{2i}|}\,\text{sgn}(P_{1i} - P_{2i}); f_i = A_{1i}w_{1i} - A_{2i}w_{2i}$$

$$R_{1i} = s^*(u_i)\sqrt{P_{si} - P_{1i}} + s^*(-u_i)\sqrt{P_{1i} - P_{ri}}; R_{2i} = s^*(u_i)\sqrt{P_{2i} - P_{ri}} + s^*(-u_i)\sqrt{P_{si} - P_{2i}}$$

16

Assumption 2: x_1, P_1, P_2 are the outputs of the system which are measured by sensors. All system states, their 1st derivatives, and all elements in the matrices $M(x_1)$ and $J_a(x_1)$ are bounded.

Assumption 3: The following Lipschitz conditions hold

$$| f_{2i}(x_{1i}, x_{2i} + \Delta x_{2i}) - f_{2i}(x_{1i}, x_{2i}) | \leq \kappa_i |\Delta x_{2i}|$$
$$\| C(x_1, x_2 + \Delta x_2)(x_2 + \Delta x_2) - C(x_1, x_2)x_2 \| \leq \kappa \|\Delta x_2\|$$
(3.12)

where κ_i and κ are positive constants.

Assumption 4: The lumped disturbance/uncertainty term f is bounded, i.e., $| f_i | \leq \Delta_i^f$ where Δ_i^f is a constant.

Remark 1: Based on assumption 1, the derivative of x_1, i.e., x_2, and the derivative of the load pressure $\dot{x}_3$ are calculated based on the well-known Levant's exact differentiator with a very small bounded calculation error [59]. The differential quantity $(\bullet)$ computed by Levant's differentiator is denoted by $\overline{(\bullet)}$. For the sake of condense, the derivation of it is omitted in this work.

3.3. Proposed observer-based control algorithm

The proposed FTC scheme is described in Error! Reference source not found. including the mismatched DOB, matched DOB, online identification, fault detection, and control reconfiguration mechanism. A full state feedback backstepping control is the main controller to guarantee the position tracking performance of the n-DOF hydraulic system under both healthy conditions and faulty conditions.

Lemma 1: Consider a time-varying positive quantity $X(t)$. One concludes that $X(t)$ will stay in a bounded region that $X(t) \leq b/a$ when $t \rightarrow \infty$ if there exist positive constants a and b that satisfies

$$\dot{X} \leq -aX + b$$
(3.13)

Proof: Multiplying both sides of (3.13) by e^{at} and taking the integral of them, one obtains

$$X(t) \leq \left(X(0) - \frac{b}{a} \right) e^{-at} + \frac{b}{a}$$
(3.14)

Because $\lim_{t \rightarrow \infty} e^{-at} = 0$, Lemma 1 is proved.
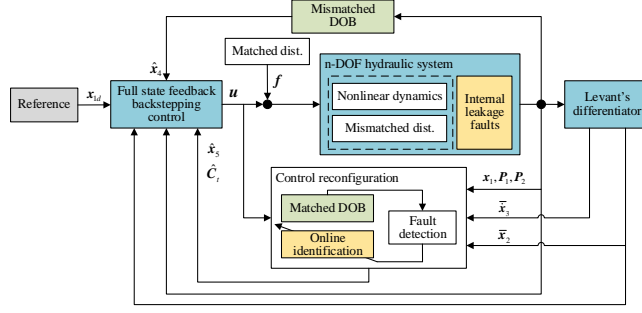
Fig. 3-3: Proposed active FTC scheme

3.3.1. Disturbance observer design

To design the matched DOB and mismatched DOB, the extended-state mechanism is adopted to generate 2 augmented state-space equations as follows:

$$\begin{cases} \dot{\boldsymbol{x}}_1 = \boldsymbol{x}_2 \\ \dot{\boldsymbol{x}}_2 = \boldsymbol{M}(\boldsymbol{x}_1)^{-1}(\boldsymbol{J}_a(\boldsymbol{x}_1)^T \boldsymbol{x}_3 \\ \qquad - \boldsymbol{C}(\boldsymbol{x}_1, \boldsymbol{x}_2)\boldsymbol{x}_2 - \boldsymbol{G}(\boldsymbol{x}_1)) + \boldsymbol{x}_4 \\ \dot{\boldsymbol{x}}_4 = \boldsymbol{h}_1 \end{cases} \qquad (3.15)$$

$$\begin{cases} \dot{\boldsymbol{x}}_3 = \boldsymbol{f}_1(\boldsymbol{x}_1)\boldsymbol{u} - \boldsymbol{f}_2(\boldsymbol{x}_1, \boldsymbol{x}_2) + \boldsymbol{x}_5 \\ \dot{\boldsymbol{x}}_5 = \boldsymbol{h}_2 \end{cases} \qquad (3.16)$$

where $\boldsymbol{x}_4 = -\boldsymbol{M}(\boldsymbol{x}_1)^{-1}\boldsymbol{d}; \boldsymbol{x}_5 = \boldsymbol{f} - \boldsymbol{f}_3\boldsymbol{C}_t$.

Assumption 5: The derivatives of lumped disturbances are bounded, i.e., $\|\boldsymbol{h}_1\| \le \delta_1, \|\boldsymbol{h}_2\| \le \delta_2$ where δ_1 and δ_2 are positive constants.

To simplify the design of mismatched disturbance observer for the system (3.15), the state equation is re-written as

$$\begin{cases} \dot{\boldsymbol{x}}_{e1} = \boldsymbol{A}_{e1}\boldsymbol{x}_{e1} + \boldsymbol{F}_{e1}(\boldsymbol{x}_1, \boldsymbol{x}_2, \boldsymbol{x}_3) + \boldsymbol{\varPsi}_{e1} \\ \boldsymbol{y}_{e1} = \boldsymbol{C}_{e1}\boldsymbol{x}_{e1} \end{cases} \qquad (3.17)$$

where

$$\boldsymbol{A}_{e1} = \begin{bmatrix} 0_{n\times n} & \boldsymbol{I}_n & 0_{n\times n} \\ 0_{n\times n} & 0_{n\times n} & \boldsymbol{I}_n \\ 0_{n\times n} & 0_{n\times n} & 0_{n\times n} \end{bmatrix}; \boldsymbol{\varPsi}_{e1} = \begin{bmatrix} 0_{n\times 1} \\ 0_{n\times 1} \\ \boldsymbol{h}_1 \end{bmatrix}; \boldsymbol{F}_{e1} = \begin{bmatrix} 0_{n\times 1} \\ \boldsymbol{M}(\boldsymbol{x}_1)^{-1}(\boldsymbol{J}_a(\boldsymbol{x}_1)^T \boldsymbol{x}_3 - \boldsymbol{C}(\boldsymbol{x}_1, \boldsymbol{x}_2)\boldsymbol{x}_2 - \boldsymbol{G}(\boldsymbol{x}_1)) \\ 0_{n\times 1} \end{bmatrix};$$

$$\boldsymbol{C}_{e1} = \begin{bmatrix} \boldsymbol{I}_n & 0_{n\times n} & 0_{n\times n} \end{bmatrix}; \boldsymbol{x}_{e1} = [\boldsymbol{x}_1^T, \boldsymbol{x}_2^T, \boldsymbol{x}_4^T]^T$$
(3.18)

The mismatched disturbance observer is designed as follows:

18

$$\dot{\hat{x}}_{e1} = A_{e1}\hat{x}_{e1} + F_{e1}(x_1, \bar{x}_2, x_3) + L_{e1}(y_{e1} - \hat{y}_{e1})$$
$$\hat{y}_{e1} = C_{e1}\hat{x}_{e1}$$

(3.19)

where $L_{e1} = [3\omega_{e1}I_n, 3\omega_{e1}^2 I_n, \omega_{e1}^3 I_n]^T$ is the observer gain, ω_{e1} is the bandwidth of the disturbance observer.

Theorem 1: For the system (3.17), the disturbance observer (3.19) guarantees a small bounded estimation performance of the mismatched disturbance x_4 if the bandwidth of the observer ω_{e1} is chosen with a large enough value.

Proof: See Section 2.3.

Similarly, to design a matched disturbance observer for the system (3.16), the state equation is re-written as

$$\begin{cases} \dot{x}_{e2} = A_{e2}x_{e2} + F_{e2}(x_1, x_2) + B_{e2}(x_1)u + \Psi_{e2} \\ y_{e2} = C_{e2}x_{e2} \end{cases}$$

(3.20)

where

$$A_{e2} = \begin{bmatrix} 0_{n\times n} & I_n \\ 0_{n\times n} & 0_{n\times n} \end{bmatrix}; F_{e2} = \begin{bmatrix} -f_2(x_1, x_2) \\ 0_{n\times 1} \end{bmatrix}; B_{e2} = \begin{bmatrix} f_1(x_1) \\ 0_{n\times n} \end{bmatrix}$$

$$\Psi_{e2} = \begin{bmatrix} 0_{n\times 1} \\ h_2 \end{bmatrix}; C_{e2} = \begin{bmatrix} I_n & 0_{n\times n} \end{bmatrix}; x_{e1} = [x_3^T, x_5^T]^T$$

(3.21)

A matched disturbance observer is designed by

$$\dot{\hat{x}}_{e2} = A_{e2}\hat{x}_{e2} + F_{e2}(x_1, \bar{x}_2) + B_{e2}(x_1)u + L_{e2}(y_{e2} - \hat{y}_{e2})$$
$$\hat{y}_{e2} = C_{e2}\hat{x}_{e2}$$

(3.22)

where $L_{e2} = [2\omega_{e2}I_n, \omega_{e2}^2 I_n]^T$ is the observer gain, ω_{e2} is the observer bandwidth.

Theorem 2: For the system (3.20), the disturbance observer (3.22) guarantees a small bounded estimation performance of the matched disturbance x_5 if the observer bandwidth ω_{e2} is chosen with a large enough value.

Proof: Similar to Proof of Theorem 1.

3.3.2. Online-fault identification

In this section, the online-fault identification algorithm is proposed based on the adaptive mechanism with the linear regression [60]. However, instead of estimating both the internal

leakage fault coefficients and the remaining unstructured uncertainty term, only the internal leakage fault coefficients are considered to simplify the algorithm but still achieve the identification performance.

Considering the 3rd equation of the system dynamics (3.10), one obtains the corresponding model as follows:

$$z = f_1(x_1)u - f_2(x_1, x_2) - f_3(x_1)C_t + f \tag{3.23}$$

where $z = \bar{\dot{x}}_3$.

The prediction model is designed by

$$\hat{z} = f_1(x_1)u - f_2(x_1, \bar{x}_2) - f_3(x_1)\hat{C}_t \tag{3.24}$$

Denote the prediction error $\tilde{z} = z - \hat{z}$. The online identification for internal leakage fault based on adaptive law is proposed as

$$\dot{\hat{C}}_t = -\Gamma f_3^T \tilde{z} \tag{3.25}$$

where Γ is a diagonal positive-definite matrix, which denotes the gain of the online identification algorithm.

Theorem 3: The bounded estimation performance $\tilde{C}_t = C_t - \hat{C}_t$ can be obtained if the persistently exciting condition is satisfied, i.e.,

$$\forall t, \exists \alpha_0, \Delta t > 0 : \int_t^{t+\Delta t} f_3^T f_3 \geq \alpha_0 I_n \Delta t \tag{3.26}$$

Proof: Substituting (3.23), (3.24) into (3.25), one obtains

$$\dot{\tilde{C}}_t = -\Gamma f_3^T f_3 \tilde{C}_t - \Gamma f_3^T (\tilde{f}_2 - f) \tag{3.27}$$

Applying the theory of time-varying linear system with noting that $\Gamma f_3^T f_3$ is a diagonal matrix, the solution is given as

$$\tilde{C}_t(t) = \tilde{C}_t(0)\Phi(t,0) + \int_0^t \Phi(t,\tau)\Gamma f_3^T(\tilde{f}_2 - f)d\tau \tag{3.28}$$

where $\Phi(t,\tau) = \exp\left(-\int_\tau^t \Gamma f_3^T f_3 d\omega\right)$.

When the persistently exciting condition (3.26) is satisfied, it is easy to state that $\tilde{C}_t(0)\boldsymbol{\Phi}(t,0) \to 0$ when $t \to \infty$. The speed of this convergence depends on the value of $\boldsymbol{\Gamma}$. Thus, to prove Theorem 3, the second term on the right-hand side of (3.28) needs to be bounded.

Based on (3.26), the following inequality holds

$$\boldsymbol{\Phi}(t,\tau) \le \exp\left(-(t-\tau)\alpha_0 \boldsymbol{I}_n\right) \tag{3.29}$$

Due to Assumptions 1, 2, and 3, there exists a constant $\delta_C > 0$ that satisfies

$$\left|\boldsymbol{\Gamma} f_3^T (\tilde{f}_2 - f)\right| \le \delta_C \tag{3.30}$$

From (3.29), (3.30), one obtains

$$\int_0^t \boldsymbol{\Phi}(t,\tau)\boldsymbol{\Gamma} f_3^T(\tilde{f}_2 - f)d\tau \le \int_0^t \boldsymbol{\Phi}(t,\tau)\left|\boldsymbol{\Gamma} f_3^T(\tilde{f}_2 - f)\right|d\tau$$
$$\le \int_0^t \delta_C \exp\left(-(t-\tau)\alpha_0 \boldsymbol{I}_n\right)d\tau = \frac{\delta_C}{\alpha_0}\left(1 - \exp(-t\alpha_0 \boldsymbol{I}_n)\right) \le \frac{\delta_C}{\alpha_0} \tag{3.31}$$

From (3.28), (3.31), it can be concluded that $\tilde{C}_t(t) \to \tilde{C}_t(\infty) \le \delta_C / \alpha_0$.

Even in the case that the persistently exciting condition (3.26) does not satisfy, i.e., $P_{1i} = P_{2i}$, from (3.27), one obtains

$$\dot{\tilde{C}}_{ti} = 0$$
$$\dot{\tilde{C}}_{tj} = -\boldsymbol{\Gamma}_j f_{3j}^T f_{3j} - \boldsymbol{\Gamma}_j f_{3j}^T(\tilde{f}_{2j} - f_j) \quad (j \ne i). \tag{3.32}$$

When these situations occur, the identification does not work at i^{th} actuator but works well at the remaining actuators. However, these specific conditions happen intermittently at a single moment, when the actuation force direction is changed, not in a period. Hence, the persistently exciting condition holds most of the time and the identification performance is not affected at all.

Remark 2: Different than most of the previous works using the adaptive mechanism to obtain the position tracking performance, the online identification law (3.25) guarantees bounded estimation performance and does not depend on the tracking error between system states and their desired values.

3.3.3. Control design

A switching term $s = \text{diag}(s_1, s_2, ..., s_n)$ is introduced here for fault detection based on the matched disturbance estimation values as follows:

$$s_i = \begin{cases} 0, & \text{if } |\hat{x}_{5i}| < \rho_i \\ 1, & \text{if } |\hat{x}_{5i}| \geq \rho_i \end{cases} \tag{3.33}$$

where ρ_i is a pre-defined threshold.

Remark 3: The switching term (3.33) is not only used for fault detection but also used to activate the adaptive law (3.25) and deactivate the matched observer (3.22) when faults are detected. Furthermore, it is well integrated into the fault-tolerant control design in the following steps.

Step 1: Define the position tracking error $z_1 = x_1 - x_d$ where x_d is a reference trajectory. Considering the first equation of (3.10), the derivative of z_1 becomes

$$\dot{z}_1 = x_2 - \dot{x}_d \tag{3.34}$$

To obtain asymptotically tracking performance of z_1, a virtual control law of x_2 is designed as follows:

$$\alpha_1 = \dot{x}_d - k_1 z_1 \tag{3.35}$$

where k_1 is a positive constant.

Step 2: Define the error between x_2 and the virtual control law α_1 by $z_2 = x_2 - \alpha_1$. From the second equation of (3.10), the derivative of z_2 is expressed as

$$\begin{aligned} \dot{z}_2 = M(x_1)^{-1}(J_a(x_1)^T x_3 - C(x_1, x_2)x_2 \\ -G(x_1) - d) - \dot{\alpha}_1 \end{aligned} \tag{3.36}$$

From (3.36), the virtual control law of x_3 is designed as

$$\begin{aligned} \alpha_2 = J_a(x_1)^{-T}(C(x_1, \bar{x}_2)\bar{x}_2 + G(x_1) \\ + M(x_1)(\dot{\alpha}_1 - z_1 - k_2 z_2 - \hat{x}_4)) \end{aligned} \tag{3.37}$$

where k_2 is a positive constant.

Step 3: Denote $z_3 = x_3 - \alpha_2$. From the third equation of the total system (3.10), the derivative of it is calculated by

$$\dot{z}_3 = f_1(x_1)u - f_2(x_1, x_2) - f_3(x_1)C_t + f - \dot{\alpha}_2 \tag{3.38}$$

Hence, the control signal is proposed by

22

$$u = \frac{1}{f_1}(f_2(x_1, \bar{x}_2) - (I_n - s)\hat{x}_5 + sf_3(x_1)\hat{C}_t$$
$$+ \dot{\alpha}_2 - J_a(x_1)M(x_1)^{-T}z_2 - k_3 z_3) \tag{3.39}$$

where k_3 is a positive constant.

3.4. Stability analysis

Theorem 4: For the system (3.10), by using the control signal (3.39) with mismatched disturbance observer (3.19), matched disturbance observer (3.22), adaptive law for fault identification (3.25) , and the fault detection (3.33), arbitrary bounded tracking performance is guaranteed under lumped disturbance/uncertainty and internal leakage faults.

Proof: Consider the following Lyapunov function

$$V = \frac{1}{2}z_1^T z_1 + \frac{1}{2}z_2^T z_2 + \frac{1}{2}z_3^T z_3 \tag{3.40}$$

Taking the derivative of it, one obtains

$$\begin{aligned} \dot{V} = {}& z_1^T(z_2 + \alpha_1 - \dot{x}_d) + z_2^T(M(x_1)^{-1}(J_a(x_1)^T(z_3 + \alpha_2) \\ & - C(x_1, x_2)x_2 - G(x_1)) + x_4 - \dot{\alpha}_1) \\ & + z_3^T(f_1 u - f_2 + (I_n - s)x_5 - sf_3 C_t + sf - \dot{\alpha}_2) \end{aligned} \tag{3.41}$$

Substituting control signals (3.35), (3.37), (3.39) into (3.41), the equation becomes

$$\begin{aligned} \dot{V} = {}& -k_1 z_1^T z_1 - k_2 z_2^T z_2 - k_3 z_3^T z_3 + z_2^T \tilde{x}_4 \\ & + z_2^T M(x_1)^{-1} J_a(x_1)^T(C(x_1, \bar{x}_2)\bar{x}_2 - C(x_1, x_2)x_2) \\ & - z_3^T(I_n - s)\tilde{x}_5 + z_3^T s(f + f_3 \tilde{C}_t) \\ & - z_3^T(f_2(x_1, x_2) - f_2(x_1, \bar{x}_2)) \end{aligned} \tag{3.42}$$

Applying Young's inequality, the following inequalities hold

$$z_2^T \tilde{x}_4 \le \frac{1}{2}z_2^T z_2 + \frac{1}{2}\tilde{x}_4^T \tilde{x}_4$$

$$-z_2^T H^T Cx_2 \le \frac{1}{2}z_2^T z_2 + \frac{1}{2}Cx_2^T HH^T Cx_2$$

$$-z_3^T(I_n - s)\tilde{x}_5 \le \frac{1}{2}z_3^T z_3 + \frac{1}{2}\tilde{x}_5^T(I_n - s)^T(I_n - s)\tilde{x}_5$$

$$z_3{}^T s(f + f_3\tilde{C}_t) \le \frac{1}{2}z_3{}^T z_3 + \frac{1}{2}(f + f_3\tilde{C}_t)^T s^T s(f + f_3\tilde{C}_t)$$

$$-z_3{}^T \tilde{f}_2 \le \frac{1}{2}z_3{}^T z_3 + \frac{1}{2}\tilde{f}_2{}^T \tilde{f}_2$$

$$(3.43)$$

where $\boldsymbol{H} = \boldsymbol{M}(\boldsymbol{x}_1)^{-1}\boldsymbol{J}_a(\boldsymbol{x}_1)^T$, $\tilde{f}_2 = f_2(\boldsymbol{x}_1, \boldsymbol{x}_2) - f_2(\boldsymbol{x}_1, \bar{\boldsymbol{x}}_2)$, $\boldsymbol{Cx}_2 = \boldsymbol{C}(\boldsymbol{x}_1, \boldsymbol{x}_2)\boldsymbol{x}_2 - \boldsymbol{C}(\boldsymbol{x}_1, \bar{\boldsymbol{x}}_2)\bar{\boldsymbol{x}}_2$.

From Theorem 1, 2, 3, Assumption 3, 4, and Remark 1, there exists a constant δ satisfying below inequality

$$\frac{1}{2}\tilde{\boldsymbol{x}}_4{}^T \tilde{\boldsymbol{x}}_4 + \frac{1}{2}\tilde{\boldsymbol{x}}_5{}^T (\boldsymbol{I}_n - s)^T (\boldsymbol{I}_n - s)\tilde{\boldsymbol{x}}_5$$

$$+ \frac{1}{2}(f + f_3\tilde{C}_t)^T s^T s(f + f_3\tilde{C}_t) + \frac{1}{2}\tilde{f}_2{}^T \tilde{f}_2$$

$$+ \frac{1}{2}\boldsymbol{Cx}_2{}^T \boldsymbol{HH}^T \boldsymbol{Cx}_2 \le \delta$$

$$(3.44)$$

Substituting (3.43), (3.44) into (3.42), one obtains

$$\dot{V} \le -k_1 z_1{}^T z_1 - (k_2 - 1)z_2{}^T z_2 - \left(k_3 - \frac{3}{2}\right)z_3{}^T z_3 + \delta$$

$$\le -\lambda V + \delta$$

$$(3.45)$$

where $\lambda = \min(2k_1, 2k_2 - 2, 2k_3 - 3)$.

By using Lemma 1, with large enough control parameters k_1, k_2, and k_3 to make $\lambda > 0$, when $t \to \infty$, $V_3(t)$ will enter a region that $V_3(t) \le \delta / \lambda$ and Theorem 4 is proved.

Remark 4: Theoretically, the arbitrary bounded error can be achieved in both disturbance observer performance, adaptive fault identification performance, and tracking performance with large enough gains. However, the effect of sampling time is not considered here, which prevents the application of the high-gain observer, identifier, and controller in the real system. In other words, there is a trade-off between tracking/estimating performance and system stability.

3.5. Numerical simulation

In this section, the HyQ leg prototype developed by the University of Genoa, Italy, and the Italian Institute of Technology (IIT) is utilized to verify the effectiveness of the proposed FTC. The original model includes 2 hydraulic cylinders to actuate the hip flexion/extension (hip f/e) and the knee flexion/extension (knee f/e), and 1 electric motor to actuate the hip

abduction/adduction (hip a/a). However, to be simple, the hip a/a joint is neglected here. The diagram of the reduced HyQ leg model is described in **Fig. 3-4**. More details about testbench configuration can be found in [61, 62].

3.5.1. Simulation setup

To verify the performance of the proposed FTC, simulation results are conducted based on the 2-DOF hydraulic manipulator model as mentioned above. Parameters for the simulation are given in **Table 3-1** and **Table 3-2**. Numerous model geometric parameters that are used to compute the kinematic problem are omitted here for simplicity, which can be found in [62].
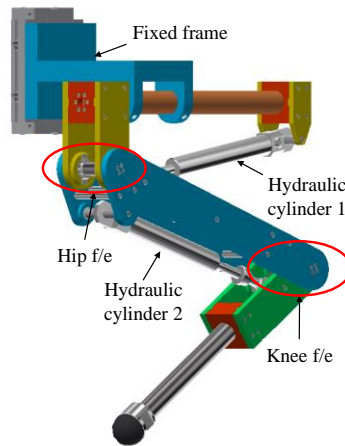
Fig. 3-4: Diagram of the reduced HyQ leg prototype.

Table 3-1: Mechanical parameters

Symbol	Quantity	Value
m_1	Mass of link 1	1.77 kg
m_2	Mass of link 2	1.48 kg
J_{C1}	Inertia moment of link 1	0.0704 kgm^2
J_{C2}	Inertia moment of link 2	0.0486 kgm^2
l_1	Length of link 1	0.35 m
l_2	Length of link 2	0.35 m
b_{C1}	Coulomb friction of link 1	1 Nm
b_{C2}	Coulomb friction of link 2	1 Nm
b_{v1}	Viscous friction of link 1	10 Nm/(rad/s)
b_{v2}	Viscous friction of link 2	10 Nm/(rad/s)

Table 3-2: Hydraulic parameters

Symbol	Quantity	Value
D	Bore diameter	0.016 m
d	Rod diameter	0.01 m
L	Stroke	0.08 m
A_1	Bore area	2.01 cm^2
A_2	Annulus area	1.23 cm^2
V_{01}	Initial volume of chamber 1	9.65 cm^3
V_{02}	Initial volume of chamber 2	5.88 cm^3
C_0	Nominal internal leakage coefficient	10^{-15}
k_u	Proportional gain of the valve	3×10^{-6} m/V
k_q	Hydraulic coefficient	4.65×10^{-4}
β_e	Bulk modulus	1.25 GPa
P_s	Supply pressure	160 bar
P_r	Return pressure	3 bar
d_{c1}	Coulomb friction of cylinder 1	5 N
d_{C2}	Coulomb friction of cylinder 2	5 N
d_{v1}	Viscous friction of cylinder 1	50 Ns/m
d_{v2}	Viscous friction of cylinder 2	50 Ns/m

The reference trajectory is chosen in a sinusoidal form as follows:

$$q_{1d} = -0.2 + 0.5\sin(4\pi t/3)\,(\text{rad})$$
$$q_{2d} = 1.4 + 0.5\sin(4\pi t/3)\,(\text{rad})$$

The mismatched disturbance includes unknown viscous and Coulomb friction at the revolute joints and the hydraulic cylinders as shown in **Table 3-1** and **Table 3-2**, and the external load acting on the end effector is chosen as $\boldsymbol{F}_d = [10, -20]^T \ (1 - \exp(-t)) \ (\text{N})$.

The matched disturbance comes from unmodeled pressure dynamics, parameter deviations, and so on. Hence, in this simulation, the matched disturbance is considered as $f_i = 3.75\times10^7 \sin(2\pi t/3) + 1.25\times10^7 \sin(4\pi t/3) \ (i = \overline{1,2})$.

To simulate the internal leakage faults in a practical system, the unknown leakage fault coefficients are selected as the following slow-varying components:

$$C_{t1} = \begin{cases} 0 & \text{if } t < 15\text{s} \\ 1.5 \times 10^{-9}(1 - e^{-0.5(t-15)}) & \text{if } t \geq 15\text{s} \end{cases}$$

$$C_{t2} = \begin{cases} 0 & \text{if } t < 25\text{s} \\ 0.7 \times 10^{-9}(1 - e^{-0.5(t-25)}) & \text{if } t \geq 25\text{s} \end{cases}$$

Remark 4: In practice, the control signals generated by the controller are limited due to the physical limitation of hardware components. Hence, they are bounded as below

$$u_{sat} = sat(u) = \begin{cases} u_{max} & \text{if } u \geq u_{max} \\ u_{min} & \text{if } u \leq u_{min} \\ u & \text{otherwise} \end{cases} \tag{3.46}$$

where $u_{max} = 12\text{V}, u_{min} = -12\text{V}$.

The structure of the simulation is described in **Fig. 3-5**.
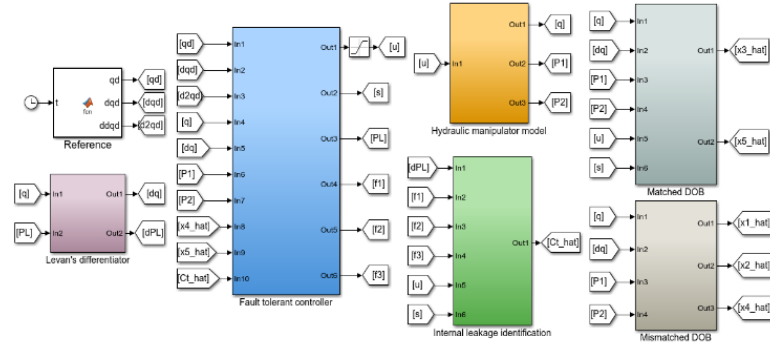
Fig. 3-5: Structure of the simulation in MATLAB Simulink.

3.5.2. Controllers for comparison

To evaluate the control performance of the proposed scheme for the hydraulic manipulator subjected to matched disturbance, mismatched disturbance, and severe internal leakage faults, the following three control algorithms are considered as follows:

1) Proposed control algorithm: The parameters of the proposed control algorithm are chosen as:

$$k_1 = 70, k_2 = 70, k_3 = 70,$$
$$\omega_{e1} = 150, \omega_{e2} = 100, \Gamma = 10^{-28}$$

2) Backstepping control with 2 disturbance observers (BC2): This type of approach has been widely applied in previous works for the position tracking control of the hydraulic system [51, 54, 56]. In this controller, the control parameters are similar to those of the proposed controller but the online identification for internal leakage fault is neglected.

3) Backstepping control with mismatched disturbance observer and online identification based on the adaptive mechanism for internal leakage faults (BCA): This control method is inspired by previous work [60]. The control parameters are similar to those of the proposed controller but the matched DOB is neglected.

To effectively evaluate the control performance of the above-mentioned controllers, besides the well-known root-mean-square error (RMSE), the maximum, average, and standard deviation of the tracking errors which are denoted as M_z, μ, and σ are utilized in this work [54].

3.5.3. Simulation results

The tracking performances of the proposed controller, BC2, and BSA are given in **Fig. 3-6**. Both controllers guarantee that the angular displacement at each joint follows its reference trajectory. However, in **Fig. 3-7**, the tracking error of each joint is clearly described which indicates that the proposed controller effectively takes advantage of both BC2 and BCA. During the period from 0s to 15s, i.e., before the faults occur, the tracking errors in both joints of the proposed controller and the BC2 are better than those of the BCA since the matched disturbance/uncertainty is the main problem. When the internal leakage faults occur at joint 1 and joint 2, the proposed controller switches from the BC2 to the BCA step-by-step. During this period, except for the transient response, the tracking performance of the proposed controller and the BCA is more accurate than it of the BC2 because the effects of the faulty conditions dominate the matched lumped disturbance effects in healthy conditions.

To quantitatively access the control performance of the comparative controllers in the steady-state phase, a similar simulation is conducted in 100s. The internal leakage faults in the 1st actuator and the 2nd actuator occur at 40s and 60s, respectively. The investigated periods include 30s in the steady-state phase of the healthy condition, i.e., from 10s to 40s, and 30s in the steady-state phase of the simultaneous faulty condition, i.e., from 70s to 100s. For the sake of simplicity, the steady-state phases of single internal leakage fault conditions are omitted here. The maximum, average, and standard deviation of the tracking errors are described in **Table 3-3**, **Table 3-4**, and **Table 3-5**, respectively. From these tables, it is obvious that the proposed

controller inherits the advantages of both the BC2 and BCA in healthy conditions and faulty conditions, respectively. Furthermore, the RMSEs of three controllers are presented in Table 3-6, which once again proves the effectiveness of the proposed controller compared to the remaining controllers.
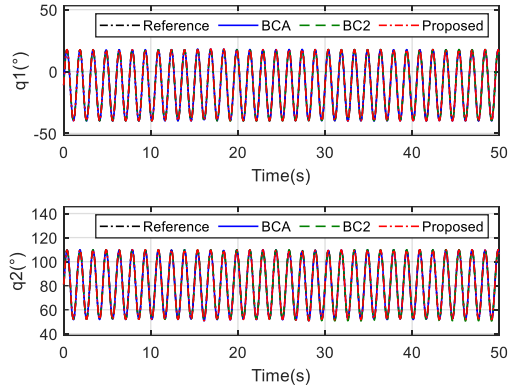
Fig. 3-6: Position tracking performances of comparative controllers
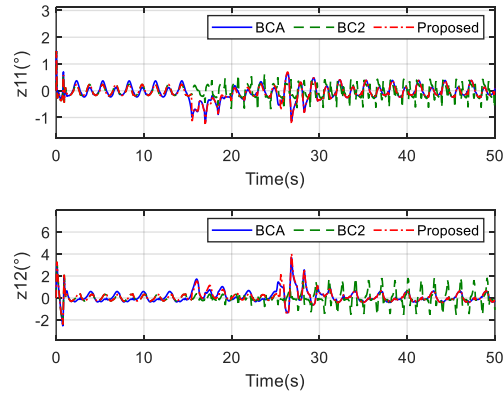
Fig. 3-7: Position tracking errors of comparative controllers

Table 3-3: Maximum of the tracking errors

Control strategies	Joint 1 (Deg)		Joint 2 (Deg)	
	Heathy	Faulty	Healthy	Faulty
Proposed control	0.2383	0.3877	0.3759	0.6513
BC2	0.2382	0.6270	0.3757	1.8136
BCA	0.3694	0.3876	0.5921	0.6515

Table 3-4: Average of the tracking erros

Control strategies	Joint 1 (Deg)		Joint 2 (Deg)	
	Heathy	Faulty	Healthy	Faulty
Proposed control	0.1343	0.1555	0.1948	0.2517
BC2	0.1342	0.2263	0.1954	0.5358
BCA	0.1453	0.1555	0.2455	0.2516

Table 3-5: Standard deviation of the tracking errors

Control strategies	Joint 1 (Deg)		Joint 2 (Deg)	
	Heathy	Faulty	Healthy	Faulty
Proposed control	0.0646	0.0945	0.1002	0.1752
BC2	0.0646	0.1191	0.1004	0.5014
BCA	0.0938	0.0945	0.1580	0.1752

Table 3-6: RMSE of the tracking errors

Control strategies	Joint 1 (Deg)		Joint 2 (Deg)	
	Heathy	Faulty	Healthy	Faulty
Proposed control	0.1490	0.1820	0.2191	0.3066
BC2	0.1490	0.2557	0.2196	0.7338
BCA	0.1729	0.1820	0.2920	0.3066

The fault detection signals are shown in **Fig. 3-8** based on the proposed decision-making mechanism (3.33). Compared to the identification performance described in **Fig. 3-9**, it is obvious that the fault detection law effectively detects the faults in a very short time. After that, the online adaptive identification algorithm (3.25) successfully identifies the magnitude and shape of the fault as shown in **Fig. 3-9**. The identification errors between the estimated values and the true values are generated by the matched lumped disturbance/uncertainty components and the imperfection when the faults are assumed to be slow-varying.
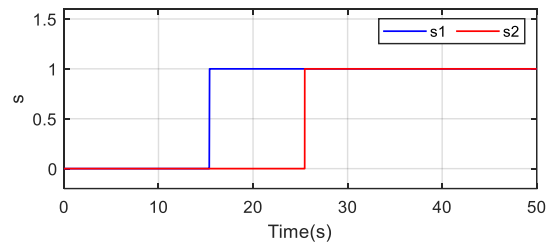
Fig. 3-8: Fault detection performance
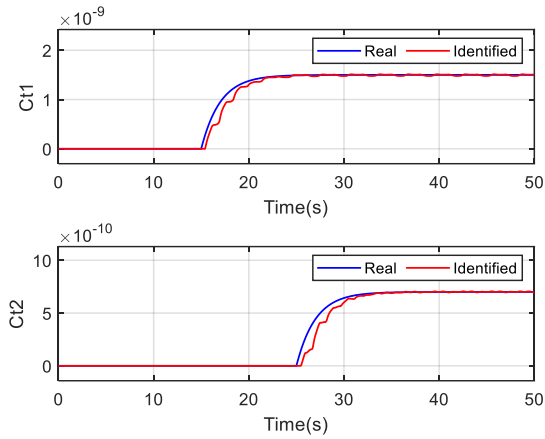
Fig. 3-9: Internal leakage fault identification performance

When the proposed controller is applied, the estimation performance of the mismatched disturbance observer is shown in **Fig. 3-10**. The mismatched lumped disturbance/uncertainty term caused by the external force, unknown viscous friction, and unknown Coulomb friction acting at both rotating joints and hydraulic actuators are effectively estimated by the mismatched DOB (3.19). An interesting point can be observed that the mismatched disturbance is not affected by the internal leakage faults and matched disturbance in the hydraulic actuation system. It is reasonable because, in the design of the mismatched DOB (3.19), the load pressure is computed based on measured pressure signals, and supplied to the DOB, which isolates the problems in the hydraulic system from the mechanical system.
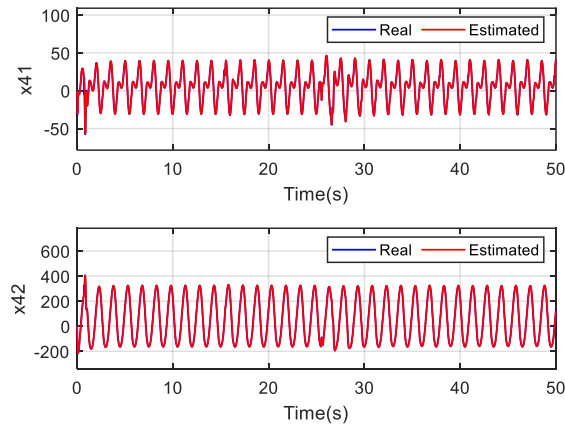
Fig. 3-10: Mismatched lumped disturbance/uncertainty estimation performance

In **Fig. 3-11**, when the proposed controller is applied, the matched disturbance terms in both joints are well estimated compared to the real term based on the matched DOB (3.22), even after the faults occur. At that time, although the lumped term is caused by both disturbance/uncertainty in healthy condition and internal leakage faults, the control performance of the BC2 is worse than it of the BCA and the proposed controller as mentioned

31

before. Note that in the proposed controller, after the faults are detected, the matched DOB can be shut down. The estimation performance after that is shown in **Fig. 3-11** is only used to check the effectiveness of it under faulty conditions.
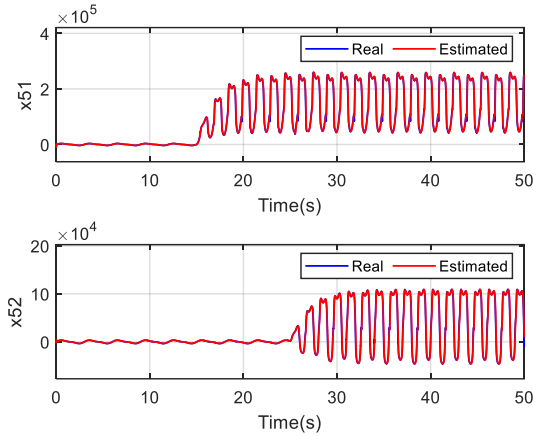
Fig. 3-11: Matched lumped disturbance/uncertainty estimation performance

To evaluate the effect of faulty conditions on the hydraulic actuation system when the proposed control method is applied, the pressures of both chambers in actuator 1 and actuator 2 are shown in **Fig. 3-12** and **Fig. 3-13**, respectively. In **Fig. 3-12**, after the internal leakage fault occurs, the pressure of both chambers consequently changes. A similar situation is realized with the internal leakage fault in actuator 2, which is described in **Fig. 3-13**. An interesting point that can be observed in these figures is that the faulty condition of an actuator does not affect the performance of the remaining actuator. This separation is achieved based on the compensation of mismatched DOB, matched DOB, the online adaptive identification, and the switching action of the fault detection law.
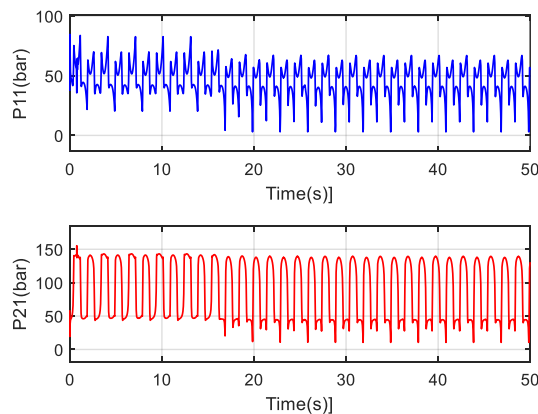
Fig. 3-12: Pressures of both chambers in cylinder 1
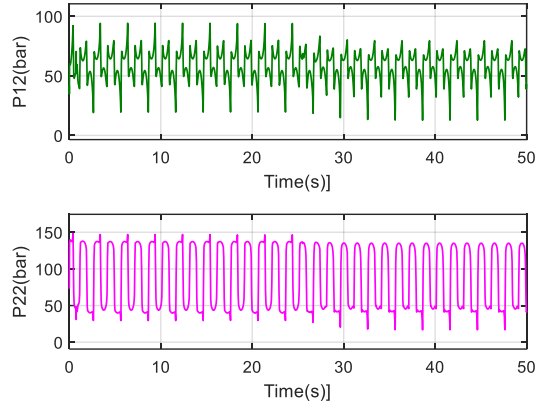
Fig. 3-13: Pressure of both chambers in cylinder 2

Finally, the control signals of both controllers are presented in **Fig. 3-14**. One can observe that when the faults occur, the magnitude of the control signal increases. This situation is reasonable because when the internal leakage fault appears in an actuator, the leakage flow rate going from the high-pressure chamber to the low-pressure chamber severely rises, which reduces the load pressure and the actuator efficiency. Therefore, the control signals need to increase to compensate for the loss of effectiveness in actuators.
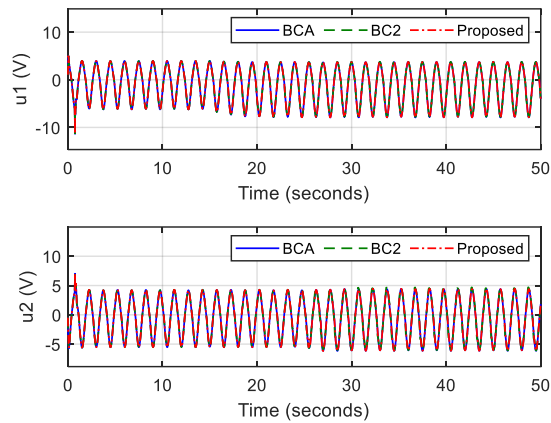
Fig. 3-14: Control signals of comparative controllers

3.6. Discussion

This paper proposes an active FTC system design for a hydraulic manipulator with internal leakage faults and matched/mismatched disturbances. A novel fault detection law is proposed to detect the internal leakage fault that occurs in each joint based on the estimated matched disturbances from the matched DOB. After that, an online adaptive identification algorithm is implemented to estimate the internal leakage fault coefficients. Besides, a mismatched DOB is designed to deal with the mismatched disturbance term caused by an external force, uncertain parameters, unknown viscous friction, and unknown Coulomb friction. The proposed FTC is

designed based on the backstepping framework, which integrates the estimated values from DOBs and the identified fault information into the control system design. Thanks to the fault detection mechanism, the actuation performance of each joint is successfully decoupled from the total system, even under simultaneous faulty conditions. Moreover, the proposed controller takes the advantages of both DOBs, which are utilized to deal with disturbances, and the adaptive law, which is effective to handle the parametric uncertainty, in a unique framework. Simulation results show that compared to the BCA and BC2, the proposed controller presents the best tracking performance under both healthy conditions and simultaneous faulty conditions.

In future works, the following interesting problems shall be investigated in the active fault-tolerant control system design for hydraulic manipulator as

1) The transient response of the hydraulic manipulation system caused by the control reconfiguration action when the actuator fault occurs has not been considered in this work. Moreover, the transient response improvement has been studied in several works with different objects [63, 64], which motivates the study about similar problems in the hydraulic manipulators.

2) Other types of hydraulic actuator faults shall be researched in future works as the drop in pressure supply, valve proportional gain variation, etc. [48]. Moreover, depending on the structure of the hydraulic actuation system in the real applications including hydraulic actuators, hydraulic circuits, and hydraulic power source, not only the number of the actuator fault scenarios but also the effects of them on the entire system are very diverse but interesting to be investigated.

3) Besides the actuator faults, the sensor faults including position sensor faults and pressure sensor faults can pose a threat to the hydraulic manipulation control system. However, the effects of sensor faults on the hydraulic manipulator have not been considered in previous works. A few studies have focused on the sensor faults in hydraulic systems, but the degree of freedom is limited to one [65, 66]. Moreover, some studies have tried to solve the fault diagnosis problem in robot manipulators [67-69]. However, the actuator dynamics are neglected for simplicity.

4) Most of the current works focusing on the fault diagnosis and fault-tolerant control design for position tracking tasks. The effects of faulty conditions on the force control problems including direct force tracking control and indirect force control, i.e., impedance control, have not received much attention.

Chapter 4
APPLICATION TO ADMITTANCE CONTROL PROBLEM OF HYDRAULIC MANIPULATORS

4.1. Introduction

Due to the advantages of high-power-to-weight ratio and large force/torque output, electrohydraulic servomechanism is widely used in many industrial and/or military applications as robot manipulator [29, 70, 71], rolling mills [72], hydraulic press [73], construction machines [74-76], aircraft actuators [77, 78], active suspension [79, 80], etc. To complete tasks, control problems of the electrohydraulic actuator have been considered as position control [36, 42, 81] and force control [82-84]. However, for the robotic application, the position tracking performance cannot be achieved when the robot motion is constrained by a stiff environment. Similarly, when the robot is operated in free motions, it is impossible to guarantee that the contact force at the end effector tracks the desired one. To deal with these problems, hybrid force/position control is developed to separate the control target to position control task in some axes and force control in the remaining one [85]. However, free motions and constraint motions cannot be handled simultaneously in the same axis by this controller, and the feedforward term in the control design requires environment position information [86]. Thus, developing a control algorithm to handle the interaction force in both free motions and contact motions is challenging.

Another approach for solving this problem is the concept of impedance/admittance which is introduced by Hogan [87], where the relationship between contact force and motion is regulated to guarantee safe and compliant interaction. Impedance can be easily obtained by adding physical components like springs and dampers to the actuation system or the end-effector [88]. This is called passive impedance. However, this implementation is difficult when the space and mass are limited [89]. The other approach called active impedance or impedance control is widely utilized because the impedance behavior is achieved by controlling the joint torques/forces to mimic the desired impedance performance. The active impedance is developed in many aspects as joint-space control/operational space control where the impedance behavior is accounted for the joints or the end-effectors, respectively, and force-based/position-based impedance control where the trade-off between simplicity and freedom in desired impedance behavior is considered [89]. However, in the case of the admittance control, i.e., the position-based impedance control, contact force measurements are needed which requires the installation of a force sensor at the contact point [90]. This approach is not cost-effective and complicates the hardware design. To overcome

these drawbacks, the force-sensorless has been proposed which utilizes observer techniques to estimate the contact force [91, 92].

In recent years, several force observer techniques have been developed. The generalized momentum observer (GMO) was early developed to estimate the contact force based on the plant dynamic information and velocity measurement [93]. Since the velocity measurement is disturbed by noise, and the installment of the velocity sensor beside the position sensor requires more effort in hardware design and increases the total cost, the GMO performance is quite limited. In contrast, the extended-state observer (ESO), which is originally developed for a general problem with nonlinear systems [94], solves these problems by not only estimating the contact force but also observing the unmeasurable velocities [95]. Inheriting the same structure as the ESO, the ESMO is introduced by utilizing the signum function instead of proportional terms with output estimation error, which can quickly react to the sudden changes in disturbances and states during operation. The ESMO is widely applied in many systems such as the permanent-magnet synchronous motor (PMSM) [96-98], Markovian jump linear systems [99], descriptor stochastic systems [100], traction network [101], satellites autonomous navigation [102], electro-optical tracking system [103], etc. However, the application of ESMO in robotics has not been realized. Hence, in this paper, the ESMO is firstly adopted to deal with unmeasurable contact forces to build the admittance control for hydraulic robots.

Besides the contact force estimation, another concern is about the effects of actuator dynamics on hydraulic robot control systems. In [89], the pressure dynamics of the hydraulic cylinder have been considered in the system modeling of the HyQ leg test bench. The study proposed two control approaches for the force control loop. The first one was a linear controller based on a linearized model around the equilibrium point with velocity compensation. The second one was the feedback linearization control which is developed based on the original nonlinear system modeling. However, matched disturbances and uncertainties were not considered in this research. In [104], an electro-hydraulic torque actuator with a backdrivable servo-valve was proposed which provided fast response and torque-source property. However, to design the compliant controller, the actuator dynamics were simplified to simple rigid actuator dynamics. A similar problem was realized in [105] where an impedance control was developed on the same electro-hydraulic torque actuator with the GMO. Overall, nonlinearities and matched uncertainties, which always exist in hydraulic actuation system and has negative impacts on the control performance, have not been appropriately addressed in previous research. Thus, it is expected that considering these problems in the control design will improve the admittance control performance of hydraulic robot systems.

Inspired by these observations, an advanced admittance controller with an ESMO is firstly developed for hydraulic robots. The ESMO is firstly designed to not only estimate the interaction force with the environment but also observe the unmeasurable joint velocities. To attenuate the effect of unknown friction in hydraulic actuators on the interaction force estimation performance, load cells are mounted on the hydraulic actuators, which provides the actuation force information. Furthermore, uncertainties and disturbances in the pressure dynamics are considered and handled by a matched disturbance observer. Finally, all of these techniques are integrated into the backstepping control framework to effectively deal with both the mechanical and hydraulic nonlinearities. Based on the Lyapunov criteria, the entire system stability is guaranteed. To verify the effectiveness of the proposed control algorithm, numerical simulations are conducted based on the 2-DOF HyQ leg model. Simulation results show that the proposed control algorithm provides high accuracy admittance performance with different scenarios.

This paper is organized as follows. In Section II, the total system modeling of hydraulic robots is presented. The admittance control design with the ESMO is developed in Section III. Simulation results and discussion is described in Section IV. Finally, section V concludes this paper.

4.2. System dynamics

The total hydraulic robot system includes two subsystems as the mechanical system and the hydraulic system [106]. These subsystem models are presented in the following section:

4.2.1. Mechanical system modeling

The dynamics of the mechanical system is modeled as follows:

$$
\begin{aligned}
\dot{x}_1 &= x_2 \\
\dot{x}_2 &= M(x_1)^{-1}(J_a(x_1)^T F + J(x_1)^T F_c - V(x_1, x_2) - G(x_1) - \tau_d)
\end{aligned}
\tag{4.1}
$$

where $x_1 \in R^n$ is joint position vector; $x_2 \in R^n$ is joint velocity vector; $M(x_1) \in R^{n \times n}$, $V(x_1, x_2) \in R^n$, and $G(x_1) \in R^n$ are the inertia matrix, centrifugal and Coriolis vector, and gravity vector, respectively; $J(x_1) \in R^{n \times n}$ and $J_a(x_1) \in R^{n \times n}$ are the Jacobian matrices computed by differentiating the end-effector position $p \in R^n$ and actuator displacement $c \in R^n$ with respect to x_1, respectively; $F_c \in R^n$ is the vector of forces generated by the contact motion with the environment; $\tau_d \in R^n$ is the vector of mismatched uncertainties and disturbances in the robot dynamics; F is the actuation force vector measured by load cells, which is given by:

$$F = x_3 - F_a \tag{4.2}$$

where $F_a \in R^n$ is the vector of model uncertainties, i.e., unknown frictions, in hydraulic actuators, and x_3 is defined in the next section.

4.2.2. Hydraulic system modeling

The hydraulic system model is described as follows:

$$\dot{x}_3 = f_1(x_1)u - f_2(x_1, x_2, P_1, P_2) + f(t) \tag{4.3}$$

where $x_3 = A_1 P_1 - A_2 P_2$ is the hydraulic power force vector with $A_j \in R^{n \times n}$ and $P_j \in R^n (j = \overline{1, 2})$ are the area diagonal matrices and pressure vectors of both sides of actuators, respectively; $f(t) \in R^n$ is the vector of matched uncertainties and disturbances in pressure dynamics; $u \in R^n$ is the control signal vector. For convenience, the remaining terms are described in Appendix A.

The remaining functions in the hydraulic model (4.3) are defined as follows:

$$
\begin{aligned}
f_{1i} &= \frac{A_{1i}\beta_e}{V_{1i}} k_{ti} R_{1i} + \frac{A_{2i}\beta_e}{V_{2i}} k_{ti} R_{2i} \\
f_{2i} &= \frac{A_{1i}\beta_e}{V_{1i}} \left[A_{1i} J_{aii} x_{2i} + C_{0i}(P_{1i} - P_{2i}) \right] \\
&\quad + \frac{A_{2i}\beta_e}{V_{2i}} \left[A_{2i} J_{aii} x_{2i} + C_{0i}(P_{1i} - P_{2i}) \right] \\
R_{1i} &= s(u_i)\sqrt{P_{si} - P_{1i}} + s(-u_i)\sqrt{P_{1i} - P_{ri}} \\
R_{2i} &= s(u_i)\sqrt{P_{2i} - P_{ri}} + s(-u_i)\sqrt{P_{si} - P_{2i}}
\end{aligned}
\tag{4.4}
$$

where k_{ti} are coefficients of servo valves; β_e is the Bulk modulus; V_{1i} and V_{2i} are chamber volumes of hydraulic actuators; P_{si} and P_{ri} are the supply pressure and tank pressure, respectively; C_{0i} is the nominal internal leakage coefficient; the subscript i denotes the order of the considered actuator. The function s is defined by

$$s(x) = \begin{cases} 1, & \text{if } x \geq 0 \\ 0, & \text{if } x < 0 \end{cases} \tag{4.5}$$

Assumption 1: x_1, P_1, P_2, and F are measured without considering measurement noises and bandwidth limitations.

Assumption 2: The following inequalities, i.e., Lipschitz conditions, hold during operation

$$
\begin{aligned}
& \mid f_{2i}(x_{1i}, x_{2i} + \Delta x_{2i}, P_{1i}, P_{2i}) \\
& \quad - f_{2i}(x_{1i}, x_{2i}, P_{1i}, P_{2i}) \mid \leq \kappa_i \left| \Delta x_{2i} \right| \\
& \left\| M(x_1)^{-1} [V(x_1, x_2 + \Delta x_2) - V(x_1, x_2)] \right\| \leq \kappa \left\| \Delta x_2 \right\|
\end{aligned}
\tag{4.6}
$$

where κ and κ_i are positive constants.
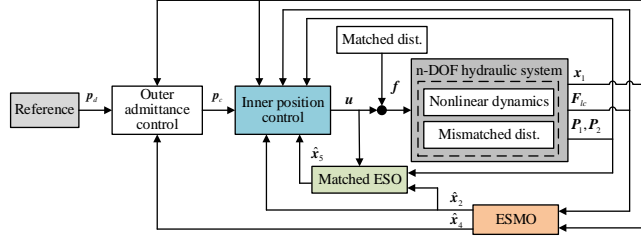
Fig. 4-1: Proposed admittance control scheme for hydraulic robots

4.3. Proposed observer-based control algorithm

The proposed admittance control structure is described in **Fig. 4-1**. The outer admittance control derives the desired end-effector position. Based on that, the inner position control loop calculates the desired actuation force. Finally, the force control loop receives it as a reference and computes the real control signals.

4.3.1. Extended sliding mode observer design

To design the ESMO, the extended-state mechanism is adopted for the mechanical system model (3.10) as follows:

$$
\begin{cases}
\dot{x}_1 = x_2 \\
\dot{x}_2 = F_1(x_1, x_2) + F_2(x_1)F + x_4 \\
\dot{x}_4 = h_1
\end{cases}
\tag{4.7}
$$

where $\quad F_1(x_1, x_2) = -M(x_1)^{-1}[V(x_1, x_2) + G(x_1)], \quad\quad F_2(x_1) = M(x_1)^{-1}J_a(x_1)^T, \quad$ and $x_4 = M(x_1)^{-1}(-\tau_d + J^T F_c)$.

Assumption 3: Derivative of the lumped disturbance term h_1 is bounded, i.e., $\left\| h_1 \right\| \leq \delta_1, \delta_1 > 0$.

Based on this assumption, the proposed ESMO is designed as follows:

$$
\begin{cases}
\dot{\hat{x}}_1 = \hat{x}_2 + v \\
\dot{\hat{x}}_2 = F_1(x_1, \hat{x}_2) + F_2(x_1)F + \hat{x}_4 + 2\omega_1 v \\
\dot{\hat{x}}_4 = \omega_1^2 v
\end{cases}
\tag{4.8}
$$

where $\mathbf{v} = \eta(\mathbf{x}_1 - \hat{\mathbf{x}}_1)/\|\mathbf{x}_1 - \hat{\mathbf{x}}_1\|$ if $\|\mathbf{x}_1 - \hat{\mathbf{x}}_1\| \neq 0$ and $\mathbf{v} = 0_{n \times 1}$ otherwise, η is a positive constant, and ω_1 denotes the bandwidth of the observer.

Theorem 1: For the system (4.7) with Assumption 3, the ESMO (4.8) guarantees arbitrarily bounded velocity and disturbance estimation errors, i.e., $\mathbf{x}_2 - \hat{\mathbf{x}}_2$ and $\mathbf{x}_4 - \hat{\mathbf{x}}_4$, if the bandwidth of the observer ω_1 is chosen with a large enough value.

Proof: See Section 2.4.

Remark 1: Because the estimated contact force is utilized in the outer admittance controller, the estimated value is expected to be chattering-free. Hence, to attenuate the chattering phenomenon, the switching action is modified as

$$\mathbf{v}_{\text{mod}} = \eta \frac{\mathbf{x}_1 - \hat{\mathbf{x}}_1}{\|\mathbf{x}_1 - \hat{\mathbf{x}}_1\| + \varepsilon} \tag{4.9}$$

where ε is a positive constant. When the position estimation error is large, the modified switching action is almost the same as the original one. However, when position estimation error is small, it behaves like a proportional term with a very high gain value.

4.3.2. Matched disturbance observer design

Considering the hydraulic system model (4.3), based on the extended state technique, this equation is rewritten as

$$\begin{aligned}\dot{\mathbf{x}}_3 &= \mathbf{f}_1(\mathbf{x}_1)\mathbf{u} - \mathbf{f}_2(\mathbf{x}_1, \mathbf{x}_2) + \mathbf{x}_5 \\ \dot{\mathbf{x}}_5 &= \mathbf{h}_2\end{aligned} \tag{4.10}$$

Assumption 4: Derivative of the lumped disturbance term $\mathbf{h}_2$ is bounded, i.e., $\|\mathbf{h}_2\| \leq \delta_2, \delta_2 > 0$.

Based on this augmented system, a matched disturbance observer is designed as [106]

$$\begin{aligned}\dot{\hat{\mathbf{x}}}_3 &= \mathbf{f}_1(\mathbf{x}_1)\mathbf{u} - \mathbf{f}_2(\mathbf{x}_1, \hat{\mathbf{x}}_2) + \hat{\mathbf{x}}_5 + 2\omega_2(\mathbf{x}_3 - \hat{\mathbf{x}}_3) \\ \dot{\hat{\mathbf{x}}}_5 &= \omega_2^2(\mathbf{x}_3 - \hat{\mathbf{x}}_3)\end{aligned} \tag{4.11}$$

Theorem 2: For the system (4.10) with Assumption 4, the matched disturbance observer (4.11) guarantees arbitrarily bounded disturbance estimation errors, i.e., $\mathbf{x}_5 - \hat{\mathbf{x}}_5$, if the observer bandwidth ω_2 is large enough.

Proof: Similar to Section 2.3.

4.3.3. Admittance control design

From (4.7), the contact force is estimated by

$$\hat{F}_c = J(x_1)^{-T} M(x_1)\hat{x}_4 \tag{4.12}$$

Based on that, the outer admittance loop is designed as

$$M_d\ddot{e}_d + B_d\dot{e}_d + K_d e_d = \hat{F}_c \tag{4.13}$$

where e_d is the desired error between the reference trajectory and the commanded trajectory which is the target for the physical end-effector position to follow to guarantee the desired admittance behavior of the system.

Remark 2: The contact force estimation (4.12) is disturbed by the lumped disturbances and uncertainties as shown in the definition of x_4. This problem is unavoidable since the contact force estimation performance always relies on the system model accuracy.

After solving (4.13), the commanded end-effector reference is computed as

$$p_c = p_d + e_d \tag{4.14}$$

where p_d is the reference trajectory of the end-effector.

Based on the commanded reference (4.14), the inner position control loop is designed in the backstepping framework as

$$
\begin{aligned}
\alpha_1 &= \dot{p}_c - k_1 z_1 \\
\alpha_2 &= -F + x_3 + J_a^{-T}\left\{ \begin{array}{l} -M[\hat{x}_4 + J^{-1}(\dot{J}(x_1,\hat{x}_2)\hat{x}_2 \\ +k_2 z_2 - \dot{\alpha}_1)] + \hat{V} + G \end{array} \right\} \\
u &= \frac{1}{f_1(x_1)}(f_2(x_1,\hat{x}_2) - \hat{x}_5 + \dot{\alpha}_2 - k_3 z_3)
\end{aligned}
\tag{4.15}
$$

where α_1 and α_2 are virtual control signals which guarantee the control performances in position and velocity loops, respectively; k_1, k_2, and k_3 are positive gains; $z_1 = p - p_c$, $z_2 = \dot{p} - \alpha_1$, and $z_3 = x_3 - \alpha_2$ are control errors.

Theorem 3: The admittance controller constructed by (4.12), (4.13), (4.14), and (4.15) together with the ESMO (4.8) and matched disturbance observer (4.10) guarantees the desired admittance behavior of the hydraulic robot, i.e., the error $p - p_c$ is arbitrarily bounded.

Proof: A Lyapunov function is selected as follows:

$$V = \frac{1}{2}z_1^T z_1 + \frac{1}{2}z_2^T z_2 + \frac{1}{2}z_3^T z_3 \tag{4.16}$$

Taking the derivative of it, one obtains:

$$\dot{V} = z_1^T(\dot{p} - \dot{p}_c) + z_2^T(\ddot{p} - \dot{\alpha}_1) + z_3^T(\dot{x}_3 - \dot{\alpha}_2) \tag{4.17}$$

From (3.10), (4.15), and (4.17), the derivative of the Lyapunov function is expressed as

$$\dot{V} = -k_1 z_1^T z_1 - k_2 z_2^T z_2 - k_3 z_3^T z_3 + z_1^T z_2$$
$$+ z_2^T J M^{-1} J_a^T z_3 + z_2^T \Phi_1 + z_3^T \Phi_2 \tag{4.18}$$

where $\Phi_1 = J(-M^{-1}\tilde{V} + \tilde{x}_4) + \dot{J}x_2$ and $\Phi_2 = -\tilde{f}_2 + \tilde{x}_5$.

Applying Young's inequality, one obtains:

$$\dot{V} \le -\lambda V + \delta \tag{4.19}$$

where

$$\lambda = \min\{2k_1 - 1, 2k_2 - 2 - \lambda_{\max}(JM^{-1}J^T)$$
$$, 2k_3 - 1 - \lambda_{\max}(J_a M^{-1} J_a^T)\} \tag{4.20}$$
$$\delta = \sup\left(\frac{1}{2}\Phi_1^T \Phi_1 + \frac{1}{2}\Phi_2^T \Phi_2\right)$$

From this, it is observed that when time goes to infinity, the Lyapunov function converges to a bounded area $V \le \delta/\lambda$. This boundary decreases when the control gains k_1, k_2, and k_3 increase. This completes the proof of Theorem 3.
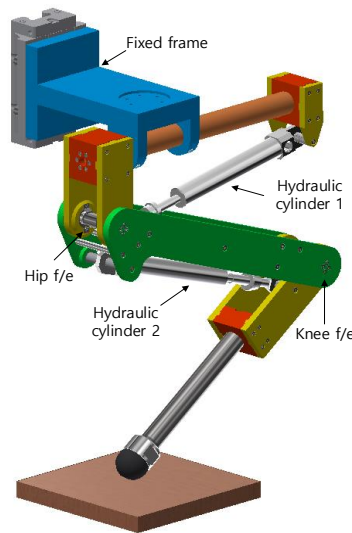
Fig. 4-2: Reduced HyQ leg prototype.

Table 4-1: Mechanical parameters

Symbol	Quantity	Value
m_1	Mass of link 1	1.77 kg
m_2	Mass of link 2	1.48 kg
J_{C1}	Inertia moment of link 1	$0.0704\,\text{kgm}^2$
J_{C2}	Inertia moment of link 2	$0.0486\,\text{kgm}^2$
l_1	Length of link 1	0.35 m
l_2	Length of link 2	0.35 m

Table 4-2: Hydraulic parameters

Symbol	Quantity	Value
D	Bore diameter	0.016 m
d	Rod diameter	0.01 m
L	Stroke	0.08 m
A_1	Bore area	$2.01\,\text{cm}^2$
A_2	Annulus area	$1.23\,\text{cm}^2$
V_{01}	Initial volume of chamber 1	$9.65\,\text{cm}^3$
V_{02}	Initial volume of chamber 2	$5.88\,\text{cm}^3$
C_0	Nominal internal leakage coefficient	10^{-15}
k_{ti}	Valve coefficient	1.395×10^{-4}
β_e	Bulk modulus	1.25 GPa
P_s	Supply pressure	160 bar
P_r	Return pressure	3 bar

4.4. Numerical simulation

In this section, the HyQ leg prototype is inherited to verify the effectiveness of the proposed admittance control algorithm [62]. The reduced model includes 2 hydraulic cylinders to actuate the hip flexion/extension (hip f/e) and the knee flexion/extension (knee f/e). The diagram of the reduced HyQ leg model is presented in **Fig. 4-2**.

4.4.1. Simulation setup

The geometric parameters of the leg model that are used to compute the kinematic problem are given in **Table 4-1** [62]. Hydraulic model parameters are inherited from previous work [106]

as shown in **Table 4-2**. The unknown friction force in hydraulic cylinders F_a is modeled as presented in the MATLAB Simscape Library [107].

To verify the effectiveness of the proposed admittance control algorithm, two case studies are investigated as follows:

- Case 1: Admittance response with a step contact force. The contact force is selected as $F_c = [10, -10]^T$ (N). It is applied to the end-effector of the robot from 5s to 15s. The reference trajectory is set as $p_d = [0, -0.595]^T$ (m).

- Case 2: Admittance response with an environment when contact motion happens. The stiffness of the environment is selected as 10000 N/m.

The matched uncertainties in pressure dynamics of hydraulic actuators are considered as a consequence of unknown internal leakage flows, which is expressed as follows:

$$f_i = \left(\frac{A_{1i}\beta_e}{V_{1i}} + \frac{A_{2i}\beta_e}{V_{2i}} \right) \sqrt{|P_{1i} - P_{2i}|} C_{ti} \, \text{sgn}\left(P_{1i} - P_{2i} \right) \tag{4.21}$$

where C_{ti} is the unknown leakage coefficient of the i$^{\text{th}}$ cylinder, which is selected as $C_{t1} = C_{t2} = 1.5 \times 10^{-10}$.

4.4.2. Controllers for comparison

To evaluate the control performance of the proposed scheme for the hydraulic robot subjected to matched disturbances/uncertainties and unmeasurable contact force, the following control algorithms as considered:

- Proposed controller: Desired admittance parameters are selected as $M_d = \text{diag}(2, 2)$, $C_d = \text{diag}(40, 40)$, and $K_d = \text{diag}(100, 100)$. Inner position control parameters are $k_1 = 200$, $k_2 = 200$, and $k_3 = 200$. The matched DOB bandwidth is $\omega_{e2} = 200$. Parameters of the ESMO are chosen as $\omega_{e1} = 20, \varepsilon = 0.001$, and $\eta = 1$.

- ESOLCC: This controller has the same configuration as the proposed controller, except for the mismatched observer design where only conventional ESO is used instead of the ESMO. The mismatched observer bandwidth is chosen as $\omega_{e1} = 20$. All the remaining parameters are selected the same as the proposed controller for a fair comparison.

- ESOC: This controller has the same configuration as the above controllers. However, this controller does not utilize the force information from load cells. Instead of that,

pressure information is used in the design of the mismatched ESO. All parameters are selected the same as the ESO-LC.

4.4.3. Simulation results
4.4.3.1. Case 1: Admittance response with a step contact force

The contact force estimation performances of the proposed controller, ESOLCC, and ESOC are given in **Fig. 4-3**. Both the ESMO and the ESO provide high-quality contact force estimation performance with actuation force information from load cells. However, the ESMO shows the best estimation performance when the step-change in contact force happens at 5s and 15s due to the quick response of the switching action. In contrast, the force estimation performance in the ESO without load cell is the worst because the unknown frictions in hydraulic cylinders cannot be covered when only pressure information is utilized. Nevertheless, in the steady-state, the estimated contact force by this observer converges to the actual one because the friction force significantly reduces with small sliding velocities between the rods and the bores of hydraulic cylinders.
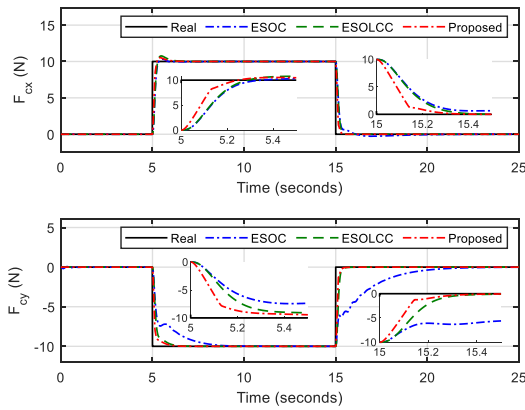
Fig. 4-3: Contact force estimation performance.
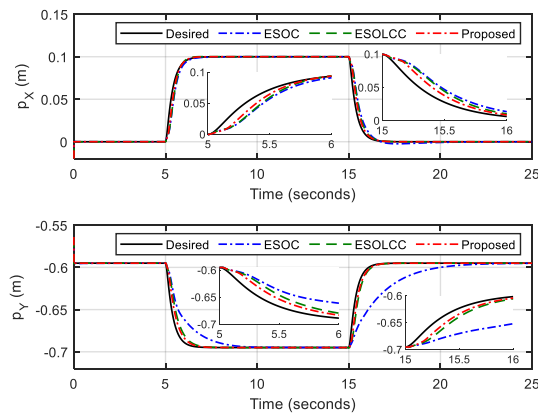
Fig. 4-4: Position of the end-effector

Table 4-3: Performance indices in case 1

Controller	M_e (mm)		μ_e (mm)		σ_e (mm)	
	p_x	p_y	p_x	p_y	p_x	p_y
Proposed	17.23	17.94	0.693	0.993	2.660	3.182
ESOLCC	23.97	25.75	1.011	1.449	3.758	4.555
ESO	25.45	51.46	1.489	7.722	4.180	12.86
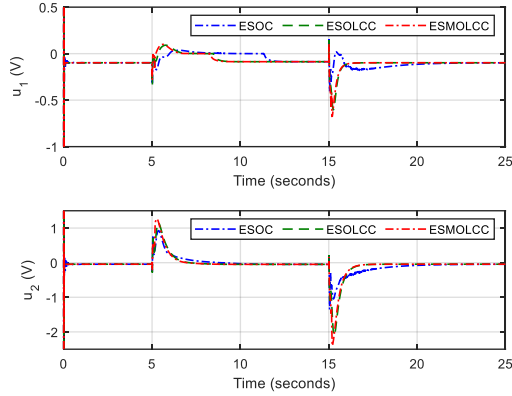
Fig. 4-5: Control signal for servo valves

The admittance behaviors of the three controllers are shown in **Fig. 4-4**. Overall, when the contact force is applied on the end effector, both controllers show the admittance control performances with deviation from the reference trajectory and follow the desired admittance behavior. However, it is observed that the contact force estimation performances strongly affect the admittance behavior of the controllers. Indeed, in Fig. 4, the proposed controller with ESMO shows the best admittance tracking performance compared to the remaining controllers. The ESOC shows the worst admittance tracking performance due to low quality-contact force estimation. To neglect the effect of initial conditions on the evaluation, performance indices including the maximum, average, and standard deviation of the tracking errors of both controllers are computed from 1s to 25s as given in **Table 4-3**, which indicates similar results.

Finally, **Fig. 4-5** presents the control signals for the proportional valves controlling the hip and knee cylinders. It is observed that the proposed controller and the ESOLCC provide similar control signals with small deviation, which is reasonable due to the similar contact force estimation performance as shown in **Fig. 4-3**. However, because the ESMO observes the contact force faster than the ESO, the control signal of the proposed controller has a higher magnitude than the control signal of the ESOLCC during the transient time. When the steady-state is achieved, control signals of both controllers remain the same due to the same contact force estimation.

4.4.3.2. Case 2: Contact motion with the environment

In this case study, an environment with constant stiffness and fixed position is selected to test the admittance behavior of the leg test bench in contact motion. The force observer bandwidths of all controllers are increased to 1500. For simplicity, the friction force at the contact point is neglected here. Hence, admittance performance in the x-axis is not necessary to be considered. The reference trajectory and environment position are given in **Fig. 4-6**.
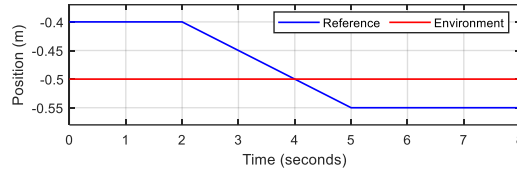
Fig. 4-6: Reference trajectory and environment position.
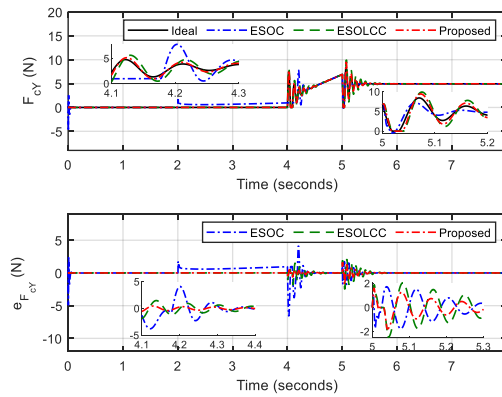
Fig. 4-7: Contact force estimation performance and contact force estimation error in the y-axis
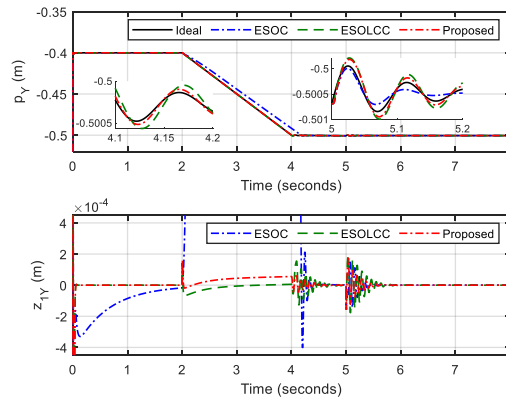
Fig. 4-8: Admittance tracking performance and the error between the actual position and the desired position in the y-axis.

Fig. 4-7 shows the contact force estimation performance and contact force estimation error in the y-axis. From 0s to 2s, contact force estimations of all controllers are zeros due to the constant reference. After that, from 2s to 4s, the robot moves down following the reference trajectory. In this period, the contact motion does not happen but the force estimation error in

47

the ESOC exists due to the lack of load cell information to cover frictions in hydraulic cylinders. From 4s to 5s, the contact motion happens, and the reference trajectory goes down. Consequently, the contact force slowly increases, and contact force estimations of all controllers successfully track it. However, in the remaining period, the reference trajectory does not move down anymore, which causes a sudden reduction in the ideal contact force. Among all force observers, it is observed that the ESMO still shows the best contact force estimation performance during this period.

The admittance behaviors and the admittance tracking accuracies of all controllers are given in **Fig. 4-8**. Due to the contact motion, one observes that the ideal admittance behavior computed by the outer admittance loop is different from the reference trajectory. Based on this desired behavior, both controllers provide good position tracking performances. However, similar to the force tracking performance mentioned above, the proposed controller shows the best admittance accuracy regardless of matched disturbance in actuator dynamics. This statement is also illustrated by performance indices in **Table 4-4**.

Table 4-4: Performance indices in case 2

Controller	M_e (mm)	μ_e (mm)	σ_e (mm)
Proposed	0.1740	0.0157	0.0233
ESOLCC	0.1953	0.0138	0.0284
ESO	8.3688	1.6958	2.7478

4.5. Discussion

In this paper, an ESMO is firstly developed for the force estimation of an admittance control algorithm of a hydraulic robot system. Together with the hydraulic actuation force information from load cells, the proposed control algorithm shows superiority in the admittance control performance compared to the remaining controller utilizing the ESO with constant external force and contact force with the environment. Actuator nonlinear dynamics are also clearly exploited to fulfill the design of the proposed admittance controller under matched disturbance, which is rarely observed in previous studies. Practical problems relating to measurement noises will be considered in future work.

Chapter 5

APPLICATION TO CONTOURING CONTROL PROBLEM OF ROBOTIC EXCAVATORS

5.1. Introduction

Motion control is one of the most important tasks in many practical applications as machine tools and manipulators. The crucial criteria to evaluate the motion control performance is the tracking accuracy which means the distance between the actual position and the desired position at each moment. However, it is not always that tracking control guarantees the quality of the product, e.g., high-quality surfaces of machined parts in a machining process. This is due to the fact that the distance between the actual position and desired contour cannot be explicitly described in the tracking accuracy, which is called the contouring error. Thus, in order to guarantee contouring accuracy, several contouring control approaches have been proposed, which can be classified into two groups. The first approach is called the cross-coupled control (CCC), in which an auxiliary contouring control signal is directly added to the tracking control signal to attenuate the contouring error [108, 109]. Based on this framework, many techniques have been integrated into the control design as adaptive nonlinear control [110], fuzzy PID control [111], iterative learning control [112], with several estimation methods as tangential line-based estimation [113], osculating circle-based approximation [114, 115], generalized CCC [116], and Taylor series [117]. Overall, the CCC structure is simple and easy to be implemented in real applications. However, the effectiveness of the control system is limited because of the omission of the system dynamics information. The other group of contouring control is the task coordinate frame (TCF)-based approach. The key idea of this method is that the system dynamics is transformed from the original described coordinate system to a more convenient coordinate system where the tracking error can be easily decoupled into tangential error, normal error, and bi-normal error [118]. Compared to the CCC, the TCF-based approach utilizes the plant information in the control design, which can offer higher contouring performance. To improve the control performance, different types of coordinate transformation methods based on this framework have been proposed as global TCF (GTCF) [119], orthogonal GTCF [120], reduced-dimension TCF [121], and polar coordinate frame [122, 123].

In recent years, besides many control problems considered in practical tasks of the excavator as position tracking control [74], energy efficiency [124-126], coordinated control [127, 128], and remote control [129], researchers have considered the contouring performance in excavator

since the surface quality has been still considered in some levels. In [130], a proportional-integral tracking control combined with CCC was proposed for the leveling work of the excavator. The equivalent joint angle errors were calculated based on the contouring error through kinematic constraints and then fed back to a simple proportional contouring control. In [131], a nonlinear PI tracking control was proposed for a robotic excavator. Instead of using two kinds of controllers as tracking controller and contouring controller, the authors modified the reference trajectory based on equivalent joint angle errors which were calculated based on the contouring error. Overall, the previous works in contouring control of excavators were limited to the CCC approach, which remains an open area to improve control performance based on the TCF approach. Moreover, although contouring precision requirements in excavator tasks are lower than those in high-precision machining tasks, model uncertainties and external disturbances usually appear in excavator operation, which significantly affects the contouring performance.

To attenuate the impact of uncertainties and disturbances, besides using robust controllers, many auxiliary components have been developed as the time delay estimation to deal with lumped disturbances/uncertainties [17, 132], the adaptive mechanism to estimate unknown model parameters [33, 133-135], and the disturbance observer (DOB) for the external disturbance [41, 94]. Originally, the DOB was designed to only estimate the external disturbance, which will be compensated in a feedforward way in control design. However, if the effect of model uncertainties can be considered as a part of the disturbance, the application of DOB can be also extended to deal with this difficulty. Recently, a special type of DOB called extended-state observer (ESO) is widely applied to not only estimate the lumped uncertainties/disturbances but also estimate the unmeasurable states of the plant. The effectiveness of ESO has been verified in many applications as hydraulic system [34, 136, 137], diesel engine [138], autonomous helicopter [139], and manipulator [57].

Motivated by these observations, a novel model-based contouring control is proposed for an excavator. One unique feature of the proposed control is that both the steady-state and transient contouring performance can be pre-defined and strictly maintained during operation. This is based on the integration of the output constraint concept with the barrier Lyapunov function (BLF) [15, 140-143] into the control design. An ESO is implemented to estimate the lumped disturbance and unmeasurable states, thus increases the robustness of the control system. Another main contribution of the paper is firstly adopting the TCF in the contouring control problem of the excavator, to transform the traditional tracking control problem into three decoupled control problems as contouring control, tangential control, and orientation control

which are separately treated due to their priority orders. The remaining tangential tracking performance and orientation tracking performance are guaranteed to be bounded by simple proportional-derivative controllers. Owing to the decoupling effect of these control objectives, the stability of each separated performance contributes to the global stability of the whole system. Finally, the effectiveness of the proposed control algorithm is verified by some simulations in the MATLAB Simulink under different surface-flattening task scenarios.

The paper is organized as follows. First, the excavator modeling with the kinematics and dynamics models is described in Section 2. Section 3 analyzes the implementation of the ESO in the control system. Then, the proposed controller is presented in Section 4. The trajectory generation algorithm of the surface flattening task is given in Section 5. Simulation results are presented and discussed in Section 6. Finally, Section 7 concludes this work.

5.2. System dynamics
5.2.1. Kinematics analysis

The model of an excavator is described in **Fig. 5-1**. The world frame is denoted by Ox_0y_0. Positive directions of angles q_1, q_2, q_3, and φ are counterclockwise. The relation between position and orientation of the bucket tip $\boldsymbol{r} = [x, y, \varphi]^T$ and the joint angle variables $\boldsymbol{q} = [q_1, q_2, q_3]^T$ are described as

$$
\begin{aligned}
x &= L_1 \cos q_1 + L_2 \cos(q_1 + q_2) + L_3 \cos(q_1 + q_2 + q_3) \\
y &= L_1 \sin q_1 + L_2 \sin(q_1 + q_2) + L_3 \sin(q_1 + q_2 + q_3) \\
\varphi &= q_1 + q_2 + q_3
\end{aligned}
\tag{5.1}
$$

where L_1, L_2, and L_3 are the lengths of the boom, arm, and bucket, respectively.

Differentiating both sides of (5.1), velocity and acceleration constraints are described as follows:

$$
\begin{aligned}
\dot{\boldsymbol{r}} &= \boldsymbol{J}\dot{\boldsymbol{q}} \\
\ddot{\boldsymbol{r}} &= \dot{\boldsymbol{J}}\dot{\boldsymbol{q}} + \boldsymbol{J}\ddot{\boldsymbol{q}}
\end{aligned}
\tag{5.2}
$$

where the Jacobian matrix $\boldsymbol{J}$ which expresses the relation between bucket tip velocity and joint angles velocity is defined by

$$
\boldsymbol{J} = \frac{\partial \boldsymbol{r}}{\partial \boldsymbol{q}}
\tag{5.3}
$$
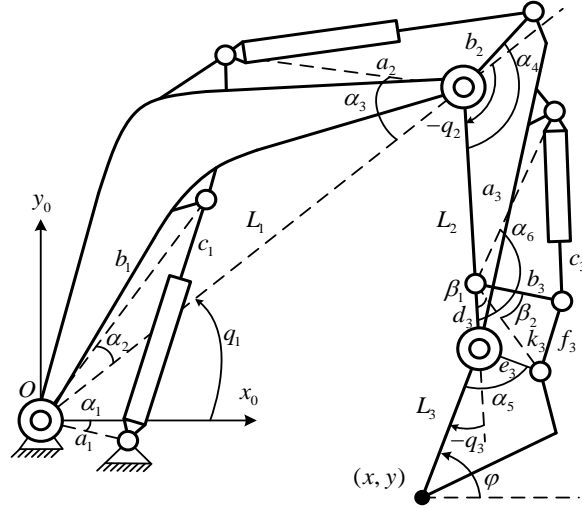
Fig. 5-1: Schematic diagram of the investigated excavator.

5.2.2. Dynamics analysis

The dynamic model of the excavator can be accurately calculated based on the method of Lagrange multiplier [144] or virtual decomposition control [145-147] due to the closed-loop structure of the configuration. However, to be simple, in this paper, the dynamics model of the excavator is approximately computed based on Lagrange's equations for the series configuration of a multi-body system as follows:

$$M(q)\ddot{q}+C(q,\dot{q})\dot{q}+G(q)q+J^{T}(q)F_{d}=\tau \tag{5.4}$$

where $q \in R^3$ is the vector of the joint variables, $M(q) \in R^{3\times3}$ is the inertia matrix, $C(q,\dot{q}) \in R^{3\times3}$ denotes the matrix of centrifugal and Coriolis forces, $G(q) \in R^3$ represents gravity vector, and $F_{d} \in R^3$ is the external disturbance acting on the bucket tips.

Toques provided at each joint is computed based on the cylinder forces by

$$\tau = J_{a}^{T}F \tag{5.5}$$

where J_{a} is the Jacobian matrix of the actuation system which is calculated based on the geometric relation between the joint angles and cylinder displacements as follows:

$$J_{a} = \frac{\partial c}{\partial q} \tag{5.6}$$

The displacements of the cylinders $c = [c_1, c_2, c_3]^T$ are computed based on the boom, arm, and bucket joint angles by

$$c_1 = \sqrt{a_1^2 + b_1^2 - 2a_1b_1\cos(q_1 + \alpha_1 + \alpha_2)}$$

$$c_2 = \sqrt{a_2^2 + b_2^2 - 2a_2b_2\cos(\pi - \alpha_3 - \alpha_4 - q_2)}$$

$$k_3 = \sqrt{d_3^2 + e_3^2 - 2d_3e_3\cos(\pi - \alpha_5 - q_3)}$$

$$\beta_1 = \arccos\left(\frac{d_3^2 + k_3^2 - e_3^2}{2d_3k_3}\right) \qquad (5.7)$$

$$\beta_2 = \arccos\left(\frac{b_3^2 + k_3^2 - f_3^2}{2b_3k_3}\right)$$

$$c_3 = \sqrt{a_3^2 + b_3^2 - 2a_3b_3\cos(\alpha_6 - \beta_1 - \beta_2)}$$

where $\alpha_1, \alpha_2, \alpha_3, \alpha_4, \gamma_1, \beta_{41}, \beta_{42}$, and β_3 are specific angles. $a_1, a_2, a_3, b_1, b_2,$ b_3, d_3, e_3, and f_3 are specific lengths. These dimensions which are defined to make the calculation process (5.7) convenient are described in **Fig. 5-1**.

Based on the hydraulic power forces $u \in R^3$ and friction forces, the cylinder forces are given by

$$F = u - D\dot{c} \qquad (5.8)$$

where $D \in R^{3\times3}$ is the matrix of unknown viscous damping coefficients of hydraulic cylinders.

From (5.4), (5.5), and (5.8), the dynamics model of the excavator becomes

$$M(q)\ddot{q} + C(q,\dot{q})\dot{q} + G(q) + \tau_f = J_a^T u \qquad (5.9)$$

where $\tau_f = J^T(q)F_d + J_a^T DJ_a\dot{q}$ is the vector of the lumped disturbance and uncertainty caused by the external load and unknown actuator friction.

5.3. Extended state observer

To estimate the lumped disturbance in the dynamics model of the excavator, an ESO is implemented in this paper. Firstly, an extended state vector is defined as $x_e = [x_{e1}, x_{e2}, x_{e3}]^T = [q, \dot{q}, -M(q)^{-1}\tau_f]$ and let $\dot{x}_{e3} = h_e(t)$ where $h_e(t)$ denotes the change rate of the lumped disturbance. Then, the model dynamics (5.4) can be represented by

$$\dot{x}_e = A_e x_e + \psi_e + H_e$$
$$y_e = C_e x_e \qquad (5.10)$$

where $A_e = \begin{bmatrix} 0_{3\times3} & I_{3\times3} & 0_{3\times3} \\ 0_{3\times3} & 0_{3\times3} & I_{3\times3} \\ 0_{3\times3} & 0_{3\times3} & 0_{3\times3} \end{bmatrix}$, $\psi_e = \begin{bmatrix} 0_{3\times3} \\ f_e \\ 0_{3\times3} \end{bmatrix}$, $C_e = [I_{3\times3}, 0_{3\times3}, 0_{3\times3}]$, $\phi_e = M(q)^{-1}(J_a^T u$

$-C(q,\dot{q})\dot{q} - G(q))$, and $H_e = [0_{1\times3}, 0_{1\times3}, h_e]^T$.

Assumption 1: The derivative of the lumped disturbance is assumed to be bounded as $\|h_e\| \le \delta_h$.

From (5.10), the ESO can be constructed as

$$\dot{\hat{x}}_e = A_e \hat{x}_e + \hat{\psi}_e + K_e (y_e - C_e \hat{x}_e) \tag{5.11}$$

where $\hat{x}_e$ is the estimated value of x_e, and $\hat{\psi}_e(q,\dot{\hat{q}})$ is the estimated value of $\psi_e(q,\dot{q})$. The observer gain K_e can be designed in the following form:

$$K_e = [3\omega_e I_{3\times3}, 3\omega_e^2 I_{3\times3}, \omega_e^3 I_{3\times3}]^T \tag{5.12}$$

where $\omega_e > 0$ is a design parameter which can be considered as the bandwidth of the ESO.
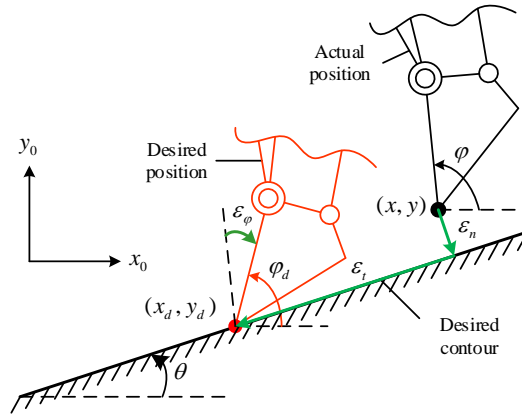
Fig. 5-2: Tracking error decomposition schematics.

5.4. Proposed observer-based control algorithm

The Cartesian tracking error is defined as $e = r_d - r$. Transform this tracking error into the following form:

$$\varepsilon = Te \tag{5.13}$$

where $\varepsilon = [\varepsilon_n, \varepsilon_t, \varepsilon_\varphi]^T$ is a new form of the tracking error e including the normal tracking error (i.e., the contouring error), tangential tracking error, and orientation tracking error, respectively. **Fig. 5-2** illustrates the relation between the tracking error and its decomposition components.

Based on **Fig. 5-2**, the transformation matrix is defined by

$$T = \begin{bmatrix} -\sin\theta & \cos\theta & 0 \\ \cos\theta & \sin\theta & 0 \\ 0 & 0 & 1 \end{bmatrix} \tag{5.14}$$

where θ is the slope angle of the target surface.

Remark 2: Control objective includes both tracking performance and contouring performance when the latter is primary. When the tracking error is transformed into a new form, the final target is how to reduce the contouring error ε_n as much as possible, while maintaining an acceptable level of the tangential tracking performance ε_t and orientation tracking performance ε_φ.
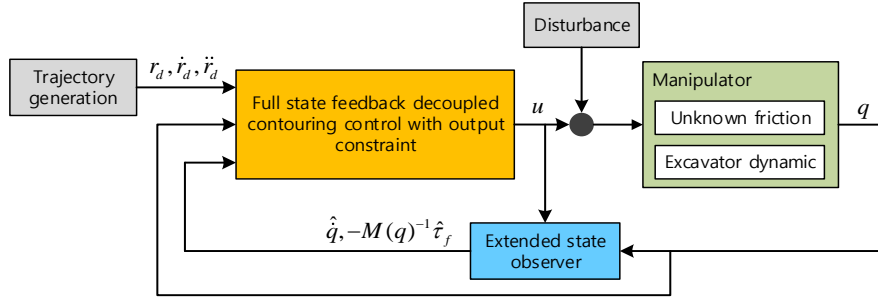
Fig. 5-3: Diagram of the proposed control.

Inspired by this idea, an extended-state observer-based output-feedback controller is given in **Fig. 5-3**. The control signal is designed by

$$\begin{aligned} \boldsymbol{u} &= \boldsymbol{J}_a^{-T}(\boldsymbol{q})(\boldsymbol{u}_1 + \boldsymbol{u}_2) \\ \boldsymbol{u}_1 &= \boldsymbol{C}(\boldsymbol{q},\hat{\dot{\boldsymbol{q}}})\hat{\dot{\boldsymbol{q}}} + \boldsymbol{G}(\boldsymbol{q}) + \hat{\boldsymbol{\tau}}_f \\ \boldsymbol{u}_2 &= -\boldsymbol{M}_x(\boldsymbol{q})\dot{\boldsymbol{J}}(\boldsymbol{q},\hat{\dot{\boldsymbol{q}}})\hat{\dot{\boldsymbol{q}}} - \boldsymbol{M}_x(\boldsymbol{q})\boldsymbol{T}^{-1}\boldsymbol{u}_3 + \boldsymbol{M}_x(\boldsymbol{q})\ddot{\boldsymbol{r}}_d \end{aligned} \tag{5.15}$$

where $\hat{\dot{\boldsymbol{q}}}$ and $\hat{\boldsymbol{\tau}}_f$ are the estimation vectors of velocities of joint angle variables and the lumped disturbances/uncertainties, $\boldsymbol{r}_d$ is the reference trajectory of the end tip, $\boldsymbol{M}_x(\boldsymbol{q}) = \boldsymbol{M}(\boldsymbol{q})\boldsymbol{J}^{-1}$, and $\boldsymbol{u}_3$ is a virtual control signal vector which will be designed later.

Substituting (5.15) to (5.9), one obtains

$$\ddot{\boldsymbol{\varepsilon}} = \boldsymbol{u}_3 + \boldsymbol{d} \tag{5.16}$$

where $\boldsymbol{d} = \boldsymbol{T}\boldsymbol{M}_x(\boldsymbol{q})^{-1}\begin{pmatrix} \boldsymbol{M}_x(\boldsymbol{q})\left(\dot{\boldsymbol{J}}(\boldsymbol{q},\hat{\dot{\boldsymbol{q}}})\hat{\dot{\boldsymbol{q}}} - \dot{\boldsymbol{J}}(\boldsymbol{q},\hat{\dot{\boldsymbol{q}}})\dot{\boldsymbol{q}}\right) \\ +(\boldsymbol{C}(\boldsymbol{q},\hat{\dot{\boldsymbol{q}}})\dot{\boldsymbol{q}} - \boldsymbol{C}(\boldsymbol{q},\hat{\dot{\boldsymbol{q}}})\hat{\dot{\boldsymbol{q}}}) + (\boldsymbol{\tau}_f - \hat{\boldsymbol{\tau}}_f) \end{pmatrix}$

From Theorem 1, it is easy to state that $\boldsymbol{d}$ is bounded as $\|\boldsymbol{d}\| \leq \delta_d$ where δ_d is a positive constant. Then, regarding Remark 2, two different control strategies are designed with different priorities as follows.

5.4.1. Normal tracking control

The first equation in (5.16) can be expressed as follows:

$$\ddot{\varepsilon}_n = u_{31} + d_n \tag{5.17}$$

The contouring error is expected to be bounded with specific lower and upper boundaries as

$$-k_n(t) \leq \varepsilon_n \leq k_n(t) \tag{5.18}$$

Theorem 2: To guarantee that the contouring error in (5.17) satisfies the prescribed performance (5.18) while suffering from the estimation error at the same time, a control signal u_{3n} can be designed by

$$u_{3n} = \dot{\alpha} - \frac{\varepsilon_n}{k_n(t)^2 - \varepsilon_n^2} + k_2 z \tag{5.19}$$

where $z = \alpha - \dot{\varepsilon}_n$, $\alpha = -(k_1 + \lambda_n(t))\varepsilon_n$, and $\lambda_n(t) = (\dot{k}_n^2(t) / k_n^2(t) + \beta)^{1/2}$. k_1, k_2 and β are positive constants.

Proof: A Barrier Lyapunov function is considered as

$$V_1 = \frac{1}{2}\log\frac{k_n^2(t)}{k_n^2(t) - \varepsilon_n^2} \tag{5.20}$$

Taking the derivative of it, one obtains

$$\dot{V}_1 = \frac{\varepsilon_n}{k_n^2(t) - \varepsilon_n^2}\left(\dot{\varepsilon}_n - \varepsilon_n\frac{\dot{k}_n(t)}{k_n(t)}\right) \tag{5.21}$$

To achieve $\dot{V}_1 \leq 0$, a virtual control law can be designed as

$$\alpha = -(k_1 + \lambda_n(t))\varepsilon_n \tag{5.22}$$

where $\lambda_n(t)$ is defined in (5.19).

Substituting into (5.21), it becomes

$$\dot{V}_1 \leq -\frac{k_1 \varepsilon_n^2}{k_n^2(t) - \varepsilon_n^2} - \frac{\varepsilon_n z}{k_n^2(t) - \varepsilon_n^2} \tag{5.23}$$

From this, it is clear that the error between the virtual control law and real contouring speed error is expected to become zero.

Thus, considering the dynamic equation (5.17), a Lyapunov function is designed as

$$V_2 = V_1 + \frac{1}{2} z^2 \tag{5.24}$$

The derivative of it is calculated by

$$\dot{V}_2 = \dot{V}_1 + z\dot{z} \leq -\frac{k_1 \varepsilon_n^2}{k_n^2(t) - \varepsilon_n^2} - \frac{\varepsilon_n z}{k_n^2(t) - \varepsilon_n^2} + z(\dot{\alpha} - u_{3n} - d_n) \tag{5.25}$$

Substituting the control signal (5.19) into (5.25) with noting that $|d_n| \leq \delta_d$, one obtains

$$\begin{aligned}
\dot{V}_2 &\leq -\frac{k_1 \varepsilon_n^2}{k_n^2(t) - \varepsilon_n^2} - k_2 z^2 - d_n z \\
&\leq -\frac{k_1 \varepsilon_n^2}{k_n^2(t) - \varepsilon_n^2} - \left(k_2 - \frac{1}{2}\right) z^2 + \frac{1}{2} \delta_d^2
\end{aligned} \tag{5.26}$$

From [148], below inequality holds

$$\log\left(\frac{k^2}{k^2 - x^2}\right) \leq \frac{x^2}{k^2 - x^2} \tag{5.27}$$

Substituting (5.27) into (5.26), it becomes

$$\dot{V}_2 \leq -k_1 \log\frac{k_n^2(t)}{k_n^2(t) - \varepsilon_n^2} - \left(k_2 - \frac{1}{2}\right) z^2 + \frac{1}{2} \delta_d^2 \tag{5.28}$$

To simplify (5.28), set $\begin{cases} a = 2 \cdot \min\left(k_1, k_2 - \frac{1}{2}\right) \\ b = \frac{1}{2} \delta_d^2 \end{cases}$

Inequality (5.28) becomes

$$\dot{V}_2 \leq -aV_2 + b \tag{5.29}$$

Multiplying both sides with e^{at} and taking the integral, one obtains

$$V_2(T) \leq \left(V_2(0) - \frac{b}{a}\right) e^{-aT} + \frac{b}{a} < V_2(0) + \frac{b}{a} \tag{5.30}$$

From (5.20) and (5.30), the contouring error is bounded as follows:

$$-k_n(T)\sqrt{1-e^{-c}} < \varepsilon < k_n(T)\sqrt{1-e^{-c}}$$

(31)

where $c = 2V_2(0) + 2b/a$.

This completes the proof of Theorem 2.

5.4.2. Tangential and angular tracking control

The last two equations in (5.16) can be written as

$$\ddot{\varepsilon}_i = u_{3i} + d_i$$

(5.32)

where $i = t, \varphi$.

As explained in Remark 2, because these tracking errors are not primary, so bounded tracking performances are acceptable. A proportional-derivative control signal is designed as

$$u_{3i} = -k_{di}\dot{\varepsilon}_i - k_{pi}\varepsilon_i$$

(5.33)

Substitute to (5.32), one obtains

$$\ddot{\varepsilon}_i + k_{di}\dot{\varepsilon}_i + k_{pi}\varepsilon_i = d_i$$

(5.34)

The transfer function of this system is expressed as

$$G_i(s) = \frac{1}{s^2 + k_{di}s + k_{pi}}$$

(5.35)

This is a conventional 2nd order system. Thus, it is easy to guarantee bounded tracking performance $|\varepsilon_i| < \delta_d / k_{pi}$ when the resonance does not occur at $k_{di} > \sqrt{2k_{pi}}$ [149, 150].

Remark 3: Bounded errors are observed in both contouring performance, tangential tracking performance, and orientation tracking performance, which leads to global stability of the control system.

5.4.3. Trajectory generation

In the surface-flattening task, the operator supplies the orientation of the bucket φ and the speed of arm angle $\dot{q}_2$ by a joystick. After that, the trajectory generation algorithm is designed to generate the reference angles of the boom, arm, and bucket to achieve the desired contour.

To locate the position of the target surface, a point $A(x_0, y_o)$ lying on the surface and the surface angle θ are pre-determined.

The bucket tip must lie on the surface which is described by the following equation:

$$(x - x_0)\sin\theta - (y - y_0)\cos\theta = 0 \tag{5.36}$$

From (5.1) and (5.36), there are four algebraic equations with four unknowns x, y, q_1, and q_3. The solution q_1 is found as

$$q_1 = \pm\gamma - \gamma_1 \tag{5.37}$$

where

$$\begin{aligned}
\gamma_1 &= \arctan 2\begin{pmatrix} L_2 \sin q_2 \sin\theta + (L_1 + L_2 \cos q_2)\cos\theta, \\ (L_1 + L_2 \cos q_2)\sin\theta - L_2 \sin q_2 \cos\theta \end{pmatrix} \\
\gamma &= \arccos \frac{(L_3 \sin\varphi - y_0)\cos\theta - (L_3 \cos\varphi - x_0)\sin\theta}{\sqrt{L_1^2 + L_2^2 + 2L_1 L_2 \cos q_2}}
\end{aligned} \tag{5.38}$$

Substituting this solution to (5.1), q_1, x, and y are computed.

5.5. Numerical simulation
5.5.1. Simulation setup

Fig. 5-4: Mini-excavator model

Table 5-1: Model parameters

Parameter	Description	Value	Unit
m_1	Mass of boom	36.863	kg
m_2	Mass of arm	13.138	kg
m_3	Mass of bucket	9.008	kg

J_{z1}	Mass moment of inertial of the boom	7306759.708		kgmm^2
J_{z2}	Mass moment of inertial of the arm	1178748.843		kgmm^2
J_{z3}	Mass moment of inertial of the bucket	348927.380		kgmm^2
r_{c1}	Center of mass of the boom	$[848.173, 213.106, 2.615]^{\mathrm{T}}$		mm
r_{c2}	Center of mass of the arm	$[336.525, 65.798, -0.000]^{\mathrm{T}}$		mm
r_{c3}	Center of mass of the bucket	$[210.471, 154.244, 0.082]^{\mathrm{T}}$		mm
L_1	Length of boom	1692		mm
L_2	Length of arm	851		mm
L_3	Length of bucket	580		mm

Table 5-2: Geometric dimensions

Parameter	Value	Unit	Parameter	Value	Unit
a_1	220	mm	f_3	200	mm
a_2	840	mm	α_1	1.05	rad
a_3	681	mm	α_2	0.27	rad
b_1	825	mm	α_3	0.6	rad
b_2	240	mm	α_4	2.67	rad
b_3	185	mm	α_5	1.66	rad
d_3	141	mm	α_6	2.86	rad
e_3	128	mm			

To verify the effectiveness of the proposed controller, simulation results are conducted based on a 1.5-tonne mini excavator which is shown in **Fig. 5-4**. Parameters for the simulation are given in **Table 5-1** and **Table 5-2**.

Remark 4: In practice, forces generated by actuators are limited due to the physical limitations of hardware components. Thus, the output of the controller is bounded as follows:

$$u_{sat} = sat(u) = \begin{cases} u_{\max} & if\ u \geq u_{\max} \\ u_{\min} & if\ u \leq u_{\min} \\ u & otherwise \end{cases} \tag{5.39}$$

where

$$Boom: u_{\max} = 50000N, u_{\min} = -50000N$$
$$Arm:\ \ u_{\max} = 50000N, u_{\min} = -50000N$$
$$Bucket:\ \ \ \ \ \ u_{\max} = 40000N, u_{\min} = -40000N$$

5.5.2. Controllers for Comparison

To compare the effectiveness of the proposed controller with that of previous works, we consider 3 controllers as follows: Controller 1 – proportional- derivative with cross-coupled control (PD-CCC); Controller 2 – decouple contouring control (DCC); Controller 3 - extended-state observer-based output-feedback decoupled contouring control (ESO-DCC).

Table 5-3: Control parameters

Controller	Parameters
PD-CCC	$K_P = diag\left(250000, 100000, 25000\right), K_D = diag\left(15000, 1500, 150\right),$ $K_P^{CC} = diag\left(50000, 0, 50000\right)$
DCC	$k_{pt} = 5000, k_{dt} = 500, k_{p\varphi} = 15000, k_{d\varphi} = 2000, k_1 = 120, k_2 = 150$
ESO-DCC	$k_{pt} = 5000, k_{dt} = 500, k_{p\varphi} = 15000, k_{d\varphi} = 2000, k_1 = 120, k_2 = 150,$ $\omega_e = 200$
Proposed controller	$k_{pt} = 5000, k_{dt} = 500, k_{p\varphi} = 15000, k_{d\varphi} = 2000, k_1 = 120, k_2 = 150,$ $k_n(t) = (0.2 - 0.005)e^{-5t} + 0.005 \text{ (m)}, \beta_1 = 0.1, \omega_e = 200$

For a fair comparison, instead of using the well-known proportional- integral-derivative with the cross-coupled control (PID-CCC), the PD-CCC is designed by

$$u = K_P\left(q_{ref} - q\right) + K_D \frac{d\left(q_{ref} - q\right)}{dt} + K_P^{CC}\varepsilon_q \tag{5.40}$$

where ε_q denotes the angle error with respect to the contouring error. Detailed information on the calculation can be found in previous work [130].

The DCC, ESO-DCC, and proposed controller are designed by using the decoupled control framework (5.15). The difference among them is that the DCC is built without disturbance compensation and the speeds of the boom, arm, and bucket angle are computed based on the derivative approximation. In contrast, the ESO-DCC and proposed controller receive the estimated speeds from the ESO as a feedback signal to construct the controller.

The DCC and ESO-DCC are similarly designed based on well-known backstepping technique as follows:

$$\begin{aligned} u_{3n} &= \dot{\alpha}_* - \varepsilon_n + k_2 z_* \\ z_* &= \dot{\varepsilon}_n - \dot{\alpha}_* \\ \alpha_* &= -k_1\varepsilon_1 \end{aligned} \tag{5.41}$$

To guarantee fair comparison, equivalent control parameters are chosen in **Table 5-3**.

5.5.3. Simulation results

In order to verify the effectiveness of the proposed controller against external disturbance, unknown viscous friction, and time-varying output constraint, some simulations are presented on the excavator with specific working tasks, which are described in the following case studies.

These simulations are conducted by MATLAB 2019b with a sampling time 10^{-4} seconds and automatic solver. The sampling time of controllers and observers is set as 10^{-3} seconds. The simulation diagram is shown in **Fig. 5-5**.
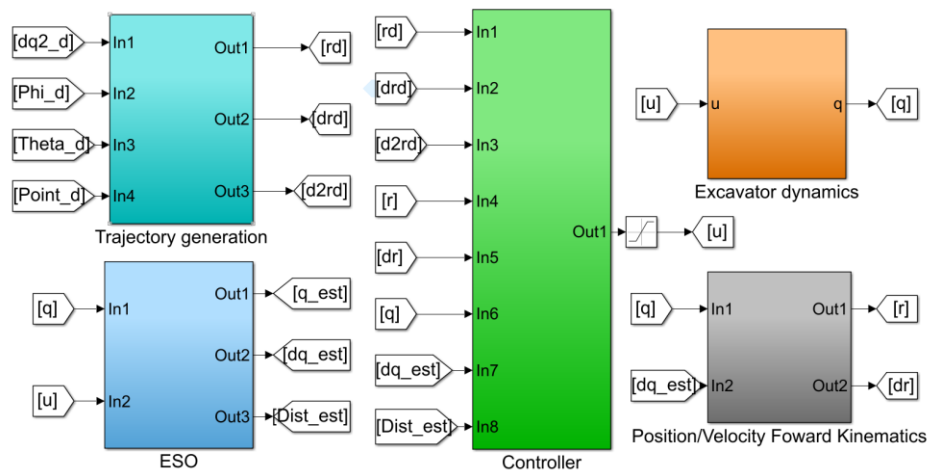
Fig. 5-5: Simulink block diagram

Fig. 5-6: Excavator reference motion in case 1

5.5.3.1. Case 1: Horizontal motion

In this case, the slope angle, orientation of the bucket, and surface height are predefined as $0°, 60°$, and -0.6m, respectively. The desired motion of the bucket is shown in **Fig. 5-6**. In **Fig. 5-7**, the arm speed signal from the joystick is set to be zero in the first 1 second to make the system states converge, in some levels, to a stable position and after that operate in the working

mode. To verify the capability to handle external disturbance, an external force and moment vector $F_d = [-300\text{N}, -100\text{N}, -300\text{Nm}]^T$ is added at 2.5 seconds.

In **Fig. 5-8a**, compared to the three remaining controllers, the proposed controller shows the best performance with the highest contouring accuracy and guarantees the prescribed performance under the external disturbance which occurs at 2.5 seconds. In contrast, even though having the largest parameters compared to the other controllers, the contouring performance of the PD-CCC is the worst with the highest overshoot at 2.5 seconds and the largest steady-state error not only before but also after the external disturbance is applied to the system since it does not get benefits from the plant information in the control design. Similar performances are observed in tangential and orientation error which is illustrated in **Fig. 5-8b-c**. It is very interesting that the tangential and orientation tracking performances of the ESO-CCC and proposed controller are almost the same due to the effectiveness of the decoupling methodology that separates the contouring task from the tangential task and orientation task. The overall contour shape is described in **Fig. 5-8d** which once again shows that the PD-CCC and CCC cannot finish the task due to poor tangential tracking performance, and their contouring accuracy is lower than the proposed controller and ESO-DCC.
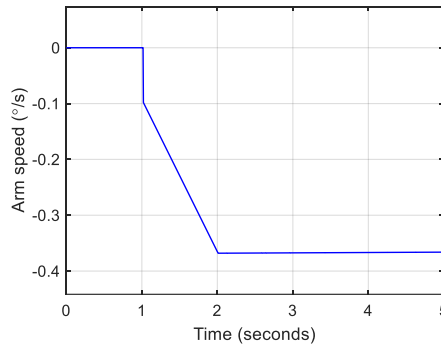
Fig. 5-7: Arm speed reference signal

(a)   (b)

(c)   (d)
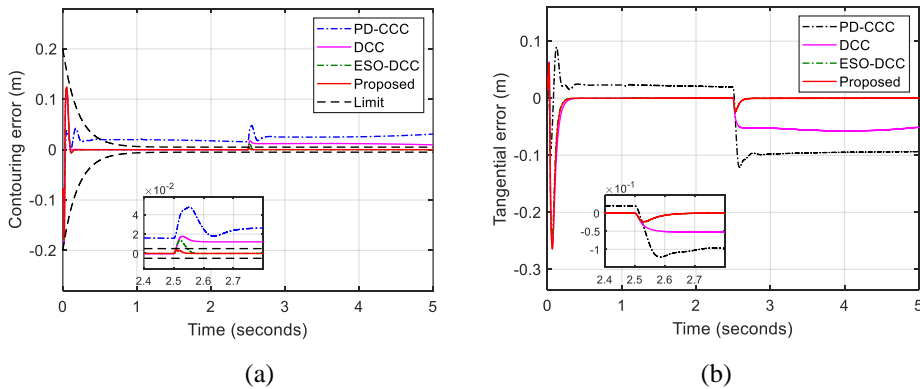
Fig. 5-8: Performance of excavator with respect to a) Contouring accuracy, b) Tangential accuracy, c) Orientation accuracy, and d) Contour shape.

(a)   (b)

(c)

Fig. 5-9: Estimation performance in terms of a) position, b) velocity, and c) lumped disturbances/uncertainties.

Fig. 5-9 shows the estimated joint angle errors, estimated joint speed errors, and estimated lumped disturbance of the ESO in the joints of the excavator. The result shows that the ESO only takes a few milliseconds to successfully estimate both position, speed, and lumped disturbance. When the disturbance suddenly occurs at 2.5 seconds, there are some overshoots at the estimation error of joint angles and speeds due to the violation of Assumption 1 that the derivative of lumped disturbance is bounded. After that, the estimation errors quickly converge to a very small boundary according to Theorem 1. In addition, in the first 2.5 seconds, although

64

the external disturbance has not been applied at the bucket tips, the estimated values of the lumped disturbance are non-zeros due to the unknown viscous damping of the cylinders. In the last 2.5 seconds, the external disturbance is provided to the bucket tips and affects the joint torque due to the kinematic relationship, which makes the estimated values change dramatically in the boom, arm, and bucket joint angles.

Fig. 5-10 presents the control signals, which mean the force generated by each cylinder, in each joint of the excavator. Besides the sudden-increasing magnitude at 2.5 seconds due to the external disturbance, it is observed that control signals abruptly rise at 1 second. The reason is that at that time, the arm speed signal is also suddenly increased by the operator as shown in **Fig. 5-7**.

(a)　　　　　　　　　　　　　　(b)

(c)
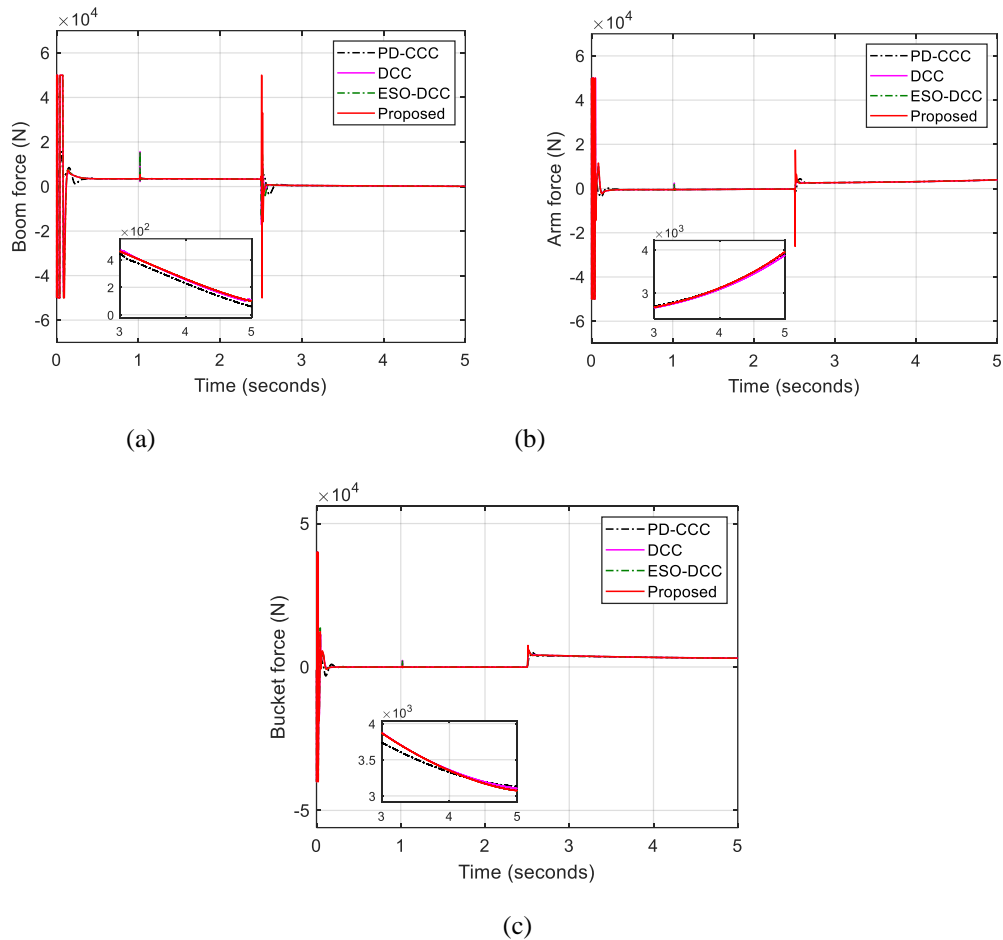
Fig. 5-10: Force control signal of a) boom cylinder, b) arm cylinder, and c) bucket cylinder.

Fig. 5-11: Excavator reference motion in case 2

5.5.3.2. Case 2: Slope motion

In this case, the slope angle is changed from $0°$ to $45°$. A point $(2, 0.5)$ is chosen to determine the surface. The desired motion of the excavator is shown in **Fig. 5-11**. The bucket orientation is calculated to make the bottom tangential to the targeted surface. The arm speed signal is the same as Case 1. An external disturbance vector $F_d = [-150\text{N}, -100\text{N}, -300\text{Nm}]^T$ is also added at 2.5 seconds to test the capability of controllers for handling external disturbance.

Fig. 5-12 shows errors in the contouring performance, tangential performance, orientation performance, and contouring shape. Similar to the previous scenario, it is observed that only the proposed controller guarantees the contouring prescribed performance and achieves the best tracking performance with respect to the tangential and orientation tracking errors, compared to the remaining controllers.

Estimation performance is verified in **Fig. 5-13** with small estimation errors in both position and velocity of joint angles. Similar to the previous case study, the estimated values of the lumped disturbance dramatically change at 2.5 seconds due to the external force and moment. At the time, undesirable changes in the estimated errors of positions and speeds of the boom, arm, and bucket angles are also not avoided as explained before. However, it does not violate the prescribed performance in the contouring error due to the implementation of the BLF in control design.
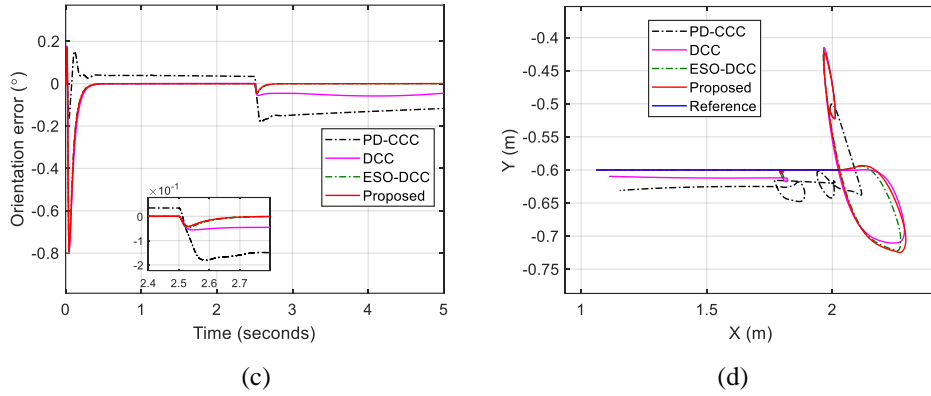
(a)

(b)

(c)

(d)
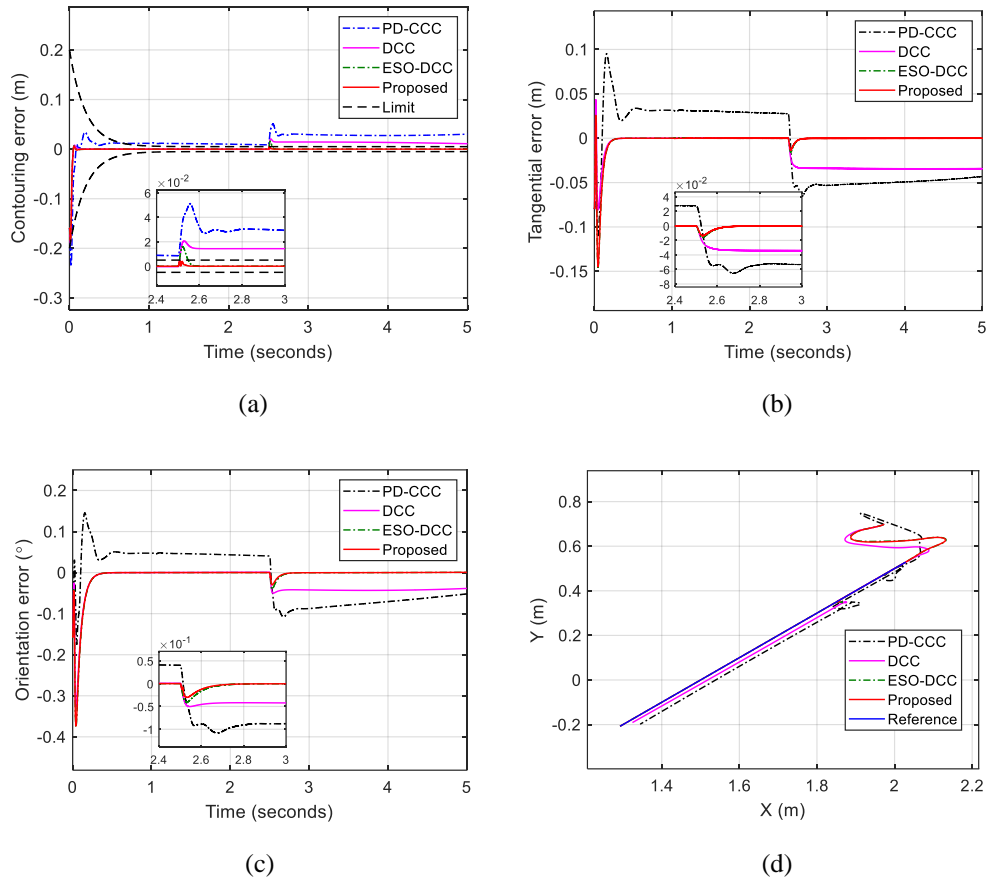
Fig. 5-12: Performance of excavator with respect to a) Contouring accuracy, b) Tangential accuracy, c) Orientation accuracy, and d) Contour shape.
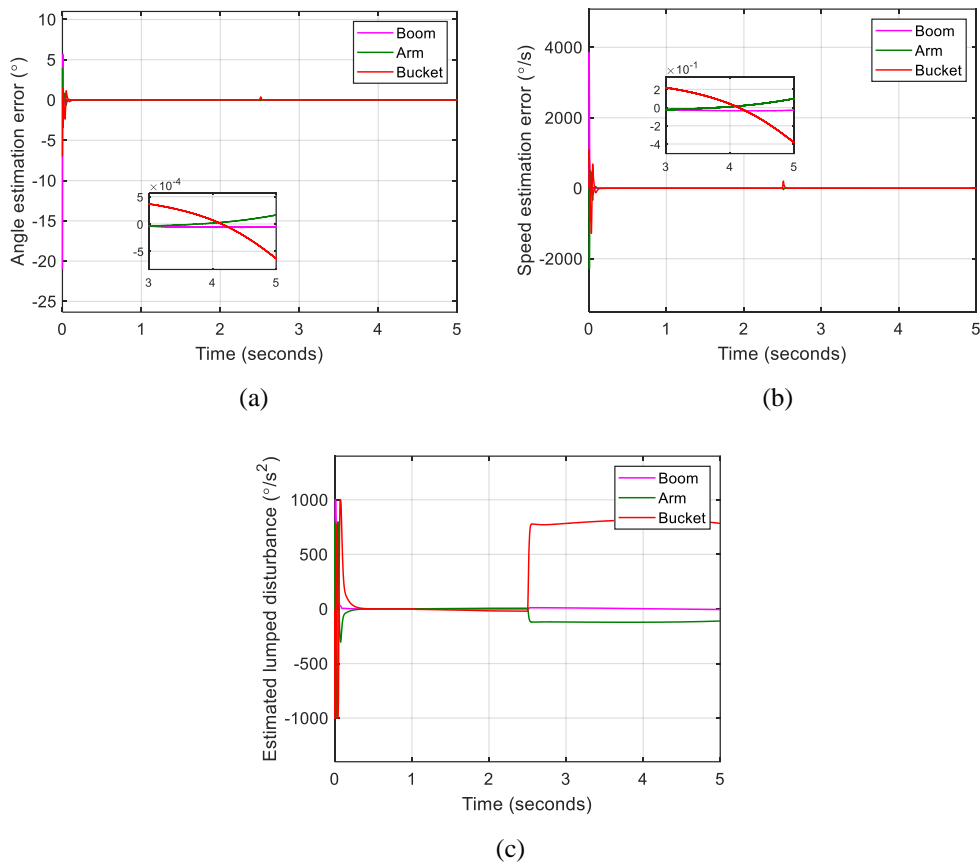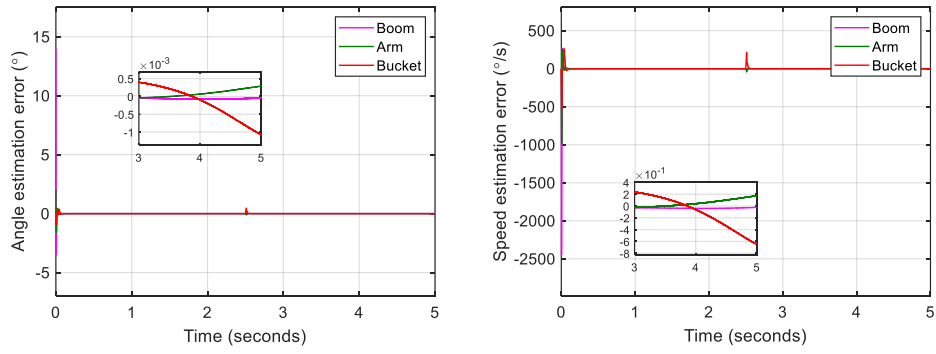
(a)

(b)
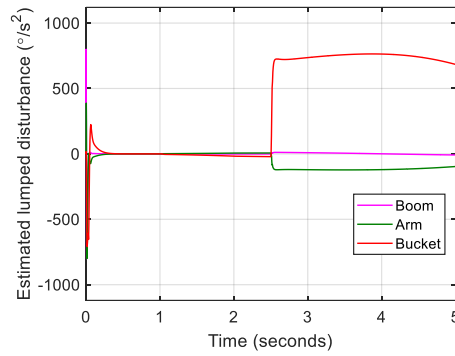
(c)

Fig. 5-13: Estimation performance in terms of a) position, b) velocity, and c) lumped disturbances/uncertainties.
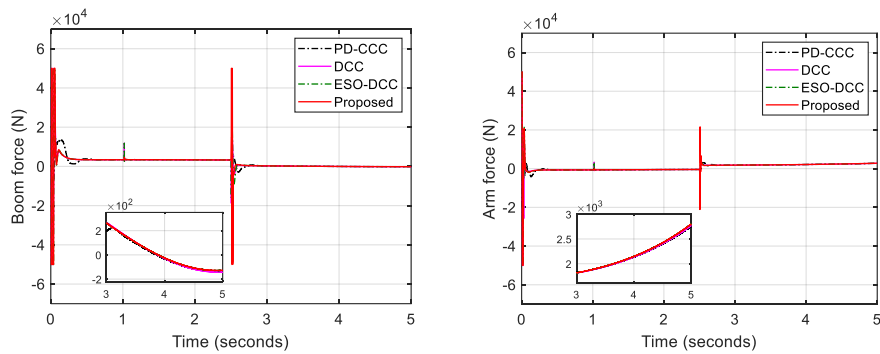
(a)

(b)
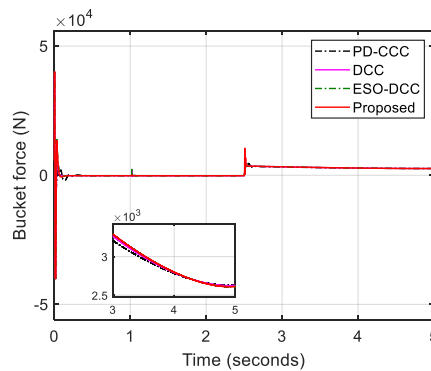
(c)

Fig. 5-14: Force control signal of a) boom cylinder, b) arm cylinder, and c) bucket cylinder.

Finally, force control signals of the boom, arm, and bucket cylinders are shown in **Fig. 5-14**. From 3 seconds to 5 seconds, the force control signal of the boom cylinder has changed its sign from positive to negative. It means that the effect of the external force and moment dominates the gravity force on the whole system, which requires the cylinder force to change its sign to make the boom move down.

5.6. Conclusion

This paper reports a novel extended-state observer-based output-feedback decoupled contouring control for an excavator in surface-flattening tasks regardless of time-varying output constraint, external load, and unknown frictions. The proposed controller was designed based on the ESO and BLF with the backstepping technique. The task coordinate methodology is utilized to separate the tracking performance into the contouring performance, tangential performance, and orientation performance, and treat them independently due to their orders of priority. Besides estimating the unmeasurable speed of each joint angle, the ESO is also applied to estimate the lumped disturbances/uncertainties presented during operation. In addition, the BLF is adopted to guarantee the contour performance not violating the pre-defined constraint performance. Moreover, the stability of the system is theoretically analyzed based on Lyapunov stability analysis. Simulation results with two surface flattening scenarios are conducted to verify the effectiveness of the proposed controller. The proposed control performance shows its superiority in improving both tracking performance and contouring performance under unknown friction, external load, and different working condition compared to the PD-CCC, DCC, and ESO-DCC.

Chapter 6
CONCLUSION AND FUTURE WORKS

6.1. Conclusions

This thesis presents some observer-based control techniques applied for different applications of robot manipulators. The key techniques are the backstepping framework and the state and disturbance observers which are proposed to improve the estimation performance. Depending on the specific problem in each application, these two techniques are skillfully utilized together with other auxiliary components to effectively solve the problem compared to the previous results. The main contributions of the dissertation are listed as follows:

Firstly, to realize the fault detection mechanism in the hydraulic robot manipulators with internal leakage fault, the ESO has been utilized to estimate the lumped disturbances in the pressure dynamics, and the estimated values are considered as an indicator to detect the fault. When the fault is detected, the online adaptive identification algorithm is activated to identify the internal leakage fault coefficient. Based on that, the normal controller is reconfigured into the fault-tolerant controller which effectively attenuates the effects of faults on the final control performance.

Secondly, in the interaction between the robot end-effector and the environment, contact force estimation is very important to achieve the desired admittance behavior on the system. To deal with this problem, an ESMO is firstly introduced which improves the transient response and the steady state force estimation performance compared to the ESO. Based on that, the estimated contact forces and velocities are fed back to the cascade controller including the outer admittance control loop and the inner position control, which guarantees the final control performance.

Finally, to improve the quality of the surface flattening tasks for robotic excavators, a high-accuracy contouring control algorithm is proposed, which relies on the task-coordinate frame approach to decouple the contouring error from the tracking error, the ESO to reduce the effects of the lumped uncertainties/disturbances on the excavation system, and the BLF to achieved pre-defined contouring control accuracy. Simulation results show that the proposed approach dominates the traditional CCC approach.

6.2. Future works

In this work, some practical problems should be considered in future work such as

- Control input saturation: This problem occurs when the actuation system tries to follow the desired trajectory but exceeds the physical limits of the hardware, which can cause instability and deteriorate the control performance.

- Time delay: In practical robotic systems, the signals come in and go out of the main controller through ADC, DAC, and communication protocol which causes delays and affects the overall system performance.

- Sensor faults: Actuator faults have been investigated in robot manipulators based on the robot nominal model and output measurement from sensors. However, when faults occur at sensors, the problem is much more difficult and requires much effort to find effective solutions.

Published papers and patents

A. International Journal

1. **Hoang Vu Dao** and K. K. Ahn, "Active Disturbance Rejection Contouring Control of Robotic Excavators with Output Constraints and Sliding Mode Observer," *Applied Sciences,* vol. 12, no. 15, 2022, doi: 10.3390/app12157453.

2. **Hoang Vu Dao** and K. K. Ahn, "Extended Sliding Mode Observer-Based Admittance Control for Hydraulic Robots," *IEEE Robotics and Automation Letters,* vol. 7, no. 2, pp. 3992-3999, 2022, doi: 10.1109/lra.2022.3147244.

3. **Hoang Vu Dao**, D. T. Tran, and K. K. Ahn, "Active Fault Tolerant Control System Design for Hydraulic Manipulator With Internal Leakage Faults Based on Disturbance Observer and Online Adaptive Identification," *IEEE Access,* vol. 9, pp. 23850-23862, 2021, doi: 10.1109/access.2021.3053596.

4. **Hoang Vu Dao**, S. Na, D. G. Nguyen, and K. K. Ahn, "High accuracy contouring control of an excavator for surface flattening tasks based on extended state observer and task coordinate frame approach," *Automation in Construction,* vol. 130, 2021, doi: 10.1016/j.autcon.2021.103845.

5. **Hoang Vu. Dao** *et al.*, "Optimization-Based Fuzzy Energy Management Strategy for PEM Fuel Cell/Battery/Supercapacitor Hybrid Construction Excavator," *International Journal of Precision Engineering and Manufacturing-Green Technology,* 2020, doi: 10.1007/s40684-020-00262-y.

B. International Conference

1. **Hoang Vu Dao** and K. K. Ahn, "Task coordinate frame-based contouring control of an excavator with sliding mode observer and prescribed performance," presented at the 2021 24th International Conference on Mechatronics Technology (ICMT), 2021.

C. Patents

1. Ahn Kyoung Kwan, Truong Hoai Vu Anh, Dang Tri Dung, **Dao Hoang Vu** "Hybrid power generation system having hydrogen generation function", Republic of Korea Patent 10-222779, Mar. 09, 2021.

2. Ahn Kyoung Kwan, **Dao Hoang Vu**, Truong Hoai Vu Anh, Dang Tri Dung "System and method for controlling temperature of fuel cell stack", Republic of Korea Patent 10-2254511, May. 14, 2021.

3. Ahn Kyoung Kwan, Truong Hoai Vu Anh, Dang Tri Dung, Do Tri Cuong, **Dao Hoang Vu** "Power management control method of vehicle having multi power source", Republic of Korea Patent 10-2153626, Sep. 02, 2020.

References

[1] Y. Sun, J. Falco, M. A. Roa, and B. Calli, "Research Challenges and Progress in Robotic Grasping and Manipulation Competitions," *IEEE Robotics and Automation Letters,* vol. 7, no. 2, pp. 874-881, 2022, doi: 10.1109/lra.2021.3129134.

[2] R.-D. Xi, X. Xiao, T.-N. Ma, and Z.-X. Yang, "Adaptive Sliding Mode Disturbance Observer Based Robust Control for Robot Manipulators Towards Assembly Assistance," *IEEE Robotics and Automation Letters,* vol. 7, no. 3, pp. 6139-6146, 2022, doi: 10.1109/lra.2022.3164448.

[3] B. Wang, S. J. Hu, L. Sun, and T. Freiheit, "Intelligent welding system technologies: State-of-the-art review and perspectives," *Journal of Manufacturing Systems,* vol. 56, pp. 373-391, 2020/07/01/ 2020, doi: https://doi.org/10.1016/j.jmsy.2020.06.020.

[4] C. L. Stewart *et al.*, "Study on augmented reality for robotic surgery bedside assistants," *Journal of Robotic Surgery,* vol. 16, no. 5, pp. 1019-1026, 2022/10/01 2022, doi: 10.1007/s11701-021-01335-z.

[5] Q. S. Mahdi, I. H. Saleh, G. Hashim, and G. B. Loganathan, "Evaluation of robot professor technology in teaching and business," *Information Technology in Industry,* vol. 9, no. 1, pp. 1182-1194, 2021.

[6] M. Vukobratović, "Humanoid robotics, past, present state, future," *Director Robotics Center, Mihailo Pupin Institute,* vol. 11000, pp. 13-27, 2006.

[7] J. Alvarez-Ramirez, I. Cervantes, and R. Kelly, "PID regulation of robot manipulators: stability and performance," *Systems & control letters,* vol. 41, no. 2, pp. 73-83, 2000.

[8] R. Middletone and G. C. Goodwin, "Adaptive computed torque control for rigid link manipulators," in *1986 25th IEEE Conference on Decision and Control*, 1986: IEEE, pp. 68-73.

[9] J. Craig, P. Hsu, and S. Sastry, "Adaptive control of mechanical manipulators," in *Proceedings. 1986 IEEE international conference on robotics and automation*, 1986, vol. 3: IEEE, pp. 190-195.

[10] N. Nikdel, M. Badamchizadeh, V. Azimirad, and M. Nazari, "Adaptive backstepping control for an n-degree of freedom robotic manipulator based on combined state augmentation," *Robotics and Computer-Integrated Manufacturing,* vol. 44, pp. 129-143, 2017.

[11] Y. Feng, X. Yu, and Z. Man, "Non-singular terminal sliding mode control of rigid manipulators," *Automatica,* vol. 38, no. 12, pp. 2159-2167, 2002.

[12] A. Mohammadi, M. Tavakoli, H. J. Marquez, and F. Hashemzadeh, "Nonlinear disturbance observer design for robotic manipulators," *Control Engineering Practice,* vol. 21, no. 3, pp. 253-267, 2013, doi: 10.1016/j.conengprac.2012.10.008.

[13]   H. Wang, "Adaptive Control of Robot Manipulators With Uncertain Kinematics and Dynamics," *IEEE Transactions on Automatic Control,* vol. 62, no. 2, pp. 948-954, 2017, doi: 10.1109/tac.2016.2575827.

[14]   D.-T. Tran, H.-V.-A. Truong, and K. K. Ahn, "Adaptive Backstepping Sliding Mode Control Based RBFNN for a Hydraulic Manipulator Including Actuator Dynamics," *Applied Sciences,* vol. 9, no. 6, 2019, doi: 10.3390/app9061265.

[15]   S. Zhang, Y. Dong, Y. Ouyang, Z. Yin, and K. Peng, "Adaptive Neural Control for Robotic Manipulators With Output Constraints and Uncertainties," *IEEE Trans Neural Netw Learn Syst,* vol. 29, no. 11, pp. 5554-5564, Nov 2018, doi: 10.1109/TNNLS.2018.2803827.

[16]   W. Sun, Y. Wu, and X. Lv, "Adaptive Neural Network Control for Full-State Constrained Robotic Manipulator With Actuator Saturation and Time-Varying Delays," *IEEE Trans Neural Netw Learn Syst,* vol. PP, Jan 27 2021, doi: 10.1109/TNNLS.2021.3051946.

[17]   J. Lee, P. H. Chang, and M. Jin, "Adaptive Integral Sliding Mode Control With Time-Delay Estimation for Robot Manipulators," *IEEE Transactions on Industrial Electronics,* vol. 64, no. 8, pp. 6796-6804, 2017, doi: 10.1109/tie.2017.2698416.

[18]   M. Jin, S. H. Kang, P. H. Chang, and J. Lee, "Robust Control of Robot Manipulators Using Inclusive and Enhanced Time Delay Control," *IEEE/ASME Transactions on Mechatronics,* vol. 22, no. 5, pp. 2141-2152, 2017, doi: 10.1109/tmech.2017.2718108.

[19]   C. Wen-Hua, D. J. Ballance, P. J. Gawthrop, and J. O. Reilly, "A nonlinear disturbance observer for robotic manipulators," *IEEE Transactions on Industrial Electronics,* vol. 47, no. 4, pp. 932-938, 2000, doi: 10.1109/41.857974.

[20]   A. D. Luca and R. Mattone, "Actuator failure detection and isolation using generalized momenta," in *2003 IEEE International Conference on Robotics and Automation (Cat. No.03CH37422),* 14-19 Sept. 2003 2003, vol. 1, pp. 634-639 vol.1, doi: 10.1109/ROBOT.2003.1241665.

[21]   H. V. Dao, S. Na, D. G. Nguyen, and K. K. Ahn, "High accuracy contouring control of an excavator for surface flattening tasks based on extended state observer and task coordinate frame approach," *Automation in Construction,* vol. 130, 2021, doi: 10.1016/j.autcon.2021.103845.

[22]   H. V. Dao and K. K. Ahn, "Extended Sliding Mode Observer-Based Admittance Control for Hydraulic Robots," *IEEE Robotics and Automation Letters,* vol. 7, no. 2, pp. 3992-3999, 2022, doi: 10.1109/lra.2022.3147244.

[23]   H. V. Dao and K. K. Ahn, "Active Disturbance Rejection Contouring Control of Robotic Excavators with Output Constraints and Sliding Mode Observer," *Applied Sciences,* vol. 12, no. 15, 2022, doi: 10.3390/app12157453.

[24]   H. E. Merritt, *Hydraulic Control Systems*. Hoboken, NJ, USA: Wiley, 1967.

[25]   Y. Huang, J. Na, X. Wu, X. Liu, and Y. Guo, "Adaptive control of nonlinear uncertain active suspension systems with prescribed performance," *ISA Trans,* vol. 54, pp. 145-55, Jan 2015, doi: 10.1016/j.isatra.2014.05.025.

[26]   M. Dong, C. Liu, and G. Li, "Robust Fault Diagnosis Based on Nonlinear Model of Hydraulic Gauge Control System on Rolling Mill," *IEEE Transactions on Control Systems Technology,* vol. 18, no. 2, pp. 510-515, 2010, doi: 10.1109/tcst.2009.2019750.

[27]   S. Ijaz, L. Yan, M. T. Hamayun, and C. Shi, "Active fault tolerant control scheme for aircraft with dissimilar redundant actuation system subject to hydraulic failure," *Journal of the Franklin Institute,* vol. 356, no. 3, pp. 1302-1332, 2019, doi: 10.1016/j.jfranklin.2018.11.018.

[28]   L. Lu and B. Yao, "Energy-Saving Adaptive Robust Control of a Hydraulic Manipulator Using Five Cartridge Valves With an Accumulator," *IEEE Transactions on Industrial Electronics,* vol. 61, no. 12, pp. 7046-7054, 2014, doi: 10.1109/tie.2014.2314054.

[29]   K.-x. Ba *et al.*, "A Nonlinear Model-based Variable Impedance Parameters Control for Position-based Impedance Control System of Hydraulic Drive Unit," *International Journal of Control, Automation and Systems,* vol. 18, no. 7, pp. 1806-1817, 2020, doi: 10.1007/s12555-019-0151-0.

[30]   D. T. Tran, D. X. Ba, and K. K. Ahn, "Adaptive Backstepping Sliding Mode Control for Equilibrium Position Tracking of an Electrohydraulic Elastic Manipulator," *IEEE Transactions on Industrial Electronics,* vol. 67, no. 5, pp. 3860-3869, 2020, doi: 10.1109/tie.2019.2918475.

[31]   H. V. A. Truong, D. T. Tran, X. D. To, K. K. Ahn, and M. Jin, "Adaptive Fuzzy Backstepping Sliding Mode Control for a 3-DOF Hydraulic Manipulator with Nonlinear Disturbance Observer for Large Payload Variation," *Applied Sciences,* vol. 9, no. 16, 2019, doi: 10.3390/app9163290.

[32]   W. Shen and J. Wang, "Adaptive Fuzzy Sliding Mode Control Based on Pi-sigma Fuzzy Neutral Network for Hydraulic Hybrid Control System Using New Hydraulic Transformer," *International Journal of Control, Automation and Systems,* vol. 17, no. 7, pp. 1708-1716, 2019, doi: 10.1007/s12555-018-0593-9.

[33]   J. Yao, Z. Jiao, D. Ma, and L. Yan, "High-Accuracy Tracking Control of Hydraulic Rotary Actuators With Modeling Uncertainties," *IEEE/ASME Transactions on Mechatronics,* vol. 19, no. 2, pp. 633-641, 2014, doi: 10.1109/tmech.2013.2252360.

[34]   J. Yao, Z. Jiao, and D. Ma, "Extended-State-Observer-Based Output Feedback Nonlinear Robust Control of Hydraulic Systems With Backstepping," *IEEE Transactions on Industrial Electronics,* vol. 61, no. 11, pp. 6285-6293, 2014, doi: 10.1109/tie.2014.2304912.

[35]   J. Yao, "Model-based nonlinear control of hydraulic servo systems: Challenges, developments and perspectives," *Frontiers of Mechanical Engineering,* vol. 13, no. 2, pp. 179-210, 2017, doi: 10.1007/s11465-018-0464-3.

[36]   Z. Yao, J. Yao, and W. Sun, "Adaptive RISE Control of Hydraulic Systems With Multilayer Neural-Networks," *IEEE Transactions on Industrial Electronics,* vol. 66, no. 11, pp. 8638-8647, 2019, doi: 10.1109/tie.2018.2886773.

[37]   B. Yao, F. Bu, J. Reedy, and G. T. C. Chiu, "Adaptive robust motion control of single-rod hydraulic actuators: Theory and experiments," in *Proceedings of the 1999 American Control Conference (Cat. No. 99CH36251),* 2-4 June 1999 1999, vol. 2, pp. 759-763 vol.2, doi: 10.1109/ACC.1999.783142.

[38]   B. Helian, Z. Chen, and B. Yao, "Precision Motion Control of a Servomotor-Pump Direct-Drive Electrohydraulic System With a Nonlinear Pump Flow Mapping," *IEEE Transactions on Industrial Electronics,* vol. 67, no. 10, pp. 8638-8648, 2020, doi: 10.1109/tie.2019.2947803.

[39]   L. Lyu, Z. Chen, and B. Yao, "Development of Pump and Valves Combined Hydraulic System for Both High Tracking Precision and High Energy Efficiency," *IEEE Transactions on Industrial Electronics,* vol. 66, no. 9, pp. 7189-7198, 2019, doi: 10.1109/tie.2018.2875666.

[40]   B. Xian, D. M. Dawson, M. S. deQueiroz, and J. Chen, "A Continuous Asymptotic Tracking Control Strategy for Uncertain Nonlinear Systems," *IEEE Transactions on Automatic Control,* vol. 49, no. 7, pp. 1206-1206, 2004, doi: 10.1109/tac.2004.831148.

[41]   D. Won, W. Kim, D. Shin, and C. C. Chung, "High-Gain Disturbance Observer-Based Backstepping Control With Output Tracking Error Constraint for Electro-Hydraulic Systems," *IEEE Transactions on Control Systems Technology,* vol. 23, no. 2, pp. 787-795, 2015, doi: 10.1109/tcst.2014.2325895.

[42]   Z. Chu, C. Wu, and N. Sepehri, "Active Disturbance Rejection Control Applied to High-order Systems with Parametric Uncertainties," *International Journal of Control, Automation and Systems,* vol. 17, no. 6, pp. 1483-1493, 2019, doi: 10.1007/s12555-018-0509-8.

[43]   S. Wang and J. Zhai, "A Trajectory Tracking Method for Wheeled Mobile Robots Based on Disturbance Observer," *International Journal of Control, Automation and Systems,* vol. 18, no. 8, pp. 2165-2169, 2020, doi: 10.1007/s12555-019-0156-8.

[44]   X. Yu and J. Jiang, "A survey of fault-tolerant controllers based on safety-related issues," *Annual Reviews in Control,* vol. 39, pp. 46-57, 2015, doi: 10.1016/j.arcontrol.2015.03.004.

[45]   Z. Gao, C. Cecati, and S. X. Ding, "A Survey of Fault Diagnosis and Fault-Tolerant Techniques—Part I: Fault Diagnosis With Model-Based and Signal-Based Approaches," *IEEE Transactions on Industrial Electronics,* vol. 62, no. 6, pp. 3757-3767, 2015, doi: 10.1109/tie.2015.2417501.

[46]   Y. Wang, W. Zhou, J. Luo, H. Yan, H. Pu, and Y. Peng, "Reliable Intelligent Path Following Control for a Robotic Airship Against Sensor Faults," *IEEE/ASME Transactions on Mechatronics,* vol. 24, no. 6, pp. 2572-2582, 2019, doi: 10.1109/tmech.2019.2929224.

[47]   Y. Wang, B. Jiang, Z.-G. Wu, S. Xie, and Y. Peng, "Adaptive Sliding Mode Fault-Tolerant Fuzzy Tracking Control With Application to Unmanned Marine Vehicles," *IEEE Transactions on Systems, Man, and Cybernetics: Systems,* pp. 1-10, 2020, doi: 10.1109/tsmc.2020.2964808.

[48]   Q.-N. Xu, K.-M. Lee, H. Zhou, and H.-Y. Yang, "Model-Based Fault Detection and Isolation Scheme for a Rudder Servo System," *IEEE Transactions on Industrial Electronics,* vol. 62, no. 4, pp. 2384-2396, 2015, doi: 10.1109/tie.2014.2361795.

[49]   M. Muenchhof, M. Beck, and R. Isermann, "Fault-tolerant actuators and drives—Structures, fault detection principles and applications," *Annual Reviews in Control,* vol. 33, no. 2, pp. 136-148, 2009, doi: 10.1016/j.arcontrol.2009.08.002.

[50]   A. S. Rezazadeh, H. R. Koofigar, and S. Hosseinnia, "Robust leakage detection for electro hydraulic actuators using an adaptive nonlinear observer," *International Journal of Precision Engineering and Manufacturing,* vol. 15, no. 3, pp. 391-397, 2014, doi: 10.1007/s12541-014-0349-2.

[51]   T. Li, T. Yang, Y. Cao, R. Xie, and X. Wang, "Disturbance-Estimation Based Adaptive Backstepping Fault-Tolerant Synchronization Control for a Dual Redundant Hydraulic Actuation System With Internal Leakage Faults," *IEEE Access,* vol. 7, pp. 73106-73119, 2019, doi: 10.1109/access.2019.2920415.

[52]   A. A. Amin and K. M. Hasan, "A review of Fault Tolerant Control Systems: Advancements and applications," *Measurement,* vol. 143, pp. 58-68, 2019, doi: 10.1016/j.measurement.2019.04.083.

[53]   V. Mien, G. Shuzhi Sam, and R. Hongliang, "Finite Time Fault Tolerant Control for Robot Manipulators Using Time Delay Estimation and Continuous Nonsingular Fast Terminal Sliding Mode Control," *IEEE Trans Cybern,* vol. 47, no. 7, pp. 1681-1693, Jul 2017, doi: 10.1109/TCYB.2016.2555307.

[54]   J. Yao and W. Deng, "Active Disturbance Rejection Adaptive Control of Hydraulic Servo Systems," *IEEE Transactions on Industrial Electronics,* vol. 64, no. 10, pp. 8023-8032, 2017, doi: 10.1109/tie.2017.2694382.

[55]   C. Wang, L. Quan, Z. Jiao, and S. Zhang, "Nonlinear Adaptive Control of Hydraulic System With Observing and Compensating Mismatching Uncertainties," *IEEE Transactions on Control Systems Technology,* vol. 26, no. 3, pp. 927-938, 2018, doi: 10.1109/tcst.2017.2699166.

[56]   T. X. Dinh, T. D. Thien, T. H. V. Anh, and K. K. Ahn, "Disturbance Observer Based Finite Time Trajectory Tracking Control for a 3 DOF Hydraulic Manipulator Including Actuator Dynamics," *IEEE Access,* vol. 6, pp. 36798-36809, 2018, doi: 10.1109/access.2018.2848240.

[57]   D. T. Tran, M. Jin, and K. K. Ahn, "Nonlinear Extended State Observer Based on Output Feedback Control for a Manipulator With Time-Varying Output Constraints and External Disturbance," *IEEE Access,* vol. 7, pp. 156860-156870, 2019, doi: 10.1109/access.2019.2949594.

[58] J. Yao, W. Deng, and Z. Jiao, "Adaptive Control of Hydraulic Actuators With LuGre Model-Based Friction Compensation," *IEEE Transactions on Industrial Electronics,* vol. 62, no. 10, pp. 6469-6477, 2015, doi: 10.1109/tie.2015.2423660.

[59] A. Levant, "Robust exact differentiation via sliding mode technique," *Automatica,* vol. 34, no. 3, pp. 379-384, 1998/03/01/ 1998, doi: https://doi.org/10.1016/S0005-1098(97)00209-4.

[60] A. Mohanty and B. Yao, "Indirect Adaptive Robust Control of Hydraulic Manipulators With Accurate Parameter Estimates," *IEEE Transactions on Control Systems Technology,* vol. 19, no. 3, pp. 567-575, 2011, doi: 10.1109/tcst.2010.2048569.

[61] N. G. T. Claudio Semini*, Emanuele Guglielmino, Michele Focchi, Ferdinando Cannella and Darwin G. Caldwell, "Design of HyQ – a Hydraulically and Electrically Actuated Quadruped Robot," 2011.

[62] C. Semini, "HyQ - Design and Development of a Hydraulically Actuated Quadruped Robot," PhD, University of Genoa & Italian Institute of Technology, 2010.

[63] J. Cieslak, D. Efimov, and D. Henry, "Transient management of a supervisory fault-tolerant control scheme based on dwell-time conditions," *International Journal of Adaptive Control and Signal Processing,* vol. 29, no. 1, pp. 123-142, 2015, doi: 10.1002/acs.2465.

[64] "Adaptive Fault-Tolerant Spacecraft Attitude Control Design With Transient Response Control," *IEEE/ASME Transactions on Mechatronics,* vol. 19, no. 4, pp. 1404-1411, 2014, doi: 10.1109/tmech.2013.2288314.

[65] S. A. Nahian, D. Q. Truong, P. Chowdhury, D. Das, and K. K. Ahn, "Modeling and fault tolerant control of an electro-hydraulic actuator," *International Journal of Precision Engineering and Manufacturing,* vol. 17, no. 10, pp. 1285-1297, 2016, doi: 10.1007/s12541-016-0153-2.

[66] S. A. Nahian, T. Q. Dinh, H. V. Dao, and K. K. Ahn, "An Unknown Input Observer–EFIR Combined Estimator for Electrohydraulic Actuator in Sensor Fault-Tolerant Control Application," *IEEE/ASME Transactions on Mechatronics,* vol. 25, no. 5, pp. 2208-2219, 2020, doi: 10.1109/tmech.2020.3013609.

[67] D. Brambilla, L. M. Capisani, A. Ferrara, and P. Pisu, "Fault Detection for Robot Manipulators via Second-Order Sliding Modes," *IEEE Transactions on Industrial Electronics,* vol. 55, no. 11, pp. 3954-3963, 2008, doi: 10.1109/tie.2008.2005932.

[68] L. M. Capisani, A. Ferrara, A. Ferreira de Loza, and L. M. Fridman, "Manipulator Fault Diagnosis via Higher Order Sliding-Mode Observers," *IEEE Transactions on Industrial Electronics,* vol. 59, no. 10, pp. 3979-3986, 2012, doi: 10.1109/tie.2012.2189534.

[69] H. Yang and S. Yin, "Actuator and Sensor Fault Estimation for Time-Delay Markov Jump Systems With Application to Wheeled Mobile Manipulators," *IEEE Transactions on Industrial Informatics,* vol. 16, no. 5, pp. 3222-3232, 2020, doi: 10.1109/tii.2019.2915668.

[70] J. Mattila, J. Koivumaki, D. G. Caldwell, and C. Semini, "A Survey on Control of Hydraulic Robotic Manipulators With Projection to Future Trends," *IEEE/ASME Transactions on Mechatronics,* vol. 22, no. 2, pp. 669-680, 2017, doi: 10.1109/tmech.2017.2668604.

[71] W. Lee, S. Yoo, S. Nam, K. Kim, and W. K. Chung, "Passivity-Based Robust Compliance Control of Electro-Hydraulic Robot Manipulators With Joint Angle Limit," *IEEE Robotics and Automation Letters,* vol. 5, no. 2, pp. 3190-3197, 2020, doi: 10.1109/lra.2020.2975724.

[72] C. Qian, L. Zhang, C. Hua, and Z. Bai, "Adaptive Fuzzy Vertical Vibration Suppression Control of the Mechanical-Hydraulic Coupling Rolling Mill System With Input Dead-Zone and Output Constraints," *IEEE Access,* vol. 8, pp. 85793-85801, 2020, doi: 10.1109/access.2020.2992610.

[73] D.-F. Zhang, S.-P. Zhang, Z.-Q. Wang, and B.-C. Lu, "Dynamic Control Allocation Algorithm for a Class of Distributed Control Systems," *International Journal of Control, Automation and Systems,* vol. 18, no. 2, pp. 259-270, 2019, doi: 10.1007/s12555-017-9768-z.

[74] S. Zhang, T. Minav, M. Pietola, H. Kauranne, and J. Kajaste, "The effects of control methods on energy efficiency and position tracking of an electro-hydraulic excavator equipped with zonal hydraulics," *Automation in Construction,* vol. 100, pp. 129-144, 2019, doi: 10.1016/j.autcon.2019.01.003.

[75] T. C. Do, T. D. Dang, T. Q. Dinh, and K. K. Ahn, "Developments in energy regeneration technologies for hydraulic excavators: A review," *Renewable and Sustainable Energy Reviews,* vol. 145, 2021, doi: 10.1016/j.rser.2021.111076.

[76] T. Lin, Y. Lin, H. Ren, H. Chen, Z. Li, and Q. Chen, "A double variable control load sensing system for electric hydraulic excavator," *Energy,* vol. 223, 2021, doi: 10.1016/j.energy.2021.119999.

[77] J. P. P. Gomes, L. R. Rodrigues, B. P. Leao, R. K. H. Galvao, and T. Yoneyama, "Using Degradation Messages to Predict Hydraulic System Failures in a Commercial Aircraft," *IEEE Transactions on Automation Science and Engineering,* vol. 15, no. 1, pp. 214-224, 2018, doi: 10.1109/tase.2016.2601261.

[78] S. Ijaz, M. T. Hamayun, H. Anwaar, L. Yan, and M. K. Li, "LPV Modeling and Tracking Control of Dissimilar Redundant Actuation System for Civil Aircraft," *International Journal of Control, Automation and Systems,* vol. 17, no. 3, pp. 705-715, 2019, doi: 10.1007/s12555-017-0399-1.

[79] J. N. Strohm, D. Pech, and B. Lohmann, "A Proactive Nonlinear Disturbance Compensator for the Quarter Car," *International Journal of Control, Automation and Systems,* vol. 18, no. 8, pp. 2012-2026, 2020, doi: 10.1007/s12555-019-0531-5.

[80] V. T. Vu, O. Sename, L. Dugard, and P. Gáspár, "An Investigation into the Oil Leakage Effect Inside the Electronic Servo-valve for an $\mathcal{H}_\infty$/LPV Active

Anti-roll Bar System," *International Journal of Control, Automation and Systems,* vol. 17, no. 11, pp. 2917-2928, 2019, doi: 10.1007/s12555-019-0060-2.

[81]   J. Na, Y. Li, Y. Huang, G. Gao, and Q. Chen, "Output Feedback Control of Uncertain Hydraulic Servo Systems," *IEEE Transactions on Industrial Electronics,* vol. 67, no. 1, pp. 490-500, 2020, doi: 10.1109/tie.2019.2897545.

[82]   L. Cheng, Z.-C. Zhu, G. Shen, S. Wang, X. Li, and Y. Tang, "Real-Time Force Tracking Control of an Electro-Hydraulic System Using a Novel Robust Adaptive Sliding Mode Controller," *IEEE Access,* vol. 8, pp. 13315-13328, 2020, doi: 10.1109/access.2019.2895595.

[83]   B. Yu *et al.*, "Design, Mathematical Modeling and Force Control for Electro-Hydraulic Servo System With Pump-Valve Compound Drive," *IEEE Access,* vol. 8, pp. 171988-172005, 2020, doi: 10.1109/access.2020.3012091.

[84]   S.-W. Kim, B. Cho, S. Shin, J.-H. Oh, J. Hwangbo, and H.-W. Park, "Force Control of a Hydraulic Actuator With a Neural Network Inverse Model," *IEEE Robotics and Automation Letters,* vol. 6, no. 2, pp. 2814-2821, 2021, doi: 10.1109/lra.2021.3062353.

[85]   M. H. Raibert and J. J. Craig, "Hybrid Position/Force Control of Manipulators," *Journal of Dynamic Systems, Measurement, and Control,* vol. 103, no. 2, pp. 126-133, 1981, doi: 10.1115/1.3139652.

[86]   T. Yoshikawa, "Dynamic hybrid position/force control of robot manipulators--Description of hand constraints and calculation of joint driving force," *IEEE Journal on Robotics and Automation,* vol. 3, no. 5, pp. 386-392, 1987, doi: 10.1109/JRA.1987.1087120.

[87]   N. Hogan, "Impedance Control: An Approach to Manipulation: Part I—Theory," *Journal of Dynamic Systems, Measurement, and Control,* vol. 107, no. 1, pp. 1-7, 1985, doi: 10.1115/1.3140702.

[88]   H. Dong, X. Li, P. Shen, L. Gao, and H. Zhong, "Interval Type-2 Fuzzy Logic PID Controller Based on Differential Evolution with Better and Nearest Option for Hydraulic Serial Elastic Actuator," *International Journal of Control, Automation and Systems,* vol. 19, no. 2, pp. 1113-1132, 2020, doi: 10.1007/s12555-020-0141-2.

[89]   T. Boaventura, J. Buchli, C. Semini, and D. G. Caldwell, "Model-Based Hydraulic Impedance Control for Dynamic Robots," *IEEE Transactions on Robotics,* vol. 31, no. 6, pp. 1324-1336, 2015, doi: 10.1109/tro.2015.2482061.

[90]   B. Siciliano and L. Villani, *Robot Force Control*, 1 ed. (The Springer International Series in Engineering and Computer Science). Springer US, 1999.

[91]   G. Sebastian, Z. Li, V. Crocher, D. Kremers, Y. Tan, and D. Oetomo, "Interaction Force Estimation Using Extended State Observers: An Application to Impedance-Based Assistive and Rehabilitation Robotics," *IEEE Robotics and Automation Letters,* vol. 4, no. 2, pp. 1156-1161, 2019, doi: 10.1109/lra.2019.2894908.

[92]   S. H. Chien, J. H. Wang, and M. Y. Cheng, "Performance Comparisons of Different Observer-Based Force-Sensorless Approaches for Impedance Control of Collaborative Robot Manipulators," in *2020 IEEE Conference on Industrial Cyberphysical Systems (ICPS)*, 10-12 June 2020 2020, vol. 1, pp. 326-331, doi: 10.1109/ICPS48405.2020.9274790.

[93]   S. Lee, M. Kim, and J. Song, "Sensorless collision detection for safe human-robot collaboration," in *2015 IEEE/RSJ International Conference on Intelligent Robots and Systems (IROS)*, 28 Sept.-2 Oct. 2015 2015, pp. 2392-2397, doi: 10.1109/IROS.2015.7353701.

[94]   W.-H. Chen, J. Yang, L. Guo, and S. Li, "Disturbance-Observer-Based Control and Related Methods—An Overview," *IEEE Transactions on Industrial Electronics,* vol. 63, no. 2, pp. 1083-1095, 2016, doi: 10.1109/tie.2015.2478397.

[95]   J. Yang and C. Peng, "Adaptive neural impedance control with extended state observer for human–robot interactions by output feedback through tracking differentiator," *Proceedings of the Institution of Mechanical Engineers, Part I: Journal of Systems and Control Engineering,* vol. 234, no. 7, pp. 820-833, 2020, doi: 10.1177/0959651819898936.

[96]   A. K. Junejo, W. Xu, C. Mu, M. M. Ismail, and Y. Liu, "Adaptive Speed Control of PMSM Drive System Based a New Sliding-Mode Reaching Law," *IEEE Transactions on Power Electronics,* vol. 35, no. 11, pp. 12110-12121, 2020, doi: 10.1109/tpel.2020.2986893.

[97]   D. Ke, F. Wang, L. He, and Z. Li, "Predictive Current Control for PMSM Systems Using Extended Sliding Mode Observer With Hurwitz-Based Power Reaching Law," *IEEE Transactions on Power Electronics,* vol. 36, no. 6, pp. 7223-7232, 2021, doi: 10.1109/tpel.2020.3043489.

[98]   C. Yang, B. Song, Y. Xie, and X. Tang, "Online Parallel Estimation of Mechanical Parameters for PMSM Drives via a Network of Interconnected Extended Sliding-Mode Observers," *IEEE Transactions on Power Electronics,* vol. 36, no. 10, pp. 11818-11834, 2021, doi: 10.1109/tpel.2021.3067328.

[99]   J. Zhang, P. Shi, and W. Lin, "Extended sliding mode observer based control for Markovian jump linear systems with disturbances," *Automatica,* vol. 70, pp. 140-147, 2016, doi: 10.1016/j.automatica.2016.03.020.

[100]   J. Yu, Y. Sun, W. Lin, and Z. Li, "Fault-tolerant control for descriptor stochastic systems with extended sliding mode observer approach," *IET Control Theory & Applications,* vol. 11, no. 8, pp. 1079-1087, 2017, doi: 10.1049/iet-cta.2016.0282.

[101]   Z. Liu, S. Liu, Z. Li, and I. A. Tasiu, "A Novel Approach Based on Extended State Observer Sliding Mode Control to Suppress Voltage Low Frequency Oscillation of Traction Network," *IEEE Access,* vol. 7, pp. 52440-52454, 2019, doi: 10.1109/access.2019.2912219.

[102] H. Yi, M. Liu, and H. Li, "Satellites Autonomous Navigation With an Extended State and Disturbance Sliding Mode Observer Method," *IEEE Access,* vol. 7, pp. 112693-112702, 2019, doi: 10.1109/access.2019.2930354.

[103] X. Zhou and X. Li, "Trajectory tracking control for electro-optical tracking system based on fractional-order sliding mode controller with super-twisting extended state observer," *ISA Trans,* Feb 19 2021, doi: 10.1016/j.isatra.2021.01.062.

[104] W. Lee and W. K. Chung, "Disturbance-Observer-Based Compliance Control of Electro-Hydraulic Actuators With Backdrivability," *IEEE Robotics and Automation Letters,* vol. 4, no. 2, pp. 1722-1729, 2019, doi: 10.1109/lra.2019.2897178.

[105] S. Yoo, W. Lee, and W. K. Chung, "Impedance Control of Hydraulic Actuation Systems With Inherent Backdrivability," *IEEE/ASME Transactions on Mechatronics,* vol. 24, no. 5, pp. 1921-1930, 2019, doi: 10.1109/tmech.2019.2932132.

[106] H. V. Dao, D. T. Tran, and K. K. Ahn, "Active Fault Tolerant Control System Design for Hydraulic Manipulator With Internal Leakage Faults Based on Disturbance Observer and Online Adaptive Identification," *IEEE Access,* vol. 9, pp. 23850-23862, 2021, doi: 10.1109/access.2021.3053596.

[107] "Cylinder Friction." MathWorks. https://www.mathworks.com/help/physmod/hydro/ref/cylinderfriction.html (accessed 13/08, 2021).

[108] Y. Koren, "Cross-Coupled Biaxial Computer Control for Manufacturing Systems," *Journal of Dynamic Systems, Measurement, and Control,* vol. 120, 265, 1980.

[109] Y. Koren and C. C. Lo, "Variable-Gain Cross-Coupling Controller for Contouring," *CIRP Annals,* vol. 40, no. 1, pp. 371-374, 1991/01/01/ 1991, doi: https://doi.org/10.1016/S0007-8506(07)62009-5.

[110] J. Lee, W. E. Dixon, and J. C. Ziegert, "Adaptive nonlinear contour coupling control for a machine tool system," *The International Journal of Advanced Manufacturing Technology,* vol. 61, no. 9-12, pp. 1057-1065, 2011, doi: 10.1007/s00170-011-3760-1.

[111] J. Yao, X. Cao, Y. Zhang, and Y. Li, "Cross-coupled fuzzy PID control combined with full decoupling compensation method for double cylinder servo control system," *Journal of Mechanical Science and Technology,* vol. 32, no. 5, pp. 2261-2271, 2018, doi: 10.1007/s12206-018-0437-9.

[112] K. L. Barton and A. G. Alleyne, "A Cross-Coupled Iterative Learning Control Design for Precision Motion Control," *IEEE Transactions on Control Systems Technology,* vol. 16, no. 6, pp. 1218-1231, 2008, doi: 10.1109/TCST.2008.919433.

[113] Y. Syh-Shiuh and H. Pau-Lo, "Estimation of the contouring error vector for the cross-coupled control design," *IEEE/ASME Transactions on Mechatronics,* vol. 7, no. 1, pp. 44-51, 2002, doi: 10.1109/3516.990886.

[114] J. Yang and Z. Li, "A Novel Contour Error Estimation for Position Loop-Based Cross-Coupled Control," *IEEE/ASME Transactions on Mechatronics,* vol. 16, no. 4, pp. 643-655, 2011, doi: 10.1109/TMECH.2010.2048718.

[115] J. R. Conway, C. A. Ernesto, R. T. Farouki, and M. Zhang, "Performance analysis of cross-coupled controllers for CNC machines based upon precise real-time contour error measurement," *International Journal of Machine Tools and Manufacture,* vol. 52, no. 1, pp. 30-39, 2012/01/01/ 2012, doi: https://doi.org/10.1016/j.ijmachtools.2011.08.015.

[116] F. Huo and A.-N. Poo, "Improving contouring accuracy by using generalized cross-coupled control," *International Journal of Machine Tools and Manufacture,* vol. 63, pp. 49-57, 2012/12/01/ 2012, doi: https://doi.org/10.1016/j.ijmachtools.2012.07.012.

[117] J. Wu, Z. Xiong, and H. Ding, "Integral design of contour error model and control for biaxial system," *International Journal of Machine Tools and Manufacture,* vol. 89, pp. 159-169, 2015/02/01/ 2015, doi: https://doi.org/10.1016/j.ijmachtools.2014.11.011.

[118] G. T. Chiu and M. Tomizuka, "Contouring control of machine tool feed drive systems: a task coordinate frame approach," *IEEE Transactions on Control Systems Technology,* vol. 9, no. 1, pp. 130-139, 2001.

[119] C. Hu, B. Yao, and Q. Wang, "Global Task Coordinate Frame-Based Contouring Control of Linear-Motor-Driven Biaxial Systems With Accurate Parameter Estimations," *IEEE Transactions on Industrial Electronics,* vol. 58, no. 11, pp. 5195-5205, 2011.

[120] B. Yao, C. Hu, and Q. Wang, "An Orthogonal Global Task Coordinate Frame for Contouring Control of Biaxial Systems," *IEEE/ASME Transactions on Mechatronics,* vol. 17, no. 4, pp. 622-634, 2012.

[121] R. Shi, Y. Lou, X. Zhang, and J. Li, "A Novel Task Coordinate Frame Reduced-Dimension 3-D Contouring Control," *IEEE Transactions on Automation Science and Engineering,* vol. 15, no. 4, pp. 1852-1863, 2018.

[122] Y. Lou, H. Meng, J. Yang, Z. Li, J. Gao, and X. Chen, "Task Polar Coordinate Frame-Based Contouring Control of Biaxial Systems," *IEEE Transactions on Industrial Electronics,* vol. 61, no. 7, pp. 3490-3501, 2014, doi: 10.1109/tie.2013.2282609.

[123] R. Shi and Y. Lou, "Three-Dimensional Contouring Control: A Task Polar Coordinate Frame Approach," *IEEE Access,* vol. 7, pp. 63626-63637, 2019.

[124] T. Lin, W. Huang, H. Ren, S. Fu, and Q. Liu, "New compound energy regeneration system and control strategy for hybrid hydraulic excavators," *Automation in Construction,* vol. 68, pp. 11-20, 2016, doi: 10.1016/j.autcon.2016.03.016.

[125] H. Kim, S. Yoo, S. Cho, and K. Yi, "Hybrid control algorithm for fuel consumption of a compound hybrid excavator," *Automation in Construction,* vol. 68, pp. 1-10, 2016, doi: 10.1016/j.autcon.2016.03.017.

[126] T. Wang, Q. Wang, and T. Lin, "Improvement of boom control performance for hybrid hydraulic excavator with potential energy recovery," *Automation in Construction,* vol. 30, pp. 161-169, 2013, doi: 10.1016/j.autcon.2012.11.034.

[127] F. Morosi, M. Rossoni, and G. Caruso, "Coordinated control paradigm for hydraulic excavator with haptic device," *Automation in Construction,* vol. 105, 2019, doi: 10.1016/j.autcon.2019.102848.

[128] R. C. Winck, M. Elton, and W. J. Book, "A practical interface for coordinated position control of an excavator arm," *Automation in Construction,* vol. 51, pp. 46-58, 2015, doi: 10.1016/j.autcon.2014.12.012.

[129] Q. H. Le, J. W. Lee, and S. Y. Yang, "Remote control of excavator using head tracking and flexible monitoring method," *Automation in Construction,* vol. 81, pp. 99-111, 2017, doi: 10.1016/j.autcon.2017.06.015.

[130] C. S. Lee, J. Bae, and D. Hong, "Contour control for leveling work with robotic excavator," *International Journal of Precision Engineering and Manufacturing,* vol. 14, no. 12, pp. 2055-2060, 2013, doi: 10.1007/s12541-013-0278-5.

[131] D. Wang, L. Zheng, H. Yu, W. Zhou, and L. Shao, "Robotic excavator motion control using a nonlinear proportional-integral controller and cross-coupled pre-compensation," *Automation in Construction,* vol. 64, pp. 1-6, 2016, doi: 10.1016/j.autcon.2015.12.024.

[132] Y. Wang, G. Luo, L. Gu, and X. Li, "Fractional-order nonsingular terminal sliding mode control of hydraulic manipulators using time delay estimation," *Journal of Vibration and Control,* vol. 22, no. 19, pp. 3998-4011, 2015, doi: 10.1177/1077546315569518.

[133] J. Baek, M. Jin, and S. Han, "A New Adaptive Sliding-Mode Control Scheme for Application to Robot Manipulators," *IEEE Transactions on Industrial Electronics,* vol. 63, no. 6, pp. 3628-3637, 2016, doi: 10.1109/tie.2016.2522386.

[134] N. Nikdel, M. Badamchizadeh, V. Azimirad, and M. A. Nazari, "Fractional-Order Adaptive Backstepping Control of Robotic Manipulators in the Presence of Model Uncertainties and External Disturbances," *IEEE Transactions on Industrial Electronics,* vol. 63, no. 10, pp. 6249-6256, 2016, doi: 10.1109/tie.2016.2577624.

[135] K. K. Ahn, D. N. C. Nam, and M. Jin, "Adaptive Backstepping Control of an Electrohydraulic Actuator," *IEEE/ASME Transactions on Mechatronics,* vol. 19, no. 3, pp. 987-995, 2014, doi: 10.1109/tmech.2013.2265312.

[136] Q. Guo, Y. Zhang, B. G. Celler, and S. W. Su, "Backstepping Control of Electro-Hydraulic System Based on Extended-State-Observer With Plant Dynamics Largely Unknown," *IEEE Transactions on Industrial Electronics,* vol. 63, no. 11, pp. 6909-6920, 2016, doi: 10.1109/tie.2016.2585080.

[137] W. Gu, J. Yao, Z. Yao, and J. Zheng, "Output feedback model predictive control of hydraulic systems with disturbances compensation," *ISA Trans,* vol. 88, pp. 216-224, May 2019, doi: 10.1016/j.isatra.2018.12.007.

[138] W. Li, J. Zhang, L. Liu, and X. Ma, "Finite-Time Fault-Tolerant Control for Diesel Engine Air Path via Extended State Observer," *IEEE Access,* vol. 7, pp. 65405-65414, 2019, doi: 10.1109/access.2019.2917515.

[139] K. Yan, M. Chen, Q. Wu, and B. Jiang, "Extended state observer-based sliding mode fault-tolerant control for unmanned autonomous helicopter with wind gusts," *IET Control Theory & Applications,* vol. 13, no. 10, pp. 1500-1513, 2019, doi: 10.1049/iet-cta.2018.5341.

[140] W. He, H. Huang, and S. S. Ge, "Adaptive Neural Network Control of a Robotic Manipulator With Time-Varying Output Constraints," *IEEE Trans Cybern,* vol. 47, no. 10, pp. 3136-3147, Oct 2017, doi: 10.1109/TCYB.2017.2711961.

[141] Q. Zhou, L. Wang, C. Wu, H. Li, and H. Du, "Adaptive Fuzzy Control for Nonstrict-Feedback Systems With Input Saturation and Output Constraint," *IEEE Transactions on Systems, Man, and Cybernetics: Systems,* vol. 47, no. 1, pp. 1-12, 2017, doi: 10.1109/tsmc.2016.2557222.

[142] W. He, C. Xue, X. Yu, Z. Li, and C. Yang, "Admittance-Based Controller Design for Physical Human–Robot Interaction in the Constrained Task Space," *IEEE Transactions on Automation Science and Engineering,* vol. 17, no. 4, pp. 1937-1949, 2020, doi: 10.1109/tase.2020.2983225.

[143] X. Yu, W. He, H. Li, and J. Sun, "Adaptive Fuzzy Full-State and Output-Feedback Control for Uncertain Robots With Output Constraint," *IEEE Transactions on Systems, Man, and Cybernetics: Systems,* pp. 1-14, 2020, doi: 10.1109/tsmc.2019.2963072.

[144] F. Ghorbel, O. Chételat, and R. Longchamp, "A reduced model for constrained rigid bodies with application to parallel robots," *IFAC Proceedings Volumes,* vol. 27, no. 14, pp. 57-62, 1994/09/01/ 1994, doi: https://doi.org/10.1016/S1474-6670(17)47295-8.

[145] J. Koivumaki and J. Mattila, "Stability-Guaranteed Force-Sensorless Contact Force/Motion Control of Heavy-Duty Hydraulic Manipulators," *IEEE Transactions on Robotics,* vol. 31, no. 4, pp. 918-935, 2015, doi: 10.1109/tro.2015.2441492.

[146] J. Koivumäki and J. Mattila, "High performance nonlinear motion/force controller design for redundant hydraulic construction crane automation," *Automation in Construction,* vol. 51, pp. 59-77, 2015, doi: 10.1016/j.autcon.2014.12.014.

[147] J. Koivumaki and J. Mattila, "Stability-Guaranteed Impedance Control of Hydraulic Robotic Manipulators," *IEEE/ASME Transactions on Mechatronics,* vol. 22, no. 2, pp. 601-612, 2017, doi: 10.1109/tmech.2016.2618912.

[148] W. He, A. O. David, Z. Yin, and C. Sun, "Neural Network Control of a Robotic Manipulator With Input Deadzone and Output Constraint," *IEEE Transactions on Systems, Man, and Cybernetics: Systems,* vol. 46, no. 6, pp. 759-770, 2016, doi: 10.1109/tsmc.2015.2466194.

[149] "Resonance." Wikipedia. https://en.wikipedia.org/wiki/Resonance (accessed 05/25, 2020).

[150] C.-C. Peng and C.-L. Chen, "Biaxial contouring control with friction dynamics using a contour index approach," *International Journal of Machine Tools and Manufacture,* vol. 47, no. 10, pp. 1542-1555, 2007/08/01/ 2007, doi: https://doi.org/10.1016/j.ijmachtools.2006.11.008.